DESIGN STRATEGIES FOR CHEMOSENSORS AND THEIR APPLICATIONS IN MOLECULAR SCALE LOGIC GATES

A DISSERTATION SUBMITTED TO
MATERIALS SCIENCE AND NANOTECHNOLOGY PROGRAM
OF THE GRADUATE SCHOOL OF ENGINEERING AND SCIENCES
OF BILKENT UNIVERSITY
IN PARTIAL FULFILLMENT OF THE REQUIREMENTS
FOR THE DEGREE OF
DOCTOR OF PHILOSOPHY

By
RUSLAN GULIYEV
January, 2013

I certify that I have read this thesis and that in my opinion it is fully adequate, in scope and in quality, as a thesis of the degree of Doctor of Philosophy.

…….

Prof. Dr. Engin U. Akkaya (Principal Advisor)

I certify that I have read this thesis and that in my opinion it is fully adequate, in scope and in quality, as a thesis of the degree of Doctor of Philosophy.

…….

Prof. Dr. Özdemir Doğan

I certify that I have read this thesis and that in my opinion it is fully adequate, in scope and in quality, as a thesis of the degree of Doctor of Philosophy.

…….

Assoc. Prof. Dr. Dönüş Tuncel

I certify that I have read this thesis and that in my opinion it is fully adequate, in scope and in quality, as a thesis of the degree of Doctor of Philosophy.

…….

Assoc. Prof. Dr. Mehmet Bayındır

I certify that I have read this thesis and that in my opinion it is fully adequate, in scope and in quality, as a thesis of the degree of Doctor of Philosophy.

…….

Assist. Prof. Dr. Serdar Atılgan

Approved for the Institute of Engineering and Sciences:

…….

Prof. Dr. Levent Onural

Director of the Graduate School

ABSTRACT

DESIGN STRATEGIES FOR CHEMOSENSORS AND THEIR APPLICATIONS IN MOLECULAR SCALE LOGIC GATES

Ruslan Guliyev
PhD in Materials Science and Nanotechnology
Supervisor: Prof. Dr. Engin Umut Akkaya
January, 2013

Rational design and synthesis of novel (fluorescent) chemosensors is an active area of supramolecular chemistry. The recognition and signaling moieties are the most important parts in the design of these chemosensors. Despite the numerous studies that were reported in the literature, finding new strategies and mechanisms in the design of fluorescent probes is still of continuing interest. In this thesis, we have proposed some novel and desirable approaches for this purpose. Targeting of medically important anions, such as cyanide and fluoride (chapters 3 and 4), and developing a multianalyte chemosensor for cations (chapter 5) were successfully achieved through a rational design.

Moreover, we realized that by the help of fluorescent chemosensors we can address some important solutions, at least to a certain point, to the troublesome issues that molecular logic concept faces. Recent research in molecular logic gates produced molecular equivalences of highly complex digital circuits. However, almost all the integration reported in the literature has been “virtual”, meaning that the output of a unimolecular system is adapted to the output of integrated set of logic gates, such that, the unimolecular system represents the equivalence of a certain complex digital design. Although this approach provides some important advantages, it does not truly solve the concatenation issue at the molecular level. Since physical concatenation of molecular logic gates is important for advanced molecular computing, some novel approaches should be introduced in order to overcome this problem. That is exactly what we are reporting in the chapter 6 of this thesis.

Keywords: fluorescence, chemosensors, energy transfer, logic gates,concatenation

ÖZET

KİMYASAL ALGILAYICILARIN TASARIMI VE BUNLARIN MOLEKÜLER MANTIK KAPILARINDAKİ UYGULAMALARI

Ruslan Guliyev
Malzeme Bilimi ve Nanoteknoloji, Doktora
Tez Yöneticisi: Prof. Dr. Engin Umut Akkaya
Ocak, 2013

Floresan moleküler algılayıcıların rasyonel tasarımı supramoleküler kimyanın aktif bir araştırma alanıdır. Tanıyıcı ve uyarıcı kısımlar bir moleküler algılayıcının en önemli parçalarıdır. Literatürde yayınlanan çok sayıda moleküler algılayıcının varlığına rağmen, yeni algılama mekanizmalarının bulunması ve literatüre katılması günümüzde halen yüksek öneme sahiptir. Bu amaca yönelik olarak da bu çalışmada bazı yeni ve umut vadeden yöntemler geliştirilmiştir. Tıbbi öneme sahip siyanür ve florür gibi anyonların tayini (Bölüm 3, 4) ve katyonlar için multi-analit algılayıcıların geliştirilmesi (Bölüm 5) rasyonel bir dizayn ile başarılı bir şekilde gerçekleştirildi.

Ayrıca, floresan moleküler algılayıcıların yardımı ile moleküler mantık kapılarının karşılaştığı çok farklı problemlerin çözülebileceği tarafımızca farkedilmiştir. Moleküler mantık kapıları ile ilgili son zamanlarda yapılan araştırmalar, gelişmiş dijital devrelerin moleküler eş değerlerinin yapılabileceğini gösterdi. Moleküler seviyede bilgi işlem, moleküler mantık kapıları arasında entegrasyon gerektirir. Bu zamana kadar literatürde yer alan entegrasyonların neredeyse tamamı ‘sanal’ nitelik taşımaktadır. Bu, tek moleküler sistemin çıktısının bir dize entegre mantık kapısının çıktısına uyarlanması anlamına gelir. Özetle, bu moleküler sistem kompleks bir dijital devreyi temsil etmektedir. Bu yaklaşım önemli avantajlar sağlamasına rağmen, moleküler düzeyde entegrasyon problemini çözememektedir. İleri düzeyde bir moleküler bilgi işlemci tasarlamak için, şüphesiz ki moleküler mantık kapılarını fiziksel bir yolla birbirine bağlayacak metotlara ihtiyaç vardır. Bu çalışmada da tam olarak bu konu üzerine yoğunlaşılmıştır (Bölüm 6).

Anahtar kelimeler: floresans, sensör, enerji transferi, mantık kapısı, entegrasyon

ACKNOWLEDGEMENT

This dissertation describes the work effectuated at the Supramolecular Chemistry Laboratory at Material Science and Nanotechnology Institute (UNAM) of Bilkent University from September-2008 until December-2012. During this time, I had the pleasure of meeting and working with so many great people from whom I have learned a lot and who have had a deep influence on my life for the past years.

With immense gratitude, I would like to express my foremost and sincere thanks to my research supervisor Prof. Engin Akkaya for giving me the opportunity to join his group and introducing me to this interesting field of research. In fact, I spent seven excellent years under his guidance and over the years, it has been an inspiration to witness his enthusiasm and vast scientific knowledge. His foresighted vision always improved the impact of our work by orders of magnitude. I feel proud for being a member of his 'SCL' group. Finally, I would also like to express my gratitude to him for always giving us the freedom to pursue our own ideas.

I owe a special thank to Dr. Ali Coşkun, Dr. Özgür Altan Bozdemir, and Dr. Serdar Atılgan for their everlasting help and support, invaluable guidance as well as their unlimited knowledge and experience that I have benefited from greatly.

I am sincerely grateful to my close friends Onur Büyükçakır, Yusuf Çakmak and his good wife Sündüs Çakmak, Tuğba Kütük and her husband İlker Kütük, Safacan Kölemen, and Bilal Kılıç for support, understanding and caring they provided through all these years. They have made my life different and because of them Ankara is going to be a significant and memorable place for me in the years to come.

I also wish to express my warm and sincere thanks to 'teaching assistants trio' - Tuğçe Durgut, Tuba Yaşar and Yiğit Altay for their necessary help, kind collaboration, joyful friendships and for always being there for me.

Special thanks are also extending to my friend Bora Bilgiç for the graphical designs and cover pictures he provided for our manuscripts.

All the present and past members of Akkaya Lab - thank you all so much for your valuable friendships, wonderful collaborations, and for the memorable experiences we had together during the past years. Dr. Fazlı Sözmen, Dr. Esra Tanrıverdi, Dr. Murat Işık, Dr. Deniz Yılmaz, Dr. Gökhan Barın, Ahmet Atılgan, Bilal Uyar, Ziya Köstereli, Ahmet Bekdemir, Nisa Yeşilgül, İlke Şimşek, Hatice Turgut, Muhammed Büyüktemiz, Gülcihan Gülseren, Tuğrul Nalbantoğlu, Merve Kaplan, Elif Ertem, Hande Boyacı Sencer Selçuk, Dr. Seda Demirel and others. It has been a great pleasure for me to work with you guys.

I also would like to thank all members of UNAM family for providing a multidisciplinary research atmosphere and for joyful friendships.

I gratefully acknowledge the scholarship fund program for foreign students, which was run by the TÜBİTAK to provide support for foreign students pursuing their PhD studies in Turkey.

I am grateful for the privilege of meeting Şeyma Öztürk who has significantly important contributions on the work presented in this dissertation. Other than being an outstanding collaborator, she is a kind lab partner and a good friend.

This thesis is dedicated to my family - my father, mother, sister and brother and to my uncle Şahid. There is no way to thank them for their love and care and endless support, trust and encouragement they have provided all these years for me.

LIST OF ABBREVIATIONS

AcOH	:	Acetic Acid
Bodipy	:	Boradiazaindacene
$CHCl_3$	:	Chloroform
DDQ	:	Dichlorodicyanoquinone
DMF	:	Dimethylformamide
ET	:	Energy Transfer
Et_3N	:	Triethylamine
FRET	:	Förster Resonance Energy Transfer
HOMO	:	Highest Occupied Molecular Orbital
ICT	:	Internal Charge Transfer
IFE	:	Inner Filter Effect
LUMO	:	Lowest Unoccupied Molecular Orbital
MALDI	:	Matrix-Assisted Laser Desorption/Ionization
MS	:	Mass Spectroscopy
NMR	:	Nuclear Magnetic Resonance
PET	:	Photoinduced Electron Transfer
TFA	:	Trifluoroacetic Acid
THF	:	Tetrahydrofuran
TLC	:	Thin Layer Chromotography
TOF	:	Time of Flight

TABLE OF CONTENTS

CHAPTERS

LIST OF FIGURES

LIST OF TABLES

CHAPTER 1

INTRODUCTION

1. INTRODUCTION

Think about a patient lying on the operating table and undergoing a specific surgery. Any mistaken or mismeasured diagnostic data before or during the operation may mislead the surgeon that could result in the unfortunate end of his or her life. That is why, measuring physiologic values are highly important, and those medical diagnosis are carried out with great care. There are wide range of parameters, such as blood dioxygen levels, glucose etc., to be monitored prior or during the specific operations. However, sometimes it is a really difficult task to determine the concentration of some important ions among the other competitive species present in bodily fluids of a patient. It is obvious that, for this kind of situations, better analytical devices or testing methods should be developed. For example, during the cardiovascular bypass surgical procedures, continuous monitoring of blood K^+ ion levels is very important. Considering the presence of excess Na^+ ions (mM levels) in the same matrix, developing a detection method for K^+ ions was challenging. Due to this reason, there wasn't a good detection method for monitoring the blood K^+, until recent past. Trend et al.[1] addressed a solution to this clinical issue by putting forward the molecule below (Figure 1).

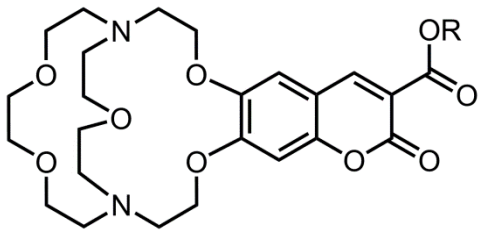

Figure 1. K^+ probe proposed by Trend et al.

Their proposed probe was a cryptand moiety tethered to a coumarin fluorophore which emits fluorescence upon binding of K^+ ions. The intensity of emitted light is proportional to the K^+ concentrations. Since, even excess amount of Na^+ ions (145 mM) didn't cause any change in the fluorescence property, the selectivity for K^+ ions was successfully achieved.

Moreover, by incorporating that molecule to a polymeric backbone, they succeeded in constructing a flow-through device, that is capable of continuously and quantitatively monitoring the blood K^+ levels. It is exactly that device, which provides an excellent example of 'supramolecular chemistry' being used for the benefits of an ordinary man in the street.

In 1987, the Nobel Prize for chemistry was awarded to triad of scientists - Donald J. Cram, Charles J. Pedersen, and Jean-Marie Lehn in recognition of their brilliant work in the field of Supramolecular Chemistry. That day, this field has proved to be a well established branch of modern chemistry. Since it lays on the crossroads between chemistry, biochemistry, physics and technology, it is highly interdisciplinary field, and has developed very rapidly in the last three decades.[2,3] Since the field is expanding as it advances, numerous definitions describing it were reported in the literature. Phrases like 'chemistry beyond the molecule', ' the chemistry of the non-covalent bond', or ' non-molecular chemistry' are some of them, to name a few. The modern concept of supramolecular chemistry was introduced by Jean-Marie Lehn, which he defined as the ‘‘chemistry of molecular assemblies and of the intermolecular bond’’.[4] From these descriptions, it can be easily inferred that, contrary to the traditional chemistry, supramolecular chemistry focuses on the weaker and reversible noncovalent interactions between molecular species. These interactions could be in the form of hydrogen bonding, metal coordination, hydrophobic forces, Van der Waals forces, π-π interactions and electrostatic forces.

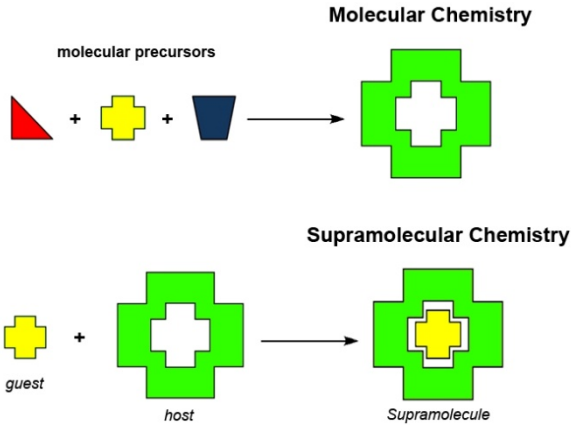

Figure 2. Comparison between molecular and supramolecular chemistry

During the early days of this field, supramolecules mainly comprised two components, a host and a guest species (Figure 2), which interact with one another in a noncovalent manner. However, dramatic developments have occurred since then, such that past decade has seen its expansion into some interesting areas of materials chemistry and nanoscience with various potential and real applications.

A wide range of chromophores, fluorophores, and redox-active chemical species have been successfully incorporated into supramolecular frameworks. Utilizing the rich host-guest chemistry, they become ideal candidates for sensing applications. Moreover, contributions of supramolecular methods in the design and manufacture of molecular scale functional devices are significantly important. Developing molecular scale logic devices, designing and synthesizing artificial biological agents, and developing new therapeutic agents, are some of the very hot and novel application areas of this field. No doubt that, as human needs are increasing, supramolecular chemistry concepts are going to be more involved in our daily life to facilitate it.

The research studies that constitute this thesis provide some novel and inspiring examples for molecular recognition in host-guest complexes, which is the oldest and generic process in supramolecular chemistry. Additionally, herein, implementation of those recognition mechanisms in the development of functional molecular logic devices was also reported.

Design and synthesis of novel (fluorescent) chemosensors constitutes the main part of this thesis. The recognition and signaling moieties are the most important parts in the design of a chemosensor. Development of receptors sensitive to specific analyte, and improvement of dye molecules (signaling part) in order to get more applicable probes are the two main research areas within this context.

Rational design of a better chemosensor, targeting a specific analyte, still remains as a challenge for the researchers working on this field. And it is an undeniable fact that, in order to be more realistic, suggested sensing probes should be applicable in biological media. Thus, water solubility becomes as one of the important barriers to be overcome. It has to be noted that, the sensing of analytes in aqueous solutions

requires strong affinity for analytes (because of their strong hydration effects) in water as well as the ability to convert analyte recognition into a fluorometric and/or colorimetric signals. So it is much more challenging to selectively recognize analytes in aqueous systems compared to organic ones. It can be concluded that, design of a sensory probe requires at least the followings: recognition between analyte and binding site should be well identified, depending on the nature of the analyte water solubility should be provided, and most importantly, selectivity of the target analyte over other concomitants should be considered. This topic is covered briefly within the second chapter of this thesis (2.3, 2.4, 2.5, 2.6).

These types of chemosensors have attracted much interest during the last two decades. Despite the numerous studies that were reported and reviewed extensively in the literature, finding new strategies and mechanisms in the design of fluorescent chemosensors is still of continuing interest. Studies presented in the chapters **3** and **4** of this thesis, briefly summarizes our recent contributions to this field.

On the other hand, by using the accumulated knowledge of chemosensor design, we are investigating their applications to different fields of supramolecular chemistry. We realized that ‘colorful’ organic molecules are very promising in the mimicking of macroscopic digital processing devices. In fact it was Professor A. Prasanna de Silva, who has reported this analogy for the first time. Contrary to the idea behind, the molecule operating as an ‘AND’ gate was very naive from synthetic perspective. Uniqueness of that study is based on the (emitted) light which is used as an output signal. It is really difficult to detect any change that happens at the molecular level. However, if the change occurs in the optical character of the molecules, then it becomes easier to detect it with high sensitivity. Molecular logic gates, based especially on fluorescence phenomenon have been widely preferred so far, due to the distinct advantages of fluorescence detection in terms of sensitivity and selectivity. Therefore, colored molecules especially fluorescent ones have become very important tools in the design and construction of molecular scale logic gates. More detailed information regarding to this topic can be found in the 'background' chapter (2.8, 2.9, 2.10, and 2.11).

Various logic gates based on organic molecules have been built due to the research work dedicated to the development of these systems so far but, molecular logic gates are still far from achieving practical applications in computing. While functional integration is possible within single molecule, at least partly because of input-output heterogeneity, integration of logic gates to implement more complex functions is far from being straight-forward. That's primarily because of the problem in the physical integration of molecules since contrary to the electronic devices we use no wiring. To solve this issue, new methodologies should be developed in terms of intermolecular communication, such that the problem of gate to gate communication is diminished. Our works along these lines are presented in chapters **5** and **6**.

CHAPTER 2

BACKGROUND INFORMATION

2. BACKGROUND

2.1. Photoluminescence

Most elementary particles are in their ground state at room temperature. When these particles are exposed to an electromagnetic irradiation, depending on the nature of the substance, absorption of a photon with proper energy may take place. This process leads to a rapid formation of an electronically excited state which is followed by dissipation of the excess energy in different forms (Figure 3). The term 'Photoluminescence' can be defined as an optical property of a substance which absorbs photon upon irradiation and release them radiatively.[5] Depending on the nature of the excited state, the emission of light can be divided into two categories as fluorescence and phosphorescence. Details related to the photoluminescence process will be discussed in the following subsections.

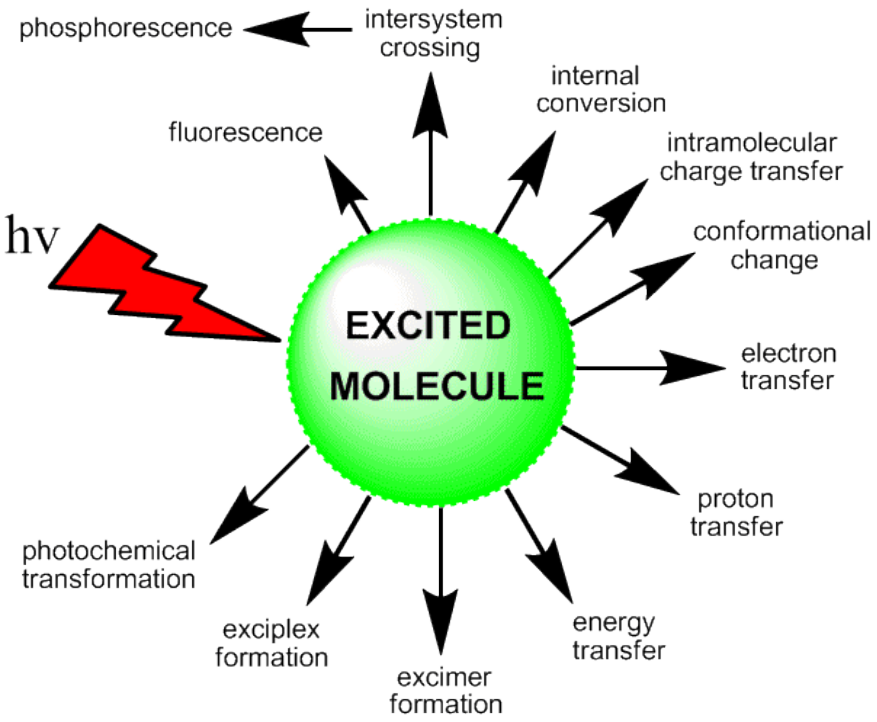

Figure 3. Possible de-excitation pathways of excited molecules

2.1.1. Absorption of Light and Electronically-Excited States

Once a molecule is irradiated by photons with proper energy, absorption of photons and transition of an electron from outer molecular orbitals (HOMO, HOMO-1 etc.) to unoccupied orbitals (LUMO, LUMO+1 etc.) of the molecule will happen very rapidly. In most cases, a photon of light of wavelength lying in the UV- Visible region of the electromagnetic spectrum is sufficient in energy for such electronic transitions. Due to this reason, the region of the spectrum covering 200- 800 nm range is sometimes named as the 'photochemical window'.[6] Moreover, other regions of the electromagnetic spectrum may induce interesting changes on the molecule upon irradiation. They are roughly summarized in the table below.

Radiation	Wavelength	Photon Energy	Results of Absorption
Gamma rays	l<0.01 nm	>1 MeV	Nuclear reactions
X rays	0.01-10 nm	124 eV-120 keV	Transitions of inner atomic electrons
UV	10-400 nm	3.1-124 eV	Transitions of outer atomic electrons
Visible	400-750 nm	1.7-3.1 eV	Transitions of outer atomic electrons
Infrared	750nm-15 μm	80meV-1.7 eV	Molecular vibrations
Far IR	15μm-1 mm	1.2meV-80meV	Molecular rotations
Radar	1mm-1 m	1.2μeV-1.2meV	Oscillation of mobile electrons

Table 1. Impact of the electromagnetic radiations on molecular structures

The absorption spectrum of a sample can be measured by UV-Vis absorption spectroscopy and at a specified wavelength the intensity of the absorption depends on the molar absorption coefficient, **ε,** of the molecule. It is the probability of an electronic transition at a given wavelength. In other words, its value gives us the information of how 'allowed' a transition is. 'Allowed' and 'forbidden' terms are beyond the classical physics, as they represent the results of quantum mechanical calculations. Since detailed quantum chemical integrations (equations) are out of the scope of this thesis, a qualitative overview will be presented within the upcoming paragraphs.

As it is stated before, the value of **ε** indicates the probability of an electronic transition from ground state to excited state of a molecule. There is a set of rules (a.k.a. selection rules) that constrain the possible transitions, and they are based mainly on two components which are spin and symmetry. Spin component displays kind of a solid property such that an electronic excitation is allowed if and only if the total spin remains unchanged during the transition. In other words, if a transition involves a spin change (e.g. singlet to triplet), then that transition is said to be forbidden. On the other hand, the symmetry component is related to the symmetry of the ground and excited states which determine the transitions to be allowed or forbidden. However, by just considering the symmetry term it is difficult to conclude that the transition is going to be forbidden. The symmetry calculations are done for the molecules in idealized conditions, but for a real molecule the symmetry may be distorted by the presence of some environmental effects like solvent or a heavy atom on the molecule. Keeping all these in mind and by analyzing the **ε** value we can comment on a transition in terms of how allowed or forbidden it is. The transition is said to be 'fully allowed' if **ε** is measured to be greater than 10^5 M^{-1} cm^{-1}. If it is smaller than 100 M^{-1} cm^{-1}, then the transition is 'forbidden', meaning that the molecule does not absorb well at this wavelength. The third option is the **ε** value lying in between 10^2- 10^4 M^{-1} cm^{-1}. In this case the transitions are said to be 'partially allowed' and this condition is coming from the symmetry component. Therefore, if a transition is spin forbidden and symmetry allowed, then the probability of it is very low (**ε**<100). On the other hand, if it is spin allowed but symmetry forbidden, then moderate absorption is observed and **ε** value is going to be between 10^2-10^4 M^{-1} cm^{-1}.

Another important consequence regarding the light absorption topic is the shape of spectra which is related to the **ε** value at each wavelength. It is a well known fact that, during the light absorption that leads to an electronic transition, number of changes in both electronic and vibrational states occurs. For an individual electronic transition, the probability of a transition between vibrational levels of each orbital (e.g. HOMO and LUMO) may be higher or lower than the others due to the overlap amount of the two vibrational wave functions. For example, when the lower and upper electronic states have similar internuclear separations, there will be greater

overlap between wave functions of vibronic states, resulting in the more intense transitions between the vibrational levels of the electronic states. Franck-Condon Principle governs all these transition, which simply states that: since the transition from one electronic state to another takes place very rapidly, nuclei of the vibrating molecule can be assumed to be fixed during the electronic transition. In other words, nuclei move much more slower than the lighter electrons, so the nuclear geometry would remain very much the same (in terms of position and velocity) as it was before the electronic transition. As a consequence of this principle, an electronic transition is represented by a vertical arrow (Figure 4), indicating the electronic transitions within stationary nuclei.[7]

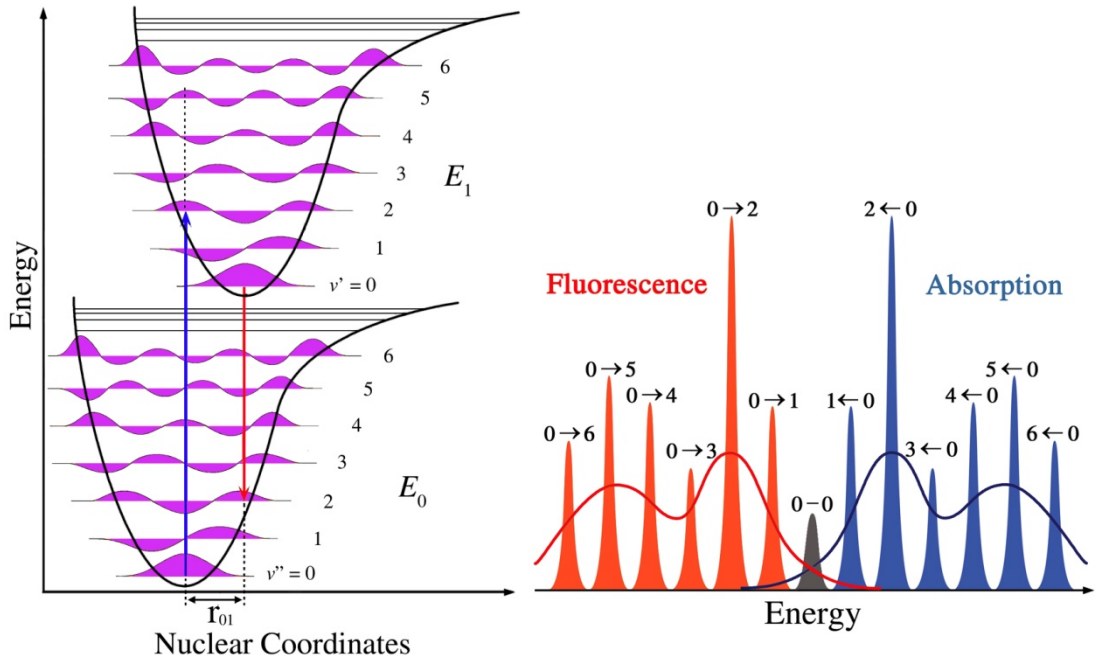

Figure 4. Morse potential diagram

A hypothetical Morse potential diagram of the ground and excited states and probable absorption and fluorescence spectra are depicted in figure 4. By looking at the diagram (left side) it can be claimed that the internuclear distance has remained unchanged during the transition. However, there is a little shift between the nuclear coordinates of ground and excited states of the molecule which is represented as r_{01}. The diagram also shows that there are many vibronic transitions that are allowed.

However, by qualitative analysis we can say that some of them are more probable than others, meaning that the intensities of vibronic transitions will be different. The most probable transition between the vibrational level in HOMO and those in LUMO will be the one where the wavefunctions overlap the most along the vertical arrow. In our case the best overlap is between ν=0 in the ground state and ν=2 in the excited state. Thus in the absorption spectrum, this transition is observed as the most intense absorption band. Due to the very large number of vibrational levels and interactions between themselves and solvent molecules, generally organic molecules do not display those fine structures in solution and solid phases. Rather, they appear as broad curves, like a line drawn over the peak maxima of the individual transition peaks. In addition, the Franck-Condon Principle is equally applicable to both absorption and fluorescence phenomena. The red arrow in the diagrams (Figure 4) represents the decay to the ground state via photon emission. Details of this and other types of relaxation processes will be covered in the next section.

2.1.2. The Physical Deactivation of Excited States

When photons with significant energy are incident on molecules, an electron in the molecule can be promoted to higher-energy molecular orbitals. These types of excitations are typical for the visible and/or ultraviolet range photon energies, producing electronically excited states. These excited states are energetically unstable thus, immediately lose their excess energy through a variety of deactivation processes. The Perrin-Jablonski diagram is convenient for visualizing in a simple way the most typical processes that may happen after photon absorption (Figure 5).

Jablonski diagram illustrates the properties of excited states as well as their relaxation processes. Following the light absorption, the vibrational levels of some upper excited states will be populated with electron density. These electrons immediately relax to the lowest vibrational level of S_1 by vibrational relaxations within picosecond or less, and this process is called as the internal conversion. All the other photochemical processes (fluorescence, quenching etc.) are more likely to

happen from the lowest vibrational state of S_1. Actually, this is the basis of Kasha's rule[8], which states that considering an excited molecule all the photochemical reactions and luminescence emission will always originate from the ν=0 of S_1, since the relaxation rate to the lowest vibrational level of S_1 is the fastest deactivation process. Depending on the nature of the excited molecule, the excited electron at S_1 now may undergo either fluorescence by emitting photons, or intersystem crossing to the triplet state or it may just relax to the S_0 via releasing the excess energy by internal conversion, as explained above.

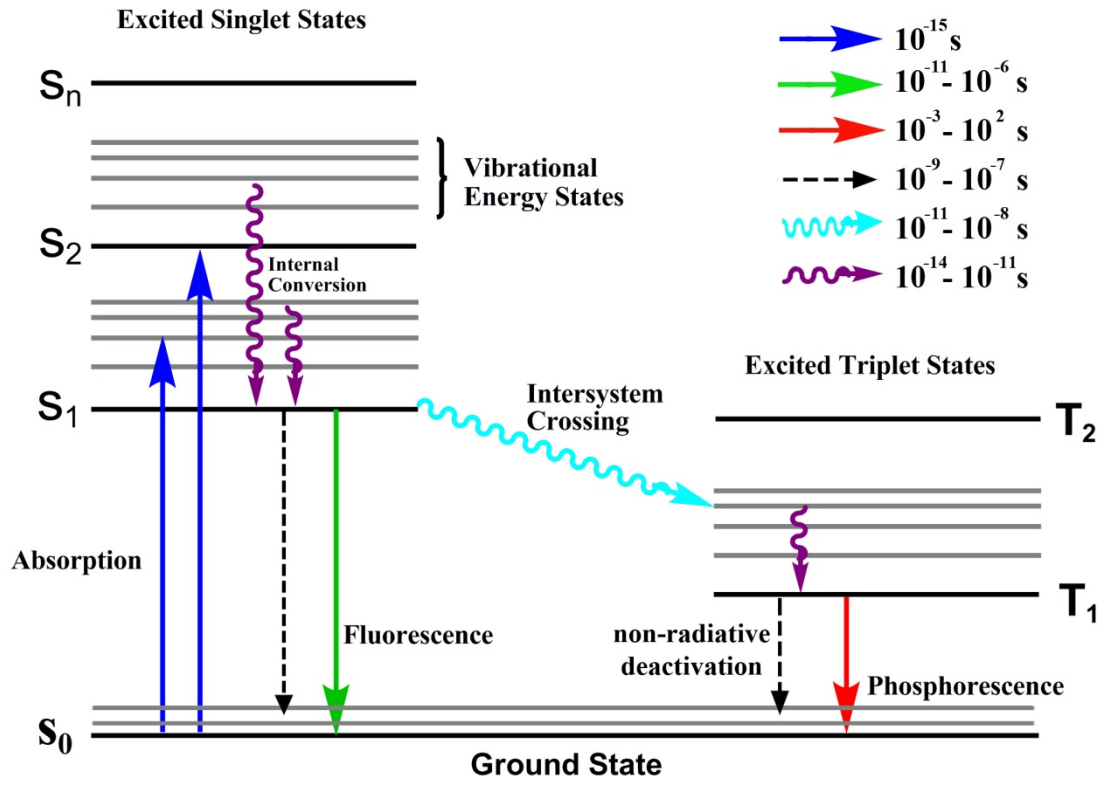

Figure 5. The Perrin-Jablonski diagram

Intersystem crossing to the triplet state T_1 is a forbidden transition in the idealized conditions, and will only happen if the electron in the S_1 state may undergo a spin conversion. There are few conditions that make such transitions favorable, such as presence of a heavy atom and/or exciton coupling within a molecule. Relaxation from T_1 is a radiative process and termed as the phosphorescence. As expected, it is a lower-energetic radiation, and because of the multiplicity of its state (T_1), the rate of

the radiative decay to the singlet S_0 state is much more slower compared to fluorescence. Details including timescales of these processes are depicted in the figure 5, shown above.

Fluorescence is a spin-allowed radiative relaxation due to the same multiplicity of the excited (S_1) and the ground states (S_0). Therefore, it occurs on relatively short timescales, presumably, within the range of picoseconds to microseconds. As can be seen in the Jablonski diagram, emitted light always has a longer wavelength (less energetic) than the absorbed light due to limited energy loss by the molecule prior to emission. The difference (usually in frequency units) between the spectral positions of band maxima of the absorption and luminescence is called Stokes' shift (Figure 6).[9] The main cause of Stokes' shift is the rapid non-radiative decay to the lowest vibrational level of S_1. In addition to this effect, fluorescent molecules can display further Stokes' shift due to solvent effects, excited-state reactions, complex formation and energy transfer.[10]

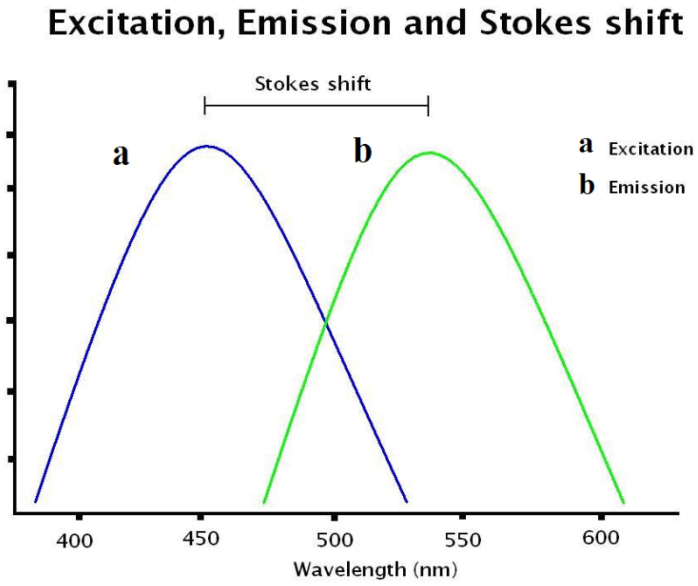

Figure 6. Stokes' shift

For a fluorescent molecule, the fluorescence quantum yield **Φ** and the lifetime **τ** are two essential photophysical parameters. The former is the ratio of the number of photons emitted by S_1 to the number of photons absorbed by S_0, which can be

determined by the below equation where k_f and k_{nr} are the rates of radiative and nonradiative transitions, respectively. The higher the quantum yield, the higher the fluorescence intensity is. Moreover, the fluorescence quantum yield of a molecule may also be determined by comparing the area under its fluorescence spectrum with that of a reference compound whose quantum yield is known.[11]

$$\Phi = k_f / k_f + k_{nr}$$

The average time the molecule remains in its excite state is called the average lifetime of the excited states $< \tau >$ and it is numerically equivalent to the fluorescence lifetime which is determined by the time-resolved measurements. Fluorescence lifetime is a kinetic parameter which is inversely proportional to the sum of the rate constants and is represented by the equation below.[12]

$$\tau = 1 / k_f + k_{nr}$$

2.2. Fluorescent Dyes

A common feature of almost all traditional dyes is that they absorb particular wavelengths of visible light, leaving the remaining wavelengths to be reflected and seen as color by the observer. For example, a traditional yellow dye absorbs violet light and thus appears yellow. The energy coming from the absorbed light is stored in the electron structure of the dye molecule and given off in the form of heat. The unique feature of a fluorescent dye is that they not only absorb light in the traditional sense, but this resulting energy is then dissipated in the form of emission of light.

Organic dyes that emit ultraviolet (UV), visible (Vis), and near infrared (IR) regions are of great interest, and have wide application fields. Especially, the advantage of low price, safety and accuracy make them very promising, considering the applications in biotechnology and medical diagnostics.[13,14] The most common dyes whose emissions span the UV to IR spectrum are shown in Figure 7 (next page).

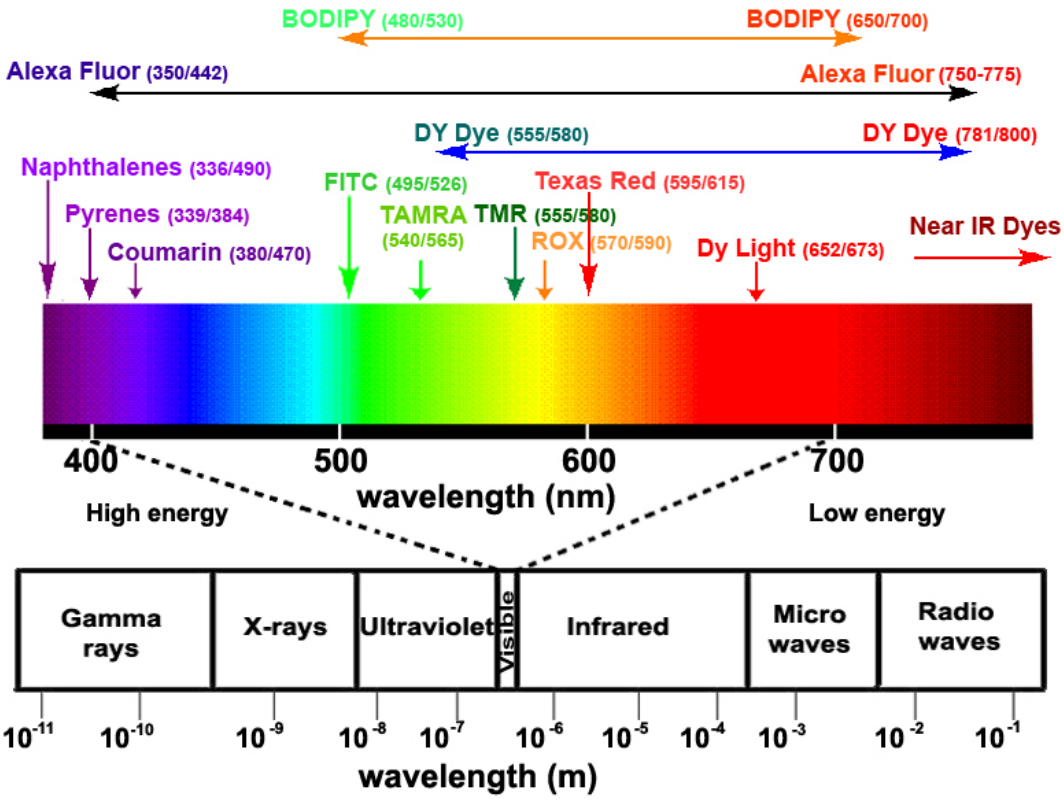

Figure 7. Distribution of dye families in the visible region

In the above figure, absorbance and emission maxima along with spectral regions covered by a particular dye family are highlighted. Tetramethyl rhodamine (TMR), carboxytetramethyl rhodamine (TAMRA), and carboxy-X-rhodamine (ROX) are all rhodamine based dyes. The UV dyes are typically pyrene, naphthalene, coumarin based structures, while the visible and near IR dyes include fluorescein, rhodamine, bodipy, and cyanine based derivatives (Figure 7). These dyes differ from each other in many aspects such as their structures, spectroscopic properties and chemical reactivities. Diversity of photochemical properties makes it easy to select a specific dye for a particular purpose.[15] Moreover, having rich chemistry (in terms of chemical modifications) is another important property of a fluorescent dye, which should be considered carefully prior to choosing it for a specific application.

Members of some dye families, such as cyanines (Cy), are closely related in structures, whereas others, such as the AlexaFluor compounds, are quite diverse. All dye families have both advantages and disadvantages depending on the intended

application. For example, fluorescein which is one of the most common used fluorophore in bio-labeling[16] is popular because of its high quantum yield, relatively high molar extinction coefficient, good water solubility, and ease of bioconjugation. On the other hand, it has a high rate of photobleaching[17], is pH sensitive[18], and can self-quench at high degrees of substitution.[19] Another important family of dyes are BODIPY based ones and will be discussed in detailed in the separate section (2.7).

As stated above, it is the emitted light that makes fluorescent dyes (fluorophores) unique when compared to traditional absorbing molecules. Depending on the substituents on it, emission intensity of a fluorophore may vary. This gives us the opportunity to design the fluorophore rationally and control the emission intensity efficiently. On-off type fluorescence control, in which the increase or decrease of fluorescence intensity at a single emission wavelength is observed, is the most frequently encountered example. This and other types of modulation mechanisms are the heart of fluorescent chemosensor design and will be covered briefly just after discussing the 'molecular sensor' phenomena.

2.3. Molecular Sensors

A molecular sensor or a chemosensor is a molecule that can report the presence of an analyte by some physical means. A sensor should ideally be selective for a particular guest molecule and it should allow the observer to monitor that analyte's concentration as well as reporting the presence of it. This is important for medical diagnostics and monitoring environmental pollution.[20]

There are numerous analytical methods that are available for the detection of various analytes, however they are expensive and often require samples of large amount. Thus, the molecular sensors gain primary importance in this area. Molecular sensors can be split into two major categories; these are electrochemical sensors and optical sensors. Electrochemical sensors can be obtained with the attachment of a redox active unit to the receptor moiety. A change in the redox properties of the receptor can be detected by an electrochemical technique such as cyclic voltametry (CV).

Optical sensors, on the other hand, constitute light based investigation methods. The most common type of it is fluorescent chemosensors which carry information regarding the analyte on the emitted light. Other methods follow the response via the changes measured in the absorbance of a sample and can be referred to as the colorimetric sensors. High sensitivity, high speed, and safety parameters make the fluorescence detection very advantageous over other optical methods. The principal advantage of a fluorescent chemosensor over a colorimetric sensor is its high sensibility. This is so because the emitted fluorescence signal is proportional to the analyte concentration whereas in absorbance measurements, the analyte concentration is proportional to the absorbance, which is related to the ratio between intensities measured before and after the beam passes through the sample. Thus, in fluorescence, an increase of the intensity of the incident beam results in a larger fluorescence signal whereas this is not so for absorbance. In other words, while fluorescent techniques can measure analyte concentrations at picomolar levels, absorbance measurements can detect concentrations only as low as micromolar scale. As a result, using fluorescence, one can monitor very rapid changes in concentrations even at very low ranges. They are, therefore, very sensitive and suitable for use in biological systems. The point of safety refers to the fact that samples are not affected or damaged during the measurements, and no hazardous by products are generated.

A recent example is provided by a sensor for saxitoxin developed in the Gawley research group shown in figure 8.[21] They reported an azabodipy derivative (**1**) containing either 18- or 27-membered crown ether rings as a synthetic sensor which is evaluated in the detection of paralytic shellfish toxin saxitoxin. According to the design, compound 1 is nonfluorescent molecule and upon complexation with the toxin its fluorescence property changes considerably, that is, a 3-fold enhancement is observed on the fluorescence spectrum. This is the way how they obtained a sensory response for the mentioned analyte. They also got some interesting results while comparing the crown ether sizes on the molecule in terms of binding constants. This and more detailed results are briefly speculated within the cited article.

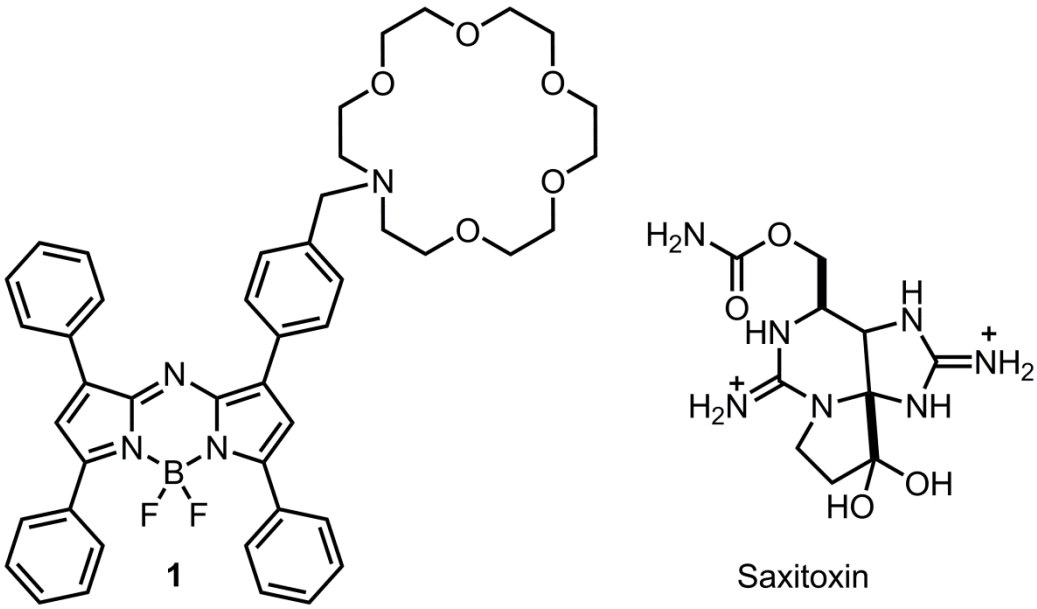

Figure 8. Molecular structure of Saxitoxin and probe compound **1**

Fluorescent chemosensors have become an important research field during the past two decades. Despite the many number of studies that were reviewed extensively in the literature, finding new strategies and mechanisms in the design of fluorescent chemosensors is of continuing interest. In the following section, fluorescent chemosensors and conventional sensing mechanisms will be discussed briefly.

2.4. Fluorescent Chemosensors

The fluorescent detection of the specific molecules and ions which are crucial in living systems has aroused attention, since it is highly sensitive, cheap and easily processed method. Therefore, fluorescent chemosensors has a significant value for their simplicity and high sensitivity. The recognition and signaling moieties are the most important parts in the design of a chemosensor. In the case of fluorescent chemosensors, the signaling part is fluorophore itself and the receptor unit (synthetic or biological) recognizing the specific guest molecule will be covalently attached to it. The importance of the receptor arises from its impact on binding and selectivity.[22] This means that, a receptor should have a strong and selective affinity towards the

target analyte. The fluorophore is a signal transformer that transforms the information into an optical signal. Binding of an analyte to the receptor part may lead to the significant changes in the photophysical properties of a fluorophore. These changes can be monitored and processed in the right way to determine the presence and the concentration of a given analyte. Design of the chemosensor determines what kind of alterations in the fluorescence signal can be observed after complexing with the targeted analyte. It could be in the form of amplification or quenching of the fluorescence signal, as well as the particular shift in the emission wavelength.[23] These fluorescent probes are either constructed as fluorophore-spacer-receptor or as integrated fluorescent probes (Figure 9). In the former case, there is a spacer in between receptor and signaling moieties that prevents the conjugation, whereas in the latter case these units are conjugatively attached to each other such that the receptor is part of the π-electron system of the fluorophore.[24]

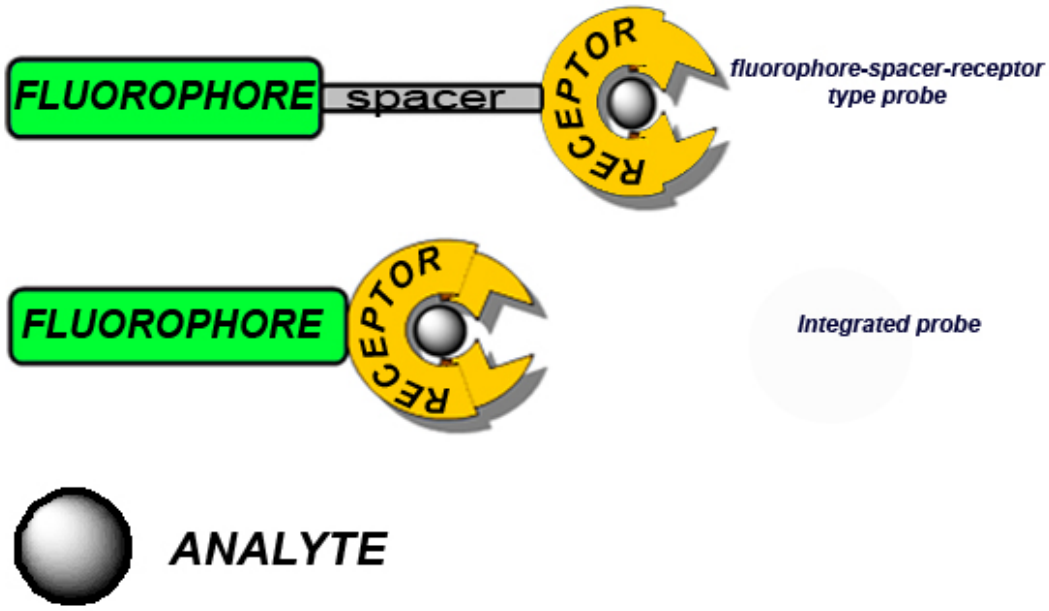

Figure 9. Schematic representations for the types of fluoroionophores

2.4.1. Photoinduced Electron Transfer (PET)

Luminescent sensors provide an easy, sensitive, and often visual method for detection of a wide range of analytes such as cations, anions or neutral molecules. In certain cases, before relaxation occurs, excited molecule either can transfer an electron from some potential donor to fill its low-lying empty orbital or it may transfer an electron to another system which is usually called a quencher. In other words, the light absorbing molecule, termed as luminophore, after excitation may accept an electron into the vacancy in the ground state or it may donate an electron from its excited state. This process has been studied well due to its major role in photosynthesis[25] and since the electron is transferred after the absorption of light, the process is called photo-induced electron transfer (PET). If both of the components, luminophore and receptor where receptor is the other component that accepts/donates an electron from/to the luminophore, exist in the same molecule and linked by a non-conjugated bridge, then this molecular sensor can be called as the PET-type chemosensor.

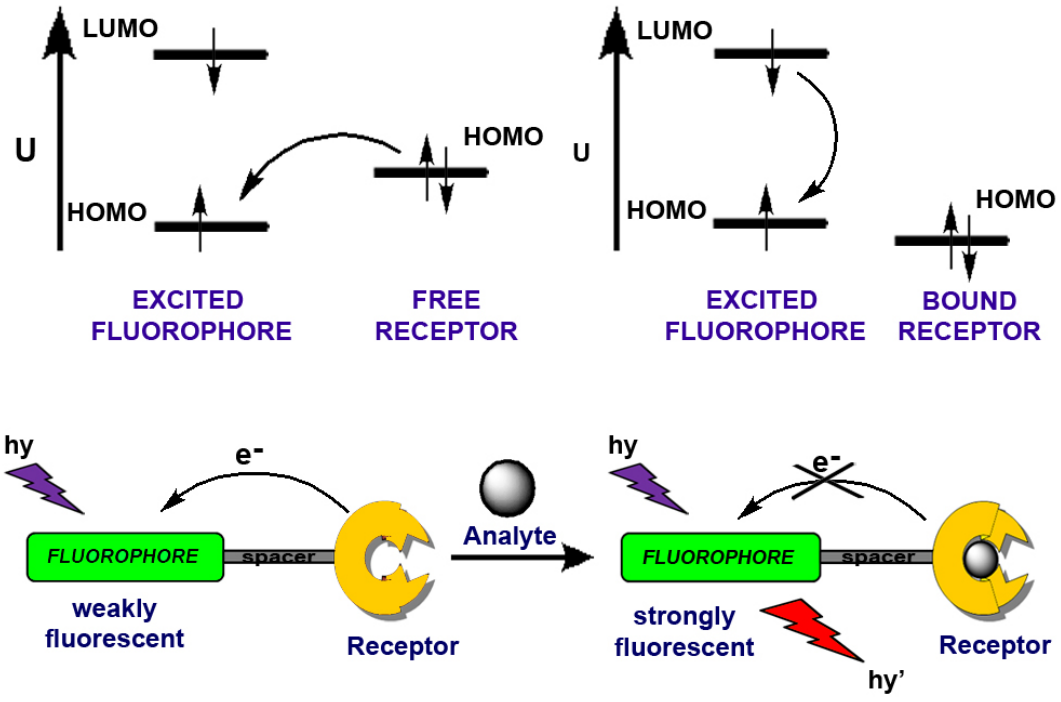

Figure 10. PET mechanism

Figure 10 illustrates the active and prohibited PET mechanisms in terms of frontier molecular orbitals. As it can be seen from the above figure, a model PET-type chemosensor is composed of three components which are luminophore, spacer and receptor units. Nature of the receptor unit determines the type of the response that luminophore will give upon analyte binding. In the above illustration the receptor unit is drawn as the electron donating component and in this particular case PET process is active via the electron transfer from HOMO of the receptor moiety to the semivacant ground state orbital of the luminophore which blocks the usual relaxation pathway of excited luminophore and quenches emission. This can also be termed as reductive photo-induced electron transfer. If the donor orbital on the receptor moiety that gives electron to the excited fluorophore can be controlled or somehow stabilized, to make PET thermodynamically less favored, an off-on type control over the fluorescence emission will be achieved. In other words, weakly luminescent sensor molecule will become strongly fluorescent when bonded to the targeted analyte. Accordingly, probes that exhibit this type of PET mechanism (reductive PET) are used widely in chemosensor designs.[26,27,28,29]

Selectivity for analytes is achieved by the correct choice of recognition moiety for the desired ions and/or molecules. For this purpose, diverse range of molecular receptors has been synthesized by organic chemists. For example, in order to recognize the alkali metal cations, crown ethers are employed as useful receptors. Depending on the size of the crown ether it is going to bind to one of the cations selectively. Moreover, structural modifications on heteroatoms or some minor functionalizations within the crown structure could yield novel receptor molecules selective to different heavy metal cations.

A very simple and classical example is compound **2**[30] (Figure 11), which contains anthracene molecule as a fluorophore and an aza-crown receptor attached to it by the CH_2 bridge. However, the recognition moiety is not necessary to be crown ether. There are also examples of cryptand- (**3**),[31] podand- (**4**),[32] dipicolylamine-,[33] and calixarene-[34] based PET sensors as selective for sodium, magnesium, potassium, calcium, and various transition metal ions. In these sensors photoinduced electron

transfer quenches the luminescence in the absence of the analyte. Binding of the desired cation inhibits the PET and switches on the emission.

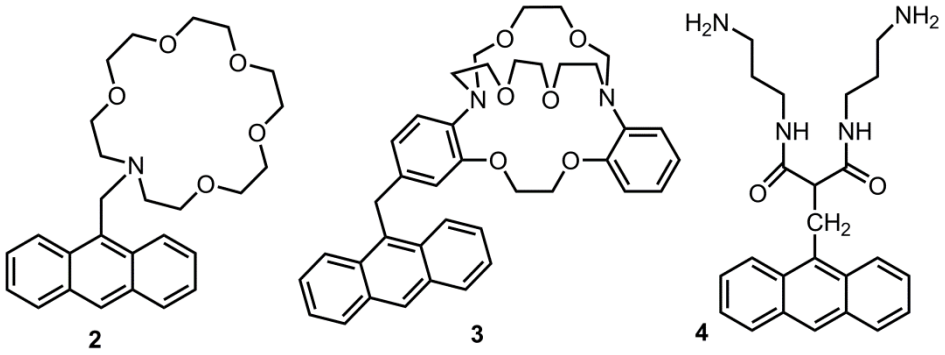

Figure 11. Some examples of PET based fluorescent chemosensors

A molecule in the excited state, when compared to its corresponding ground state, not only is a better electron acceptor because of the created electron vacancy in the HOMO, it is also a better electron donor because of the promoted electron to a higher energy level. In the previous paragraphs, working principle of a PET type chemosensor that contains electron accepting fluorophore is briefly discussed. What if the receptor unit were to accept electron upon excitation? (Next page)

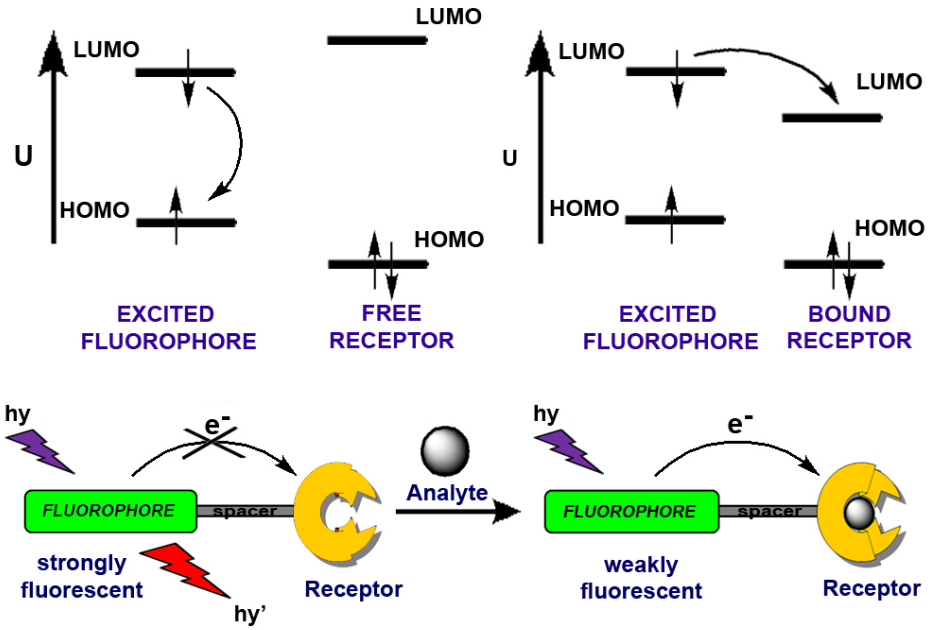

Figure 12. Oxidative PET mechanism

This of course depends on the redox potentials of both the fluorophore and receptor units and the process in turn, can be referred to as the oxidative PET. Figure 12 illustrates the possible mechanism of the process in terms of the molecular orbitals involved. Contrary to the previous case, this time unbound form of the chemosensor exhibits strong luminescence, while the fluorescence of the bound species is quenched because of the active oxidative PET process. This is called an on-off system, since the emission intensity decreases significantly by the presence of an analyte.

Compound **5**[35] is a clear example exhibiting this mechanism. In that particular case depicted in figure 13, Bodipy dye was chosen as a fluorophore and 2,2-bipyridine for the receptor part. While the fluorophore has bright-green fluorescence in the absence of zinc cation, complexation with the mentioned ion quenches the fluorescence via oxidative PET mechanism.

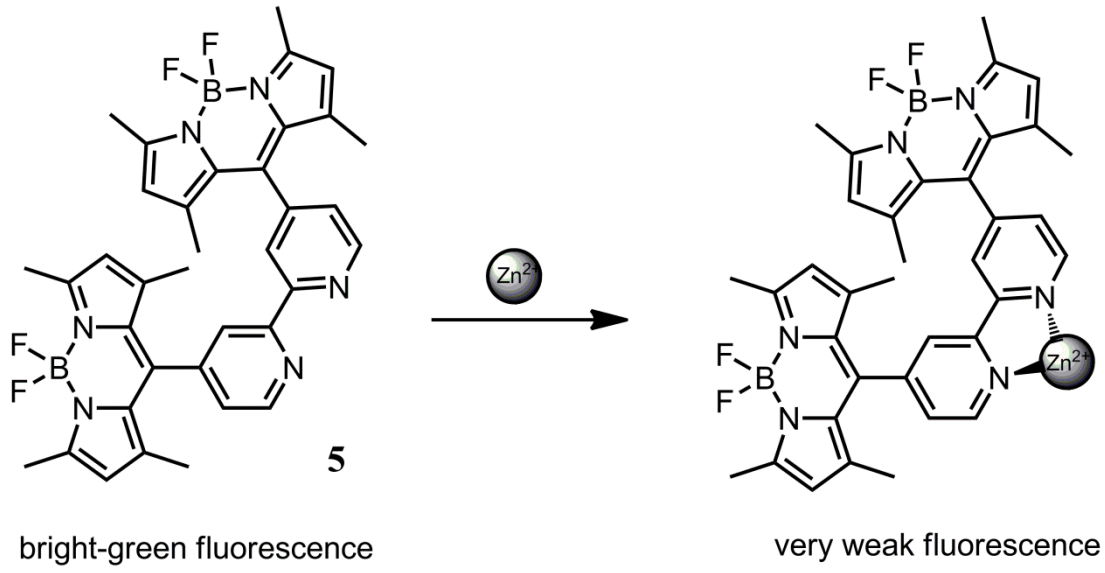

Figure 13. Coordination of zinc triggers the oxidative PET mechanism

Another study is a thiol sensor reported by Nagano, which again utilizes Bodipy derivative as the fluorophore and maleimide moiety as the receptor part (Figure 14).[36] This example displays very interesting results when compared with the previous example (Figure 13). Although the reported sensor here exhibits oxidative PET mechanism, in the paper they call it as donor-excited PET, the probe is strongly

quenched before the maleimide part reacts with thiol. After the raction, the oxidative PET mechanism is blocked and the bright fluorescence of the Bodipy is restored back. Proposed schematic representation of the oxidative PET from excited Bodipy to maleimide in terms of molecular orbitals is also illustrated in figure 14. They have also synthesized meta- and para-maleimide bound structures to study the distance effect (between fluorophore and receptor) on the PET efficiency. More details are discussed briefly within the cited article.

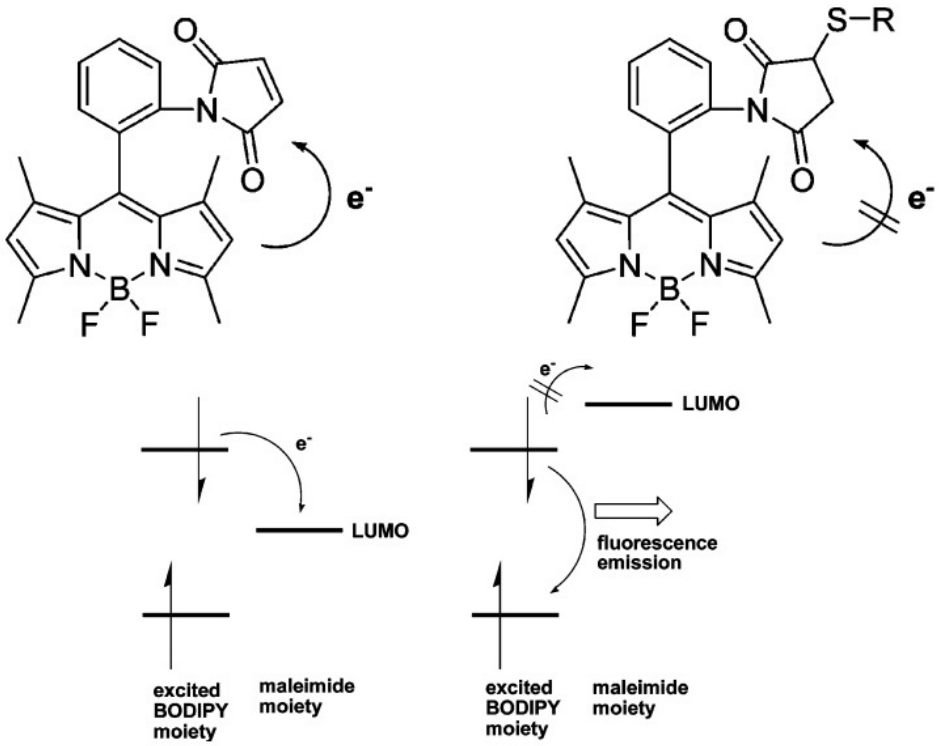

Figure 14. Reverse PeT (d-PeT) mechanism

In this section, principles of photo-induced electron transfer (PET) and its utilization in the development of molecular sensors have been discussed. Proposed mechanisms of PET process were illustrated schematically within the above figures. Literature examples for the PET type chemosensors were examined in terms of how blocking or activating this process will provide information on the nature of the analyte. No doubt that, among other conventional sensing mechanisms, PET, has been the most widely applied mechanism employed in the design of fluorescent chemosensors.

2.4.2. Intramolecular charge transfer (ICT)

Intramolecular charge transfer is another type of signaling mechanism that generally lead to a red or blue shift in the emission spectrum of a fluorophore upon enhancement and/or suppression of this process. Contrary to PET-type chemosensors, there is no spacer unit between fluorophore and receptor units in ICT-based probes. The receptor unit is part the of π-electron system of the fluorophore such that one terminal is likely to be electron rich (electron donor) whereas the other one is electron poor (electron acceptor).

When such a fluorophore-receptor system is excited with photons, a redistribution of electron density occurs and thus a dipole is created. This triggers an internal charge transfer (ICT) from donor to acceptor. Analyte binding leads to a positive or negative interaction with the excited state dipole, which results in significant changes in the both emission and absorption spectra.[37]

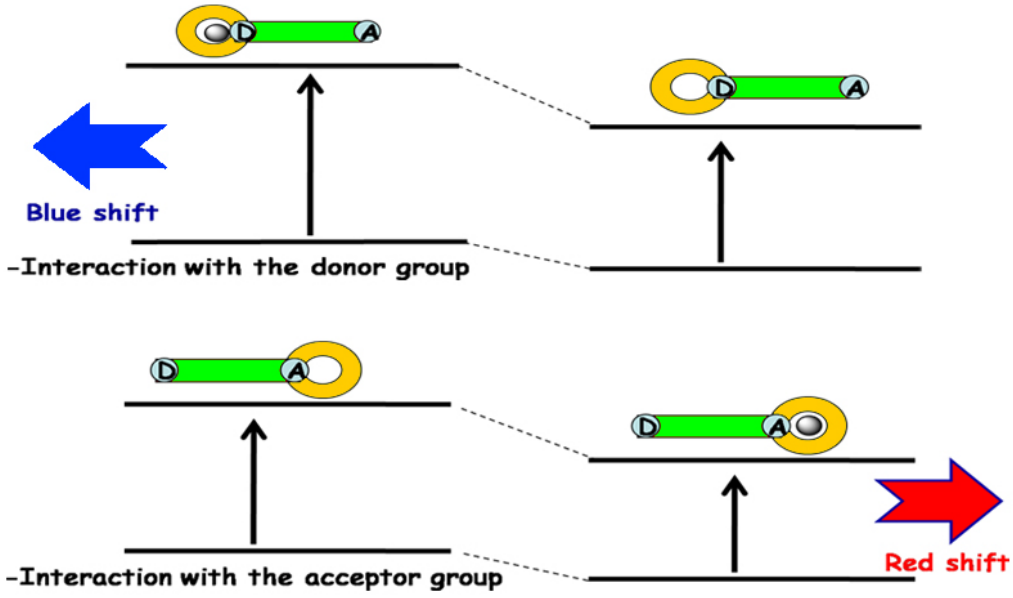

Figure 15. Spectral displacements of PCT type sensors

If the receptor unit contains an electron donating group (such as amino group) conjugated to the fluorophore, its interaction with a cation will decrease the electron donating capability of that group. In other words, this type of interaction leads to a

reduction of conjugation and a blue shift is monitored in the absorption spectrum. However, if the cation is in close interaction with the acceptor group (such as carbonyl group), this improves the electron withdrawing character of that group, resulting in the stabilization of the system and red shift in the absorption spectrum.[38]

Photophysical changes occurring upon cation binding can also be explained by charge dipole interactions.[39] The electron donating group will be positively charged in the excited state and its interaction with the cation will destabilize the excited state more than the ground state. Hence, this increase in the energy gap between ground and excited states will cause a blue shift in the both absorption and emission spectra. Conversely, if the receptor unit contains an electron accepting group (such as carbonyl group) conjugated to the fluorophore, its interaction with a cation will stabilize the excited state more than the ground state. As a result, the energy gap between the ground state and the excited state will decrease and red-shift will be monitored in the both absorption and emission spectra (Figure 15).

Many fluoroionophores have been designed according to this (ICT) mechanism so far. Compounds **6**[40] and **7**[41] (Figure 16) exhibit blue shift in both absorption and emission spectra upon cation binding.

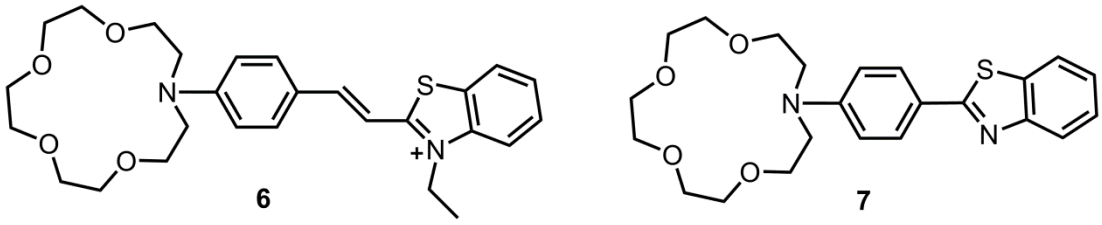

Figure 16. Crown containing PCT sensors

Depending on the receptor moiety, similar compounds can display different spectral shifts upon the binding of the same analyte. For example, two bodipy dyes showing similar spectral properties (Figure 17) exhibit opposite spectral shifts upon protonation.[42] One of the dyes includes electron donating aniline moiety whereas the other contains electron accepting pyridine unit as receptor parts. Consequently, those

two compounds demonstrate spectral shifts in the opposite directions in their proton bound form, due to the reasons explained above.

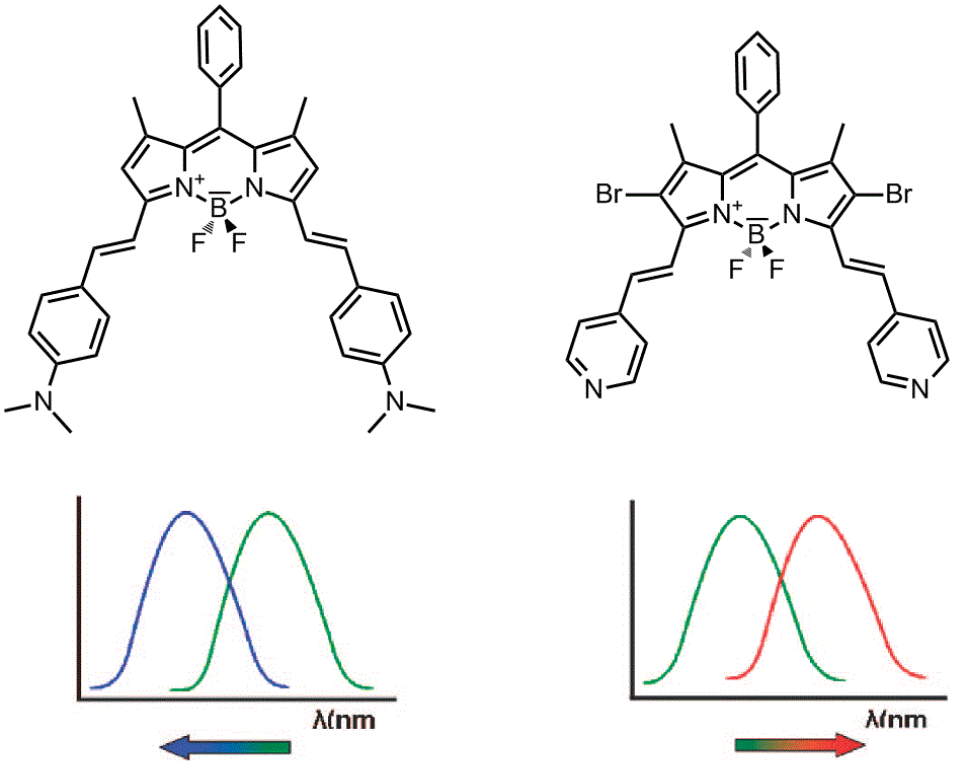

Figure 17. Bidirectional switching of the dyes related to ICT donor and acceptor characteristics

Conjugated compounds containing both electron donor (D) and electron withdrawing (A) groups that exhibit intramolecular charge transfer (ICT) through the π-conjugated bridge are also termed as the 'Push-Pull' systems (D-π-A systems). Apart from the chemosensing and analyte monitoring applications described above, this kind of systems has also found wide range of optical-electrical applications, such as organic light emitting devices,[43,44] nonlinear optical devices,[45] and solar cell materials.[46,47]

2.4.3. Energy Transfer (ET)

Energy transfer is another signaling event, which can be classified as electronic energy transfer (EET) and/or fluorescence resonance energy transfer (FRET) depending on the interaction distance between energy donor and energy acceptor units within a multichromophoric dye systems. It is the process where the energy of donor chromophore (D), which absorbs light at relatively short wavelength, is transferred to acceptor dye (A) that fluoresces at longer wavelength (as long as it is not a 'quencher' type dye molecule). In other words, energy of the donor (D) at its excited state is used to excite the acceptor through energy transfer.

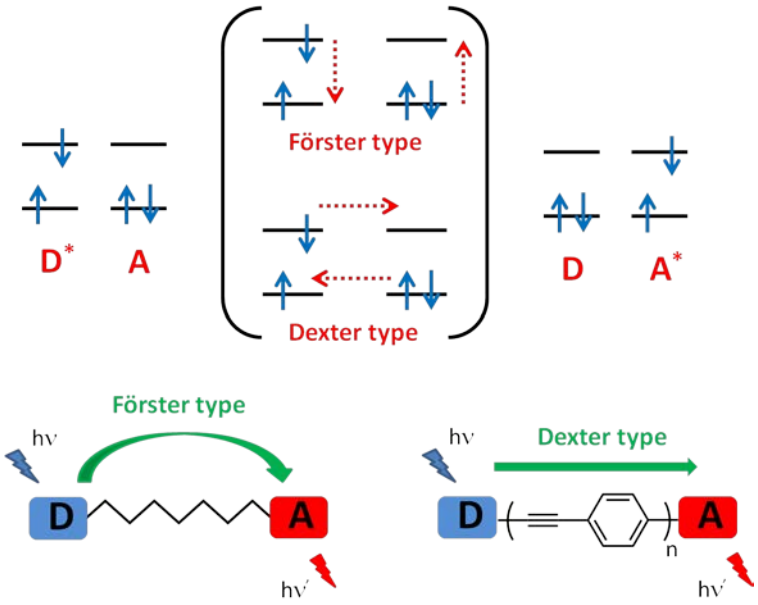

Figure 18. Förster type (through space) and Dexter type (through bond) ET

As it is stated above, it is the interaction distance between donor and acceptor units that determine the type of energy transfer mechanism occurring efficiently. EET, which is also called as Dexter electron transfer, is taking place if the distance mentioned above remains within 10Å range. On the other hand, for an efficient FRET to occur the distance between donor and acceptor should be from 10 to 100 Å. However, this is not the only requirement for efficient FRET, there should be a certain degree of overlap between the emission spectrum of donor and the absorption spectrum of acceptor moieties (Figure 18).

These two types of energy transfer mechanisms, also known as Dexter and Förster type, will be covered briefly in the following subsections.

Energy transfer characterizations can be done following various parameters such as relative lifetimes, quantum yields, and decrease in the donor emission and increase in the acceptor emission intensities. It is also influenced from the rate of deactivation pathways from the excited system and therefore, chromophores must be appropriate to compete with those pathways.[48] Besides, excited state lifetime of donor has to be longer than the time required for energy transfer.

2.4.3.1. Förster type Energy Transfer

Fluorescent labels that emit light at wavelengths distant from that of the source used to excite them have many applications in biotechnology. Generally, a simple florescent organic dye molecule has a very small Stokes' shift. When the Stokes` shift of a single dye is insufficient for a particular application, bi(multi)chromophoric systems that exploit through-space energy transfer between two dyes are frequently used. Fluorescence resonance energy transfer (FRET) occuring here is also called Förster type Energy Transfer, and is a nonradiative process whereby an excited state donor (D) transfers energy to a spatially close ground state acceptor (A), and the fluorescence of the latter is observed (Figure 19).

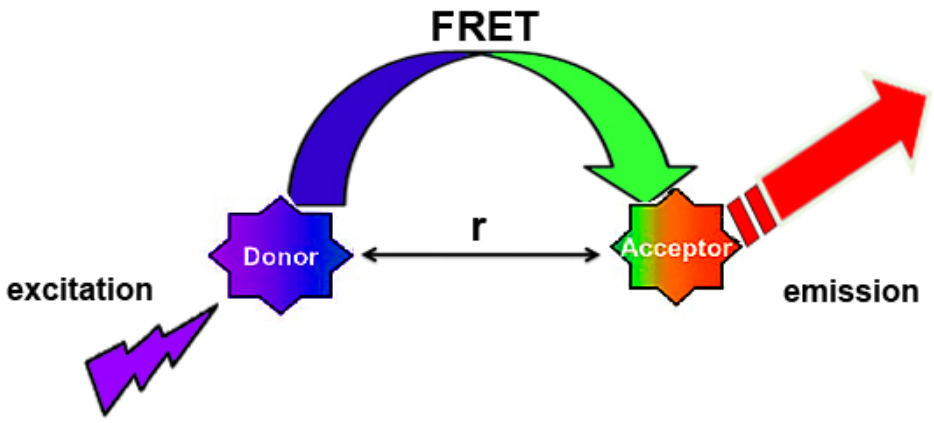

Figure 19. Schematic representation of the FRET process

In other words, an electron in HOMO of the acceptor is excited to its LUMO through the energy released during the relaxation of an electron in the LUMO of the donor to its HOMO. The energy absorbed by the acceptor unit matches the emission wavelength of the donor (spectral overlap).

As donor and acceptor moieties are usually connected via non-conjugated linker, FRET does not depend on the orbital interaction between these units (D an A). Thus, a large distance between donor and acceptor groups (10-100 Å) would still allow this type of energy transfer to occur. Spectral overlap between donor emission and acceptor absorption, the distance between donor and acceptor and relative orientations of their transition dipoles are significantly important parameters for an efficient FRET process.[49,50]

FRET efficiency can be determined using two different approaches; one is steady state approach and the other is time-resolved approach.[19] Decrease in quantum yield of donor is followed in the former case. In this method, self absorption, which refers to re-absorption of the emitted light by the same molecule, is an important problem that should be avoided. This problem might be solved by the use of very dilute solutions.[51] FRET efficiency with steady state approach can be formulated as follows:

$$\mathbf{E = 1 - (\Phi_{DA} / \Phi_{D})}$$

where $\mathbf{\Phi_{DA}}$ and $\mathbf{\Phi_{D}}$ are the quantum yields of donor molecule in the presence and the absence of acceptor, respectively. It can also be calculated with a different formula, which is based on the increase in the fluorescence of acceptor:

$$\mathbf{E = A_A (\lambda_D) / A_D (\lambda_D) * [I_{AD}(\lambda_A^{em}) / I_A(\lambda_A^{em}) - 1]}$$

where $\mathbf{A_A}$ and $\mathbf{A_D}$ refer to absorbance values of acceptor and donor at the maximum absorbance wavelength of donor. $\mathbf{I_{AD}}$ and $\mathbf{I_A}$ refer to integrated emission area of acceptor in the presence and absence of donor at $\mathbf{\lambda_A^{em}}$ respectively.

Time resolved approach enables a more accurate FRET efficiency calculation, which is determined using time-resolved emission data of donor and acceptor units. When the decay of emission is a single exponential, FRET efficiency can be formulated as follows:[19]

$$E = \tau_D * k_{FRET} / (1 + \tau_D * k_{FRET})$$

$$k_{FRET} = 1/\tau_{DA} - 1/\tau_D$$

where τ_D and τ_{DA} refer to excited state decay time (lifetime) of donor in the absence and presence of acceptor, respectively.

A very common example exhibiting Förster type energy transfer process is shown below (Figure 20). In this article Bodipy dyes were selected as the energy donor molecules, whereas perylene diimide as the acceptor unit. Four Bodipy molecules are covalently attached to a perylene core via 'click' reaction. The extinction coefficient of the final molecule at Bodipy's maximum absorption wavelength (526 nm) dramatically increases up to 250000 $M^{-1}cm^{-1}$ due to four Bodipy units in the structure. The emission of the core has enhanced, as expected, with the increasing number of terminal Bodipy donors. FRET efficiency is calculated as 99% with a critical Förster radius of 4.7 nm.[52]

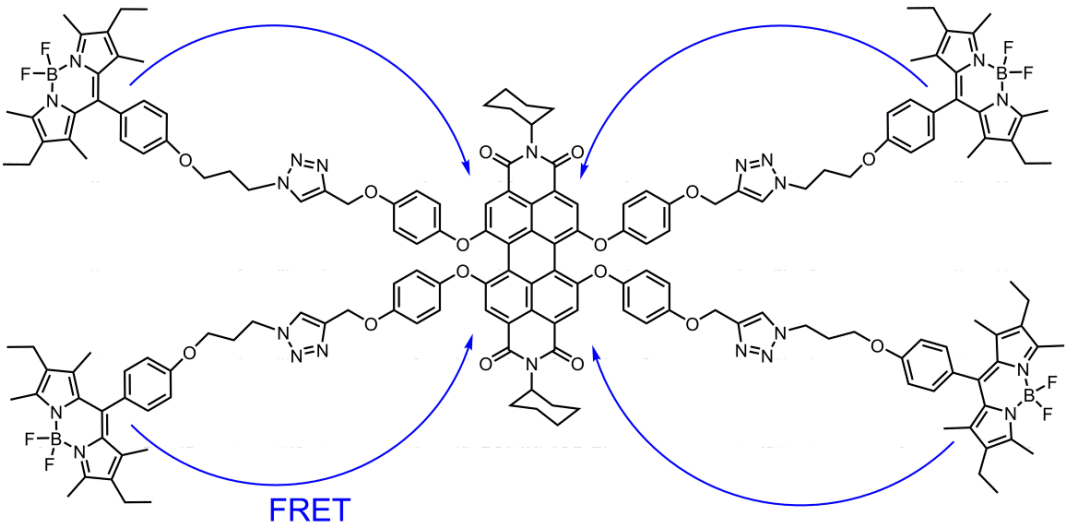

Figure 20. A Bodipy based Förster type energy transfer system

Within the past three decades, the use of Förster energy transfer has found applications in highly diverse fields, including light frequency conversion, cascade systems, artificial photosynthetic antenna, singlet oxygen generation and switching element in molecular machines.

2.4.3.2. Dexter type Energy Transfer

On the contrary to the Förster type, Dexter type energy transfer requires donor-acceptor orbital interaction which can be provided either directly or by the bridge.[53] It usually happens in the systems where donor and acceptor units are connected by a conjugated linker. That's why it is also called as 'through-bond' energy transfer. In this kind of energy transfer, an exchange of electrons occurs between both HOMOs and LUMOs of donor and acceptor (Figure 18). As it is highly dependent on the orbital overlap, which requires a short-range interaction (<10 Å), the rate constant of energy transfer decreases exponentially with distance:[54]

$$\mathbf{k_{ET} = K\ J\ exp(-2R_{DA} / L)}$$

where **K** represents orbital interaction, **J** is the overlap integral between donor emission and acceptor absorbance, $\mathbf{R_{DA}}$ is the donor acceptor separation and **L** is the Van der Waals radii.

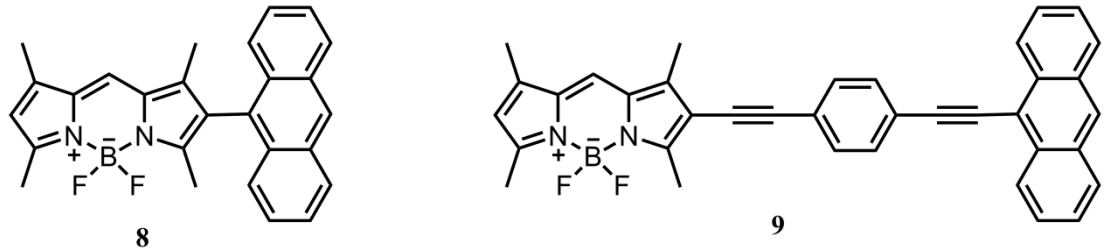

8 **9**

Figure 21. Through-bond energy transfer cassettes

Burgess et al synthesized a series of Anthracene-Bodipy cassettes in order to measure the rates of energy transfer when the orientation of donor and acceptor moieties are changed (Figure 21).[55]

When anthracene is excited a very fast energy transfer (~200 fs) is observed from anthracene to Bodipy in compound **9** that occurs as a result of parallel alignment of S_1 - S_0 transition dipole moments of donor and acceptor respectively. On the other hand, the anthracene and the BODIPY are directly attached in compound **8** and steric interactions prevent the planarity of the structure which makes it a true cassette.

Another example of Dexter type energy transfer is illustrated in Figure 22.[56] Such ligand-metal based systems provide unidirectional energy transfer in a linear array of system that would be used in molecular wires. In this example, an efficient energy transfer occurs from Ru and Os complexes to anthracene.

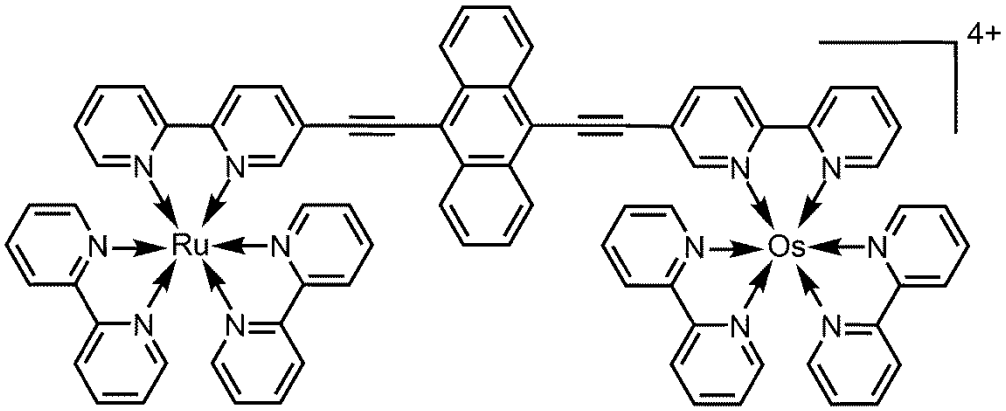

Figure 22. Ligand-metal based Dexter type energy transfer system

In the above section, fluorescent chemosensors and conventional signaling mechanisms (PET, ITC, and FRET) were discussed briefly. They constitute the important part of this thesis. Enthusiastic readers can further find different types of sensing mechanisms and examples in recent reviews and cited articles therein.[57,58,59,60] Although there are sufficiently many reported studies (regarding aforementioned topic), exploration of new sensing mechanisms is still a highly challenging part in the design and development of new fluorescent chemosensors.

2.5. Cation Recognition

Cations play many roles in biological processes. They trigger muscle contraction and are involved in the transmission of nerve impulses. They are also present at the active sites of many enzymes playing catalytic roles in the biological environment. In some cases their absence or overdoses are known to have some direct and/or indirect effects on specific diseases. For example, it is important to control the serum levels of lithium in patients under treatment for manic depression, and potassium in the case of high blood pressure. Besides, Zinc and Aluminum cations known to have some possible implications in Alzheimer`s disease.

In addition to this, heavy and transitional metals (TM) play important roles in the areas of biological, environmental and chemical systems. Therefore monitoring their activities and concentrations is of great importance for scientists, concerning the toxicity and pollutant effects of these cations such as Pb(II), Cd(II), Hg(II), etc. and the early detection in the environment is desirable. Thus, there have been great efforts exerted on the development of new and selective recognition sites or receptors for cationic guests. Though, it's still a greater challenge to design a receptor unit that selectively binds to a targeted cation in the presence of other competitive ions.

Selectivity for the targeted cation is achieved by the correct choice of recognition moiety. For this purpose, a very wide range of molecular receptors have been synthesized and reported by organic chemists. For example, in order to recognize the alkali or alkali earth metal cations, which are also known as hard cations, oxygen atom containing crown ethers are employed as useful receptors. Depending on the size of the crown ether it is going to bind to one of the cations selectively. Moreover, by playing with the heteroatoms or by making some minor modifications within the crown structure, novel receptor molecules selective to different heavy metal cations can be obtained too. According to the hard and soft acids and bases theory,[61] mercuric cation, which is a soft acid, should bind to soft bases. Therefore, in order to increase the selectivity and binding constant, most of the Hg^{2+} receptors contain sulphur (S) which is a soft atom.

Some examples from the literature are given in figure 23. Compound **10**,[62] developed by Shiguo Sun et al., is a non-fluorescent dye with a very low quantum yield (Φ=0.008), which is indicative of efficient photo-induced electron transfer (PET) mechanism occurring. The dye molecule chosen here is a Bodipy fluorophore and the phenyl group between the receptor and the dye molecule is a non-conjugated linker. Because of the steric effect caused by the methyl groups at 1 and 7 positions, phenyl ring remains orthogonal to the Bodipy skeleton. When Hg^{2+} is added on it in water/ethanol system (7/3, v/v), a 160 fold increase is observed in the fluorescence intensity. This is due to the coordination of mentioned cation with heteroatoms of the receptor unit, followed by blocking of the PET process. They have also tested some other alkali and alkaline earth metal ions together with transition and heavy metal cations to test the selectivity of the proposed probe. Yet their probe showed excellent fluorescence selectivity only towards Hg^{2+} among all other cations. Most of the reported fluorescent PET sensors are highly pH dependent. However, this probe exhibits intense fluorescence only at pH<3, when it is higher the fluorescence intensity stay very low and does not vary, which means that its fluorescence emission is pH independent under a large physiological pH range. Thus it has potential applications for biological toxicities.

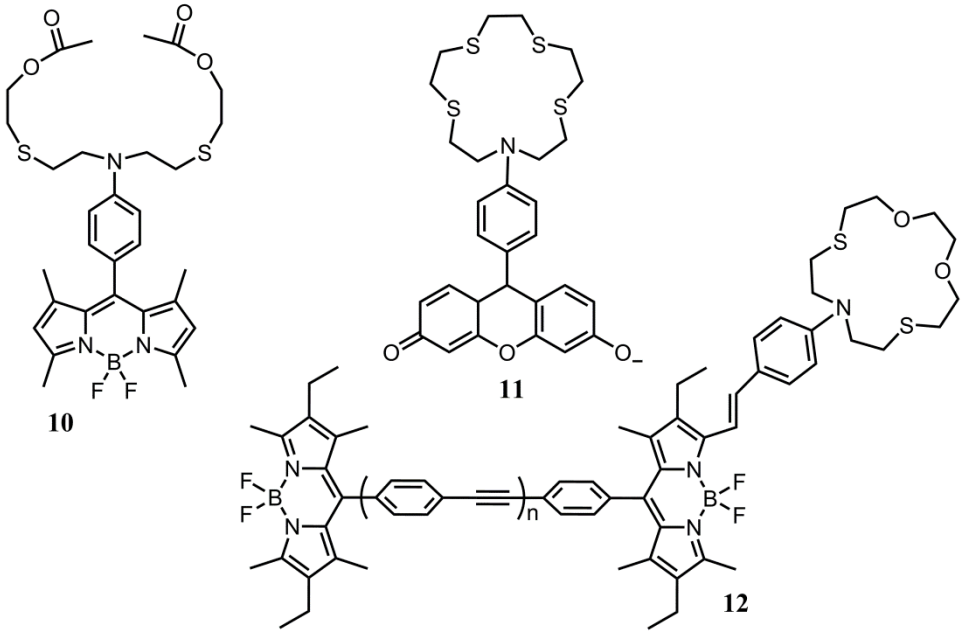

Figure 23. Hg^{2+} selective chemosensors

Chemosensor **11**[63] also behaves as a PET type chemosensor again for mercuric cation in aqueous media. In this case fluorescein dye is employed as the reporter unit. Although the receptor moiety displays quite good selectivity for Hg^{2+} over other cations, the probe shows only a small change in the emission spectrum for Cd (II) ions too.

Compound **12**[64] was developed by Akkaya et.al. In this work they have introduced a new strategy for the ratiometric chemosensor design such that the range of ratios can be significantly improved. If the chemosensor is designed as energy transfer dyad, and once the interchromophoric distance is carefully adjusted, binding of the analyte increases the spectral overlap between the donor emission and the acceptor absorption peaks. Binding of mercuric cation to the receptor unit shows ICT type behavior. As a result of this, absorbance of the acceptor unit is blue-shifted while the emission of the donor part remains the same. This change increases the spectral overlap between donor and acceptor parts, resulting in the spectacular increase in the efficiency of the energy transfer. All the measurements were carried out in the organic solvents, however, with the attachment of water soluble groups to the final molecule this approach can easily be extended to the aqueous media.

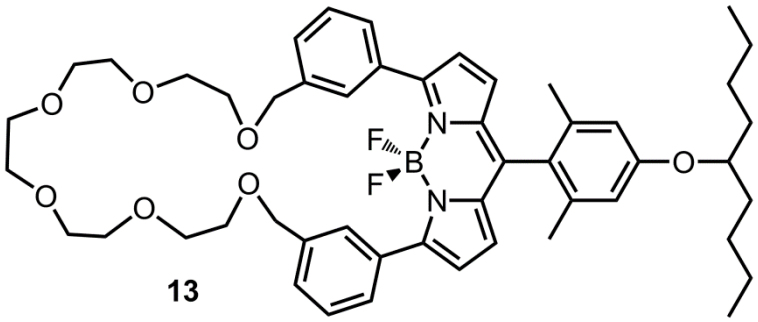

13

Figure 24. Sodium selective fluoroionophore

Compound **13**[65] is a highly selective chemosensor for Na(I) cation (Figure 24). Although there are many chemosensors designed for sodium ion and are already used in practice, this probe uses different sensing mechanism which is called conformational restriction approach besides PET and ICT mechanism. Cation binding causes significant red-shift in the emission and absorption spectra, which is

due to the restriction of phenyl units which are directly linked to Bodipy skeleton, and such extended conjugation causes red-shift in the spectrum.

Magnesium ion is one of the most abundant divalent cation in cells, which plays an important role in many cellular processes such as proliferation[66], cell death[67], DNA synthesis[68] and protein phosphorylation[64] as enzyme cofactors. Farruggia et al reported a PET-based fluorescent probe for the detection of magnesium in living cells (Figure 25).[69] Diaza-18-crown-6 is used for magnesium receptor and it showed negligible interference with Ca^{2+}. When complexed with the Mg^{2+} cation, fluorescence is increased through inhibition of the active PET mechanism.

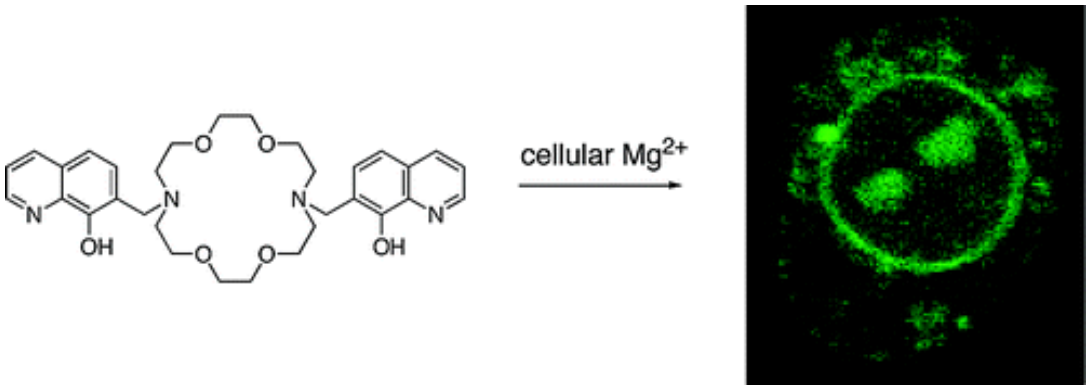

Figure 25. 8-Hydroxyquinoline derivatives with diaza-18-crown-6 for sensing magnesium ion in living cells[65]

Another important cation should be selectively monitored is Zinc(II) cation, which is quite important due to its effects on Alzeimer`s disease and human metabolism. Compound **14**[70] is a ratiometric chemosensor for Zn(II) cation. This novel two fluorophore approach gives opportunity for intracellular ratiometric sensing of Zn(II). Coumazin group which is attached to fluorescein through an ester linkage is hydrolyzed in the cell by esterase enzyme. After hydrolysis, Zn(II) sensitive fluorescein and insensitive coumazin fluorophore is created and Zn(II) concentration can be signaled from the fluorescein emission signal at 534 nm (Figure 26).

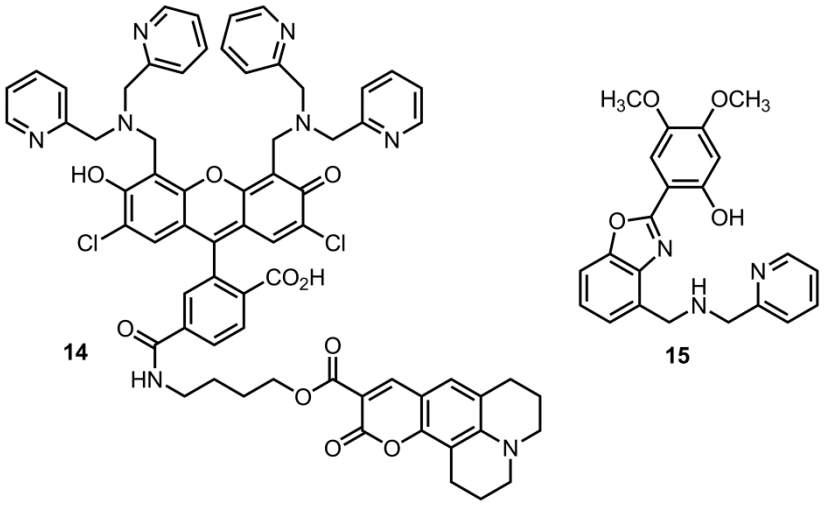

Figure 26. Selective fluorescent chemosensors for Zn(II) ions

O`Halloran et al. developed benzoxazole type fluorescent chemosensor **15**[71] which shows great selectivy towards Zn(II) cation in aqueous media. Emission ratio imaging experiments of **15** reveals changes in intracellular zinc availability.

Since there has been an increasing interest in monitoring Zn(II) cation due to its special biological relevance, many reporter units connected to various fluorophores have been reported in the literature. Yoon's *tutorial review*,[72] Lippard's *account* on zinc metalloneurochemistry,[73] and Yongshu's review[74] on DPA derived Zn(II) sensors are the some important articles, to name a few.

2.6. Anion Recognition

Like cations, anions also play a crusial role in a wide range of chemical and biological processes, and considerable effort has been dedicated to the development of receptors for anionic species. After Pedersen's first report on cation coordination of crown ether moieties in the late 1960s, coordination chemistry of alkali and alkali earth metal cations has attracted significant interest in 1970s and as a result it constitutes one of the well developed and mature branches of supramolecular chemistry. However, at the same time anion recognition received comparatively minor attention than cations, and it has only been three decades since the consistent

effort has been addressed to solve the problems regarding anion binding. Since then extensive studies were performed by different researchers which led to a remarkable scientific progress in this field.[75,76]

This was important because there are numerous reasons suggesting how crucial the improvement of this field is. First of all, anions are very common within biological systems, it should be noted that DNA itself is a polyanion and most of enzyme substrates and cofactors are also anionic species.[77] They are also involved in the areas of medicine and catalysis as well as the environmental pollution. As a result, it can be concluded that design of anion receptors for this kind of targets is particularly important and challenging. Contrary to analogous cations carrying the same charge, anions are significantly larger species with the lower charge to radius ratio which makes their electrostatic binding interactions less effective. Moreover, they are also highly sensitive to pH values of the environment and thus, the chosen receptors should function within the pH window of the target anion. Solvent effect is another important factor that should be considered carefully in the design of anion receptor. Because, solvation has a great influence on the controlling anion binding strength and selectivity. Especially hydroxyl group containing solvents may form strong hydrogen bondings with anions. Considering aqueous media, since hydrogens of water approach more closely to the anion than the oxygen of water to the cation, anions hydrate more strongly than cations. Therefore, a potential anion receptor should be able to effectively compete with the solvent environment in which the anion recognition event takes place. On the other hand, hydrophobicity can also influence the selectivity of a receptor. Obviously, hydrophobic anions are generally bound more strongly in hydrophobic binding sites.

Anslyn group reported several studies on the recognition of tricarboxylate anion and triphosphate polyanions utilizing trisguanidinium receptor species such as **16**[78] (Figure 27). This molecule contains three guanidinium groups and is therefore complementary to guests containing three carboxylate groups. Guests containing three anionic moieties, such as citrate, are bound more strongly than those with fewer

anionic parts (for example, acetate). This receptor has been used to produce a displacement-assay-type chemosensor for citrate anion.

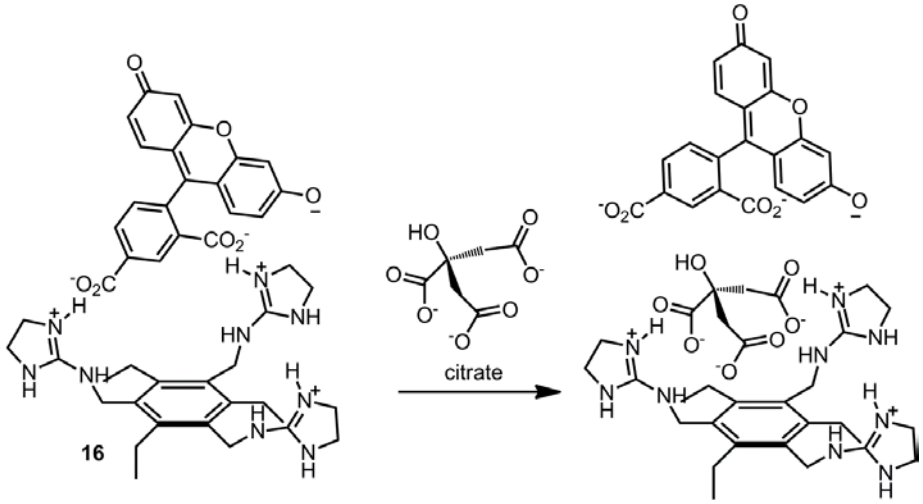

Figure 27. Displacement assay for citrate anion

5-Carboxyfluorescein is one of the common commercially available fluorescent probes and contains two carboxylate groups. Its fluorescence is highly dependent on the pH values of the environment. The two carboxylate groups present in fluorescein are used to coordinate to cationic receptor. When tricarboxylate citrate is added to the mixture of guanidinium and carboxyfluorescein that was initially prepared, the citrate ion displaces the carboxyfluorescein. The fluorescent properties of substrate changes considerably on its release from the complex, and in this way sensory response to the addition of citrate is obtained.

The development of molecular recognition systems that can detect and sense biologically relevant anions are of great interest. Especially chemosensors that can work under aqueous conditions and physiological pH are valuable for detecting substances of biological significance, since they are soluble only in aqueous solutions. Nucleosides and nucleotides are very important biomarkers because they form the fundamental units of all the life forms.[79] Therefore, monitoring their activities is of great significance for scientists. Among all the nucleotides, the recognition of adenosine-triphosphate (ATP) is of growing interest, because of its vital roles in the metabolic processes.[80]

Recently Amitava et al reported a new chromogenic complex **17**-Zn, which can be used to bind ATP in aqueous solutions at physiological pH.[81] The zinc dipicolylamine moiety in **17**-Zn acts as the receptor fragment for ATP, whereas the dimethylamino- phenylazo group acts as the signaling group for reporting the binding, inducing a visibly detectable color change. On addition of an aqueous solution of ATP, the absorption maximum was shifted to 484 nm. An associated color change from pale yellow to light pink was observed (Figure 28). No change in the absorption spectra was observed on addition of AMP, PPi, or $H_2PO_4^-$. Upon addition of ADP to a **17**-Zn solution, a much smaller red shift (8 nm) in λmax occurred and no change in color could be registered by the naked eye. Furthermore, they used this receptor molecule as a colorimetric staining agent for yeast cells, and managed to view the staining by simple light microscopy.

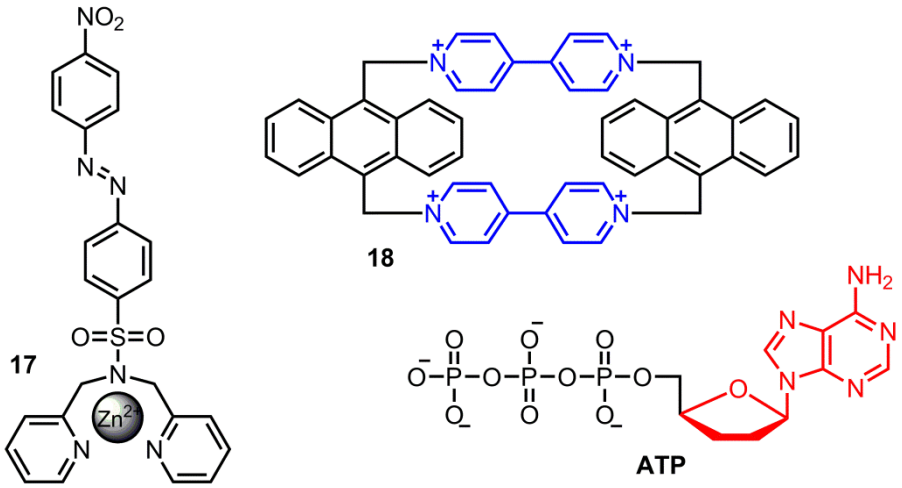

Figure 28. Chemosensors for ATP

Ramaiah et al demonstrated another interesting work, by reporting a novel molecular recognition system for the selective detection of ATP in buffer.[82] That system is devoid of hydrogen bonding but recognizes the guest molecule through synergistic effects of cavity size, π-π stacking, and electrostatic interactions. They have synthesized novel cyclophane **18**, and investigated its interactions with phosphate, adenosine, AMP, ADP, and ATP (Figure 28). With addition of ATP, significant decrease in the absorbance of **18** was observed, whereas other guest molecules showed negligible effects. The complex between **18** and ATP was confirmed through

cyclic voltammetry and ^{1}H NMR experiments. The uniqueness of this system is that it complexes selectively with ATP in a cavity and involves synergistic effects of both electrostatic and π-π stacking interactions.

Solutions of **19**[83] in methanol exhibited an absorption band centered at 450 nm responsible for the orange color of the solutions. In the presence of halides such as chloride, bromide, and iodide, only an increase in intensity of the 450 nm band was observed; however, addition of fluoride resulted in a red shift from up to 563 nm with a simultaneous color shift from orange to dark red. This was due to the formation of a tetrahedral boronate anion upon reaction with one equivalent of fluoride (Figure 29).

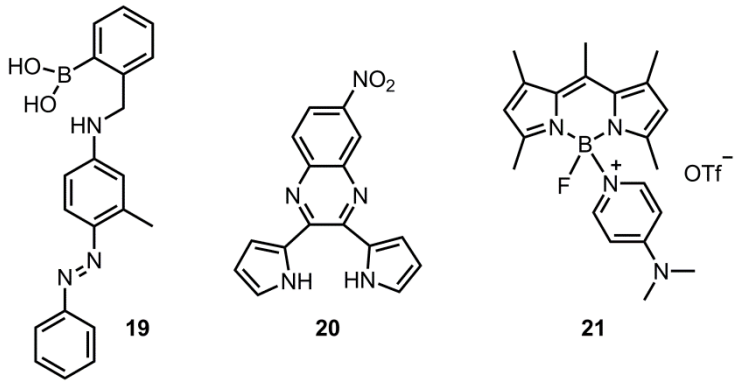

Figure 29. Fluorogenic and Chromogenic sensors for fluoride anion

Compound **20**[84] developed by Sessler et al, showed a remarkable color change from yellow (λ_{max} = 455 nm) to purple (λ_{max} = 560 nm) upon fluoride addition in DMSO, whereas chloride and dihydrogen phosphate did not produce any noteworthy color variation. Recognition of fluoride was also monitored by the quenching of the emission fluorescence. The color change was in agreement with the quite large stability constant found between **20** and F^- whereas formation constants with chloride and dihydrogen phosphate were much smaller (Figure 29).

Gabbai et al reported a Bodipy based chemosensor **21**[85] for the sensing of fluoride ions. They describe a new approach for the fluorescence turn-on sensing of mentioned anion. The key step was the preperation of boronium cation, which is in turn converted into a Bodipy dye in the presence of fluoride ions (Figure 29).

2.7. Bodipy Dyes

General characteristics and properties of fluorescent dyes and their utilization in the design and development of fluorogenic probes for sensing trace amounts of analytes were discussed within previous sections. Bright colors and wide range of wavelengths make these dyes applicable in different fields of study, such as photochemistry, biochemistry, physical chemistry and supramolecular chemistry. In this section, among the large variety of known fluorescent dyes, Boradiaza indacenes (a.k.a. Bodipy), will be discussed in terms of its synthesis, photophysical properties, and application fields.

In 1968, Treibs and Kreuzer first identified this compound while they were trying to acylate the 2,4-dimethylpyrrole with acetic anhydride in the presence of borontrifluoride as Lewis acid catalyst.[86] This compound was obtained by acid catalyzed condensation of pyrrole and keto-pyrrole yielding dipyrrin, followed by its complexation with borontrifluoride to form the final product (Figure 30).

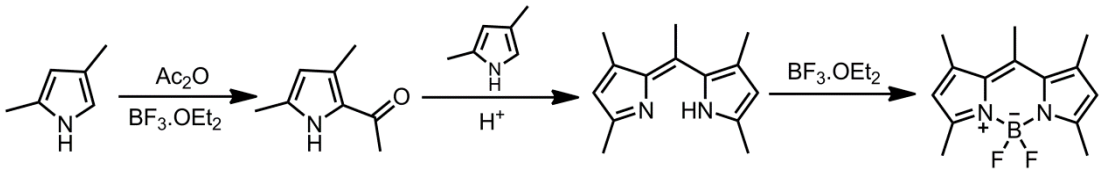

Figure 30. First synthesis of boron-dipyrrin dye

Bodipy dyes have high molar absorption coefficients; usually display strong absorption and fluorescence bands in the visible region with a smaller Stokes' shift, and higher fluorescence quantum yields, depending on their structure and the environmental conditions.[87] They are neutral molecules, and unless otherwisely designed, their characteristics mostly do not depend on the solvent polarity and pH values. Generally, they are stable in physiological pH range and start to decompose in strong acidic and/or basic conditions. In addition, good solubility, intense and tunable photophysical profile (500–900), negligible triplet state formation, higher photostability and wide versatility of synthetic pathways are additional advantages of Bodipy dyes.

Numbering of the Bodipy skeleton is slightly different from that of its precursors dipyrrin and dipyrromethane (Figure 31). The central carbon is named as *meso* position which comes from the porphyrin nomenclature. Today it is well known that all positions (1–8) of the BODIPY skeleton are labile to chemical modifications. Making structural modifications brings out new members of BODIPY family with some shifted photophysical properties.

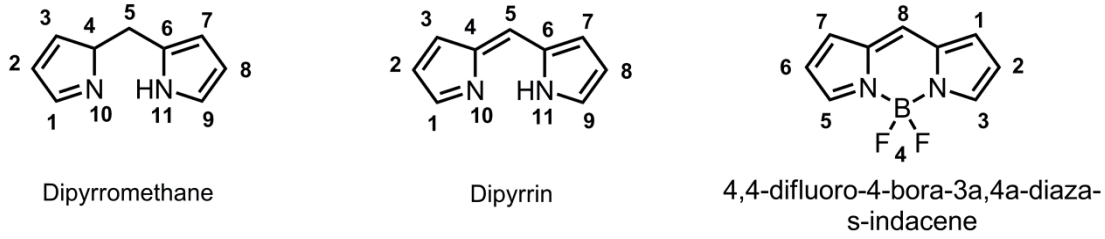

Figure 31. Structures and numbering of dipyrromethane, dipyrrin and Bodipy

For example, aromatic substituent on position-8 (a.k.a. *meso* site) significantly affects the quantum yield of the compound. The fluorescence quantum yield of the phenyl-Bodipy, depicted in figure 30, is very low. This is due to the possible conjugation between phenyl ring and Bodipy core that adapts these units in a co-planar arrangement, so that internal quenching mechanisms are enabled. If methyl substituents are installed on the 1,7 positions, that will inhibit free rotation of the phenyl ring, and therefore, energy loss via non-radiative processes will be prevented (Figure 32). Consequently, a dramatic enhancement in the fluorescence intensity will be observed.

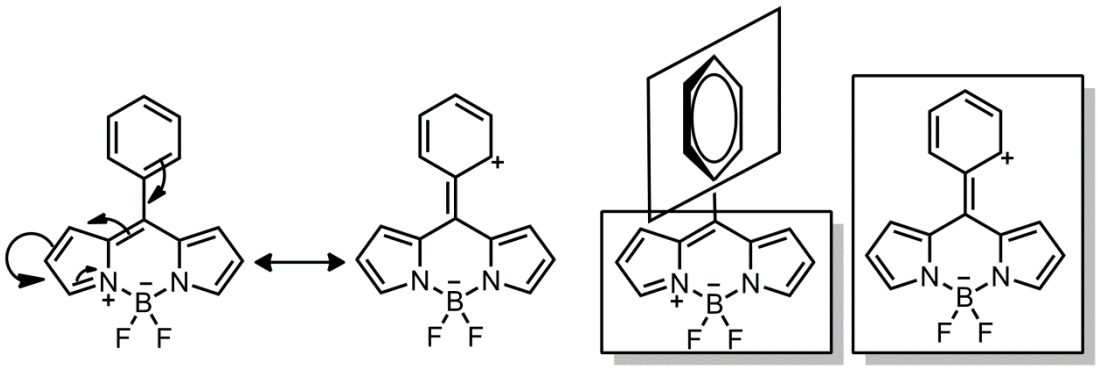

Figure 32. Tautomers of phenyl-Bodipy that affect the fluorescence quantum yields

2.7.1. Routes to Bodipy Synthesis

There are two major synthetic approaches in the formation of Bodipy skeleton. First one is acid catalyzed condensation of pyrroles with aldehides affording dipyrromethanes. Dipyrromethanes are very sensitive to air and light, and should be oxidized to dipyrromethene form (a.k.a. dipyrrin), which is rather stable compound, immediately for the best. DDQ or p-chloroanil can be used as an oxidazing agents. Addition of base then borontrifluoride on the dipyrrin affords borondifluoride complex in moderate yields (Figure 33).

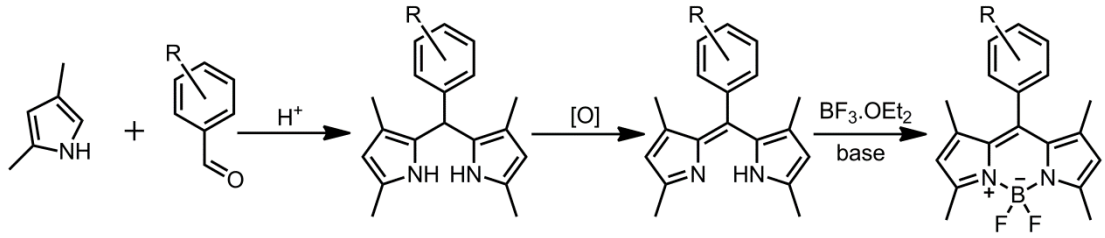

Figure 33. Acid catalyzed condensation of aromatic aldehydes with pyrroles

Second method is also similar to the first one. This time same condensation reaction is being carried out by using the acylium equivalent not aldehyde. It can be in the form of acylchloride[88], anhydride[89] or an orthoester[90], and with excess of pyrrole they directly form dipyrrin moiety. Again subjecting the formed dipyrrin to excess base and borontrifluoride yields the Bodipy derivative. With this approach asymmetric Bodipy derivatives can also be synthesized. Isolation of acylpyrrole and trituration of it with different pyrrole moieties will afford asymmetric Bodipy dyes.

Recently Burgess et al reported an alternative symmetrical Bodipy synthesis that was discovered serendipitously.[91] They claim that second pyrrole equivalent is not needed if pyrrole-2-carbaldehyde is used together with $POCl_3$ in the Bodipy synthesis. $POCl_3$ here assures the condensation of pyrrole-2-carbaldehyde with itself, and depending on the substituents on the pyrrole component, yields of the resultant Bodipy derivatives can be significantly higher. The postulated mechanism for this reaction is illustrated in figure 34, and it is based on the fact that the additional carbon cleaves from the intermediate molecule in the form of carbon monoxide.

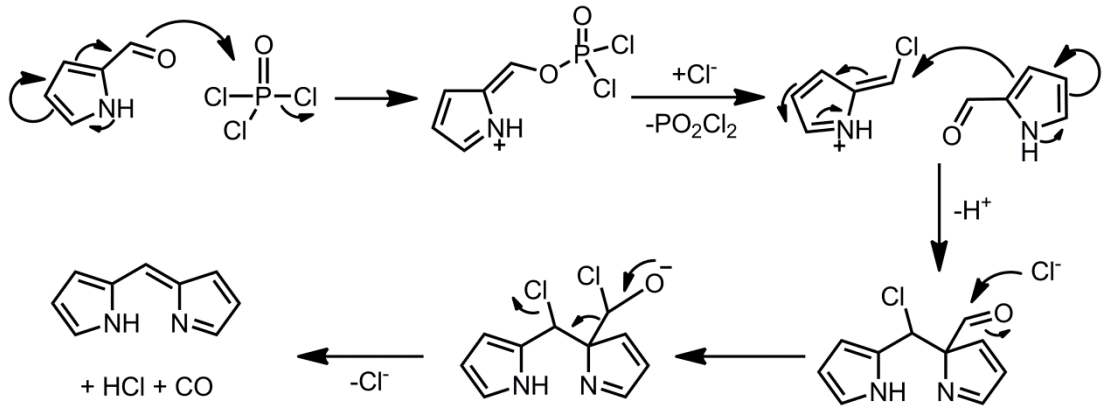

Figure 34. Proposed mechanism for the formation of dipyrrin

The key step is the removal of PO_2Cl_2 from the intermediate and formation of chlorinated azofulvene moiety which is in turn attacked by another pyrrole-carbaldehyde to form some other intermediate. Subsequent chloride anion attack and followed decomposition of the unstable intermediate yields the desired dipyrrin which can undergo complexation with borontrifluoride in a standard fashion to form the Bodipy derivative.

Due to their versatile chemical and photochemical properties, Bodipy dyes have found wide range of applications in many hot research areas, such as photosensitizers for solar energy conversion,[92] sensitizers for photodynamic therapy,[93] probes and labeling agents for biological systems,[94] light harvesting arrays in the artificial antenna systems,[95] and so on. This list has enormously grown since last decade, and no doubt that it will keep growing in the near future too.

Starting from its initial discovery, Bodipy chemistry has come a long way and is now has proven itself as a well established, versatile fluorophore. Especially within the last decade, numerious synthetic approaches and wide range of structural variations has been reported in the literature. Among them there are significantly important review articles that cover synthesis, spectroscopic properties and various applications of Bodipy derivatives briefly.[96,97,98,99] Besides this, an increasing number of novel and ingenious applications of these dyes are being reported every passing year. Considering this trend, it would not be an exaggeration to claim that there is still plenty of room to be discovered and adapted to the modern synthetic chemistry.

2.8. Logic Gates: Fundamental Building Blocks of Digital Systems

There is no doubt that computer is one of the most important invention of the last century, which has a significant impact on society since its introduction. Computers were invented primarily for their capability to solve complex mathematical calculations much faster than humans. However, they have enormously expanded their area of influence and revolutionized the fields of communications, information handling and computing, as well as the social life and the business, worldwide. A digital computer contains integrated circuits (ICs) that are constructed from logic gates. By concatenating these gates to each other in the designed way, and connecting their inputs and outputs, functions of the computer are performed.[100]

Logic gates,[101] known as electronic devices implementing Boolean functions, are fundamental building blocks of all digital systems. They process data by performing a logical operation upon one or more inputs and creating a single output. During the data processing, transmission and storage, digital electronic devices use binary logic to operate and electrical signals are used as the information carriers. Considering the binary logic, each input and output can only be either true (1) or false (0), which are represented by high and low voltage values, respectively. The output of a logic gate is directly determined by the values of its inputs, such that the output of the gate instantly changes if an input changes. In conventional computers that are based on silicon circuitry, binary logic is used for information processing, and data is encoded in series of zeros and ones.[102]

There are 16 possible Boolean logic functions[103] for the two binary variables and six of these functions (AND, OR, XOR, NAND, NOR, and XNOR) are very common in digital electronics. NOR, NAND and XNOR operations are created by the concatenation of basic OR, AND and XOR with Complement (NOT) operation. These most common operations together with their symbols and truth tables are summarized in figure 35 (next page).

Considering AND gate, the output is 1 (the state above a specified threshold), only if both inputs are 1, otherwise the output is 0 (the state below a specified threshold).

In an OR gate, the output is 1 when at least one of the inputs are 1. The output is 0 only when both inputs are 0. For an XOR gate, the inputs set to different logic states yields 1 as the output. When both inputs are set to same logic state, the output is 0. For NOR, NAND and XNOR logic gates, the outputs are exactly the reverse of the ones in OR, AND, and XOR gates (Figure 35).

INPUTS		OUTPUTS					
A	B	OR	AND	XOR	NOR	NAND	XNOR
0	0	0	0	0	1	1	1
1	0	1	0	1	0	1	0
0	1	1	0	1	0	1	0
1	1	1	1	0	0	0	1

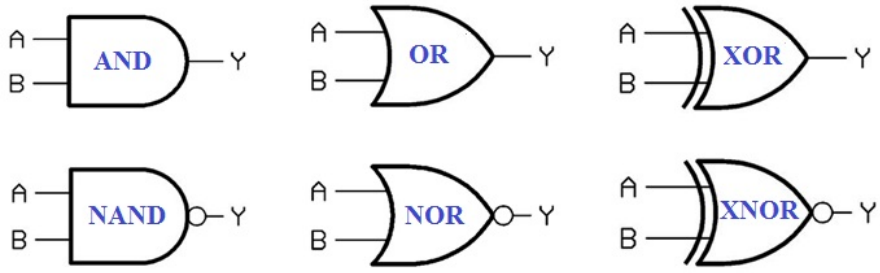

Figure 35. Truth tables and schematically representations for common logic gates

Fundamental logic gates can perform only basic logic operations; however, practical application of any digital device requires more complex logic systems that carry out higher degree of logic functions. These more complex systems are usually formed by the integration of a couple of 16 fundamental logic gates. They perform arithmetic and some other complex operations in binary fashion and yield bits of information.

In the world of digital electronics, a logic gate is constructed from transistors, which are semiconductor devices capable of amplifying and switching electrical signals. Switching between two binary states occurs in a transistor, by altering the gate voltage the current is either turned off (0) or on (1).[104] Since one computer chip have millions of continuously switching transistors connected in certain ways, massively complex tasks can be completed on a computer. The integration of large numbers of tiny transistors into a small chip, known as *miniaturization*, has provided great

improvements in electronics in terms of performance, cost and size. By the miniaturization of electronics equipment, highly complex electronic functions were included in limited space with minimum weight.

Miniaturization is still essential step for the development of new technologies. Nevertheless, the end of the miniaturization is about to come by around 2020, according to Intel co-founder Gordon Moore's predictions.[105,106,107] Miniaturization cannot continue forever because of some future technological and fundamental barriers. Further increase in the integration density of computer chips is expected to face a physical boundary due to the limited number of transistors to be placed on a particular chip, the number of interconnections to be made on that chip and obviously the heat dissipation problems. Some day in the near future transistor sizes will eventually drop to single-atomic levels,[108] facing the fundamental barrier of the universe. Most probably this is the way how the 'miniaturization history' would end.

2.9. Molecular Logic Gates: An Alternative Perspective

Recently, scientists have started to consider some potential alternatives to the digital information processing, as it is rapidly approaching to its physical and technological limits especially in terms of miniaturization. Among many proposals, the 'bottom-up' approach is thought to be one of the most promising. It is just the reverse of 'top-down' approach, in which the nanoscale devices are made from macroscopic materials. The possibility of manufacturing nanostructures within 10 nanometer range is a great advantage of bottom up approach. In this approach, basically, fundamental building blocks of matter, atoms and/or molecules (at least from an ordinary chemist's perspective), are brought together in such a way that nanoscale structures or objects are established. Chemists can be thought to be at an advantageous point considering the bottom-up manufacturing of nanostructures, because they have sufficient experience on manipulating the smallest components of matter, atoms and/or molecules. Especially, synthetic chemistry has reached to a certain degree of maturity where most plausible molecules can be synthesized.

However, arraging nanoscale structures to form some complex and functional device is not as easy task as just manufacturing or synthesizing those a few nanometer sized building blocks. In other words, while top-down approach has difficulties in going below 15-20 nm, for the bottom-up techniques the major challenge is building advanced and functional structures that exceeds beyond that size range.

As discussed in the previous section, data processing in conventional digital electronics based on silicon circuitry requires binary encoding of information in electrical signal. However, binary logic is not only applicable to electrical signal; it can also be integrated to chemical and optical ones. This means that, appropriately designed molecular systems can be used to mimic the logic functions. Uploading basic logic operations on a single molecule means a lot in terms of bottom-up approach. Most important and obvious advantage of using molecular system carrying logic functions is that they can operate in much smaller spaces (such as inside the cell), where silicon based analogs could not reach.[109] Organic molecules have been realized to be very promising candidates for this purpose.

Molecular mimicry of logic gates has aroused a great deal of interest since the pioneering study of de Silva in 1993.[110] In that particular study, first receptor molecule that operates as a two-input AND gate was reported (Figure 36). Compound **22** constitutes two different binding sites for the selective recognition of Na^+ cation and proton. That molecule exhibits fluorescence only in the presence of both cations, otherwise, it remains quenched. The input/output characteristics of this molecular logic device correspond to that of an AND gate. Uniqueness of that study was based on the emitted light which is used as output signal.

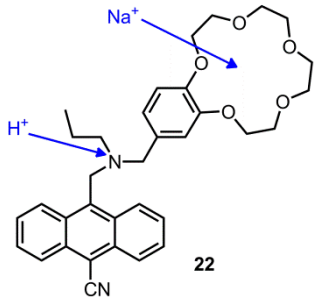

22

In1 (Na^+)	In2 (H^+)	Output (F. Intensity)	Q. Yield	F. Enhancement
0	0	0	0.011	1.0
1	0	0	0.020	1.8
0	1	0	0.013	1.2
1	1	1	0.068	6.2

Figure 36. Two-input molecular AND-logic gate by de Silva et. al.

It is really difficult to detect any change that happens at the molecular level. However, if the change occurs in the optical character of the molecules, then it becomes easier to detect it with high sensitivity. Molecular logic gates, based especially on fluorescence phenomenon have been widely preferred so far due to the distinct advantages of fluorescence detection in terms of sensitivity and selectivity. Such systems, in which fluorescence switches between 'on' and 'off' states by chemical stimuli, are commonly designed according to various photophysical principles such as photoinduced electron transfer (PET), intamolecular charge transfer (ICT) and energy transfer (ET). Therefore, colored molecules especially fluorescent ones have become very important tools in the design and construction of molecular scale logic gates.

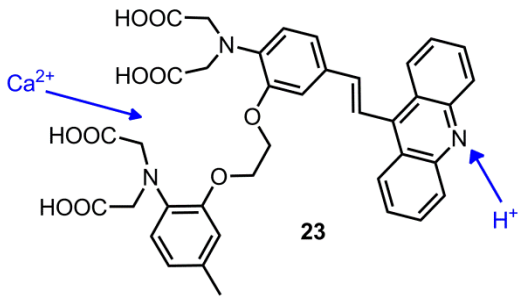

Figure 37. XOR & XNOR gate designed by de Silva et al.

Compound **23**, developed by de Silva et al, is a chemically driven example of XOR gate (Figure 37).[111] It has two recognition sites, one of which selectively binds to Ca^{2+} cations, whilst the other one is capable of capturing protons. When none of Ca^{2+} and H^{+} ions is present, the molecule displays absorption at 390 nm. Blue shift is observed in the presence of only Ca^{2+} ions, whereas red shift occurs in the presence of only H^{+} ions. Coexistence of both ions don't cause any change on the absorption profile of the molecule. This molecular system operates as XNOR logic gate in terms of absorbance at 390 nm and XOR logic gate in terms of transmittance at 390 nm.

During the last two decades, a great progress has been accomplished in the field of molecular logic gates. Large number of molecular systems mimicking most of the fundamental logic gates have been reported and well reviewed in the literature.[112,113,114]

2.10. Higher Functions with Molecular Logic

Fundamental logic gates carry out only basic logic operations, however, practical application of any digital electronic device requires more complex logic systems including arithmetic operations, complex functions performed on large data sets and so forth. These more complex logic systems performing higher level functions are usually generated by the concatenation of simple logic gates. Considering the classical silicon based microprocessor systems, it can be easily claimed that the most important feature of these systems is input-output signal homogeneity. In other words, the output of one logic gate, which is an electronic voltage signal in silicon based systems, can also be used as the input of another or even the identical gate. However, this is not the case in molecular logic gates. Since they may use different types of input-output signals (optical, electrical, chemical etc), often input-output signal homogeneity is not guaranteed. Of course there are some examples, such as all-photonic molecular logic gates,[115] where input-output signals belong to the same category. In that specific case, light is used for both input and output signals. However, it should be noted that, light is a multidirectional signal, and in terms of concatenation, it would be very difficult to assure the communication between two distinct molecular logic gates by just means of a random emission-reabsorption mechanism. Consequently, it can be concluded that, physical concatenation of simpler gate molecules remains as a difficult task for molecular scale logic studies.

Realizing the above mentioned issue, scientists started to think over some other approaches in order to address this issue and promote molecular logic concept to an advantageous position. Fortunately, thinking chemically (from the point of view of synthetic chemistry) has shed some light on this difficult task. And this approach constitutes, uploading some higher functions directly onto a single molecule instead of struggling to concatenate them. Rational design is the key step in this approach, and it eliminates the problem of physical integration of simpler gate molecules to a certain degree. And so far, a large number of molecular systems mimicking those higher functions, such as half adder, full adder, encoder/decoder, multiplexer/demultiplexer and sequential logic have been reported in the literature.[116]

2.10.1. Half Adder and Half Subtractor

The logic circuits that perform addition operations are called adders. They are able to add three bits and in order to perform a multibit addition (larger integers), they should be cascaded to yield serial adders. A half-adder is a key device in the construction of full adder, and it is able to add two bits of information. It composes of an AND and an exclusive OR (XOR) gates, that share the same inputs and provide output on carry and sum digits, respectively (Figure 38).

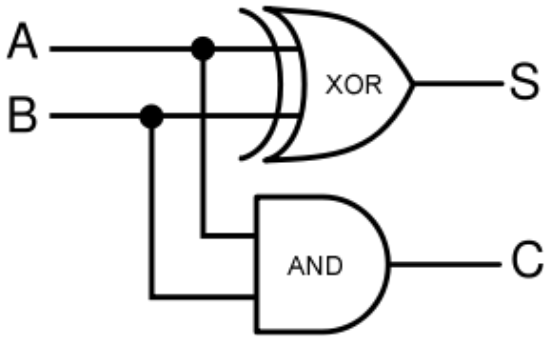

Inputs		Outputs	
A	**B**	**Sum**	**Carry**
0	0	0	0
0	1	1	0
1	0	1	0
1	1	**0**	**1**

Figure 38. Half-adder logic diagram along with its truth table

The first molecular half adder[117] was demonstrated by de Silva et al is depicted in figure 39. This was a bimolecular system, compounds **24** and **25**, responsive to the same inputs (cations), and functioning in the same solution. Anthracene and quinoline moieties were selected as the signaling parts. Both molecules operate at the same time with the same chemical inputs (Ca^{2+} and H^{+}). Compound **24** operates as XOR gate in transmittance mode (at 390 nm), while **25** operates as an AND gate in fluorescence mode (Figure 39). Authors developed a novel approach towards XOR logic (compound **24**) in this work. The tricky part of XOR gate was handled intelligently, without using annihilating inputs. While one of the inputs caused blue shift, the other one did just the reverse, a red shift. As a result, by carefully selecting the optical output signal, no net change is observed when both inputs coexist in the solution. To sum up, XOR and AND molecular logic gates operated in parallel making a binary addition. After this study, lots of molecular half adder systems have been developed and published.[118,119,120]

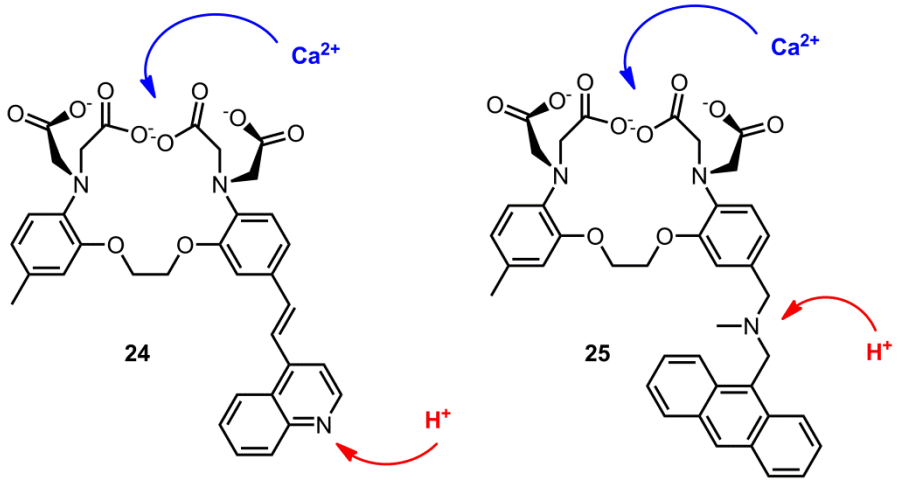

Figure 39. First molecular half adder (XOR and AND gates)

Half-subtractor on the other hand, carries out a reverse operation of half adder, which is subtraction in two bits. Similarly, it has two inputs and two outputs (Difference and Borrow), and composes of XOR and INH gates. Molecular implementation of half subtractor is more difficult than half adder. Truth table and logic representation of half-subtractor is given in figure 40 below.

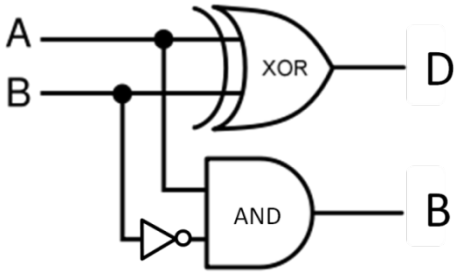

Inputs		Outputs	
A	B	Diff	Borrow
0	0	0	0
0	1	1	1
1	0	1	0
1	1	0	0

Figure 40. Logic representation and truth table of half-subtractor

First example on molecular half-subtractors was reported in 2003 by Langford and Yann.[121] In that study, the operation of the molecular device relies on the red shift in absorption band of tetraphenylporphyrin and the change in the emission intensity upon protonation/deprotonation. The absorption band of tetraphenylporphyrin (H_2TPP) is localized at 417 nm. It shifts to 440 nm on protonation (H_4TPP^{2+}) and 430 nm on deprotonation (TPP^{2-}) (Figure 41). Besides, only protonated and deprotonated forms of tetraphenylporphyrin exhibit a strong emission.

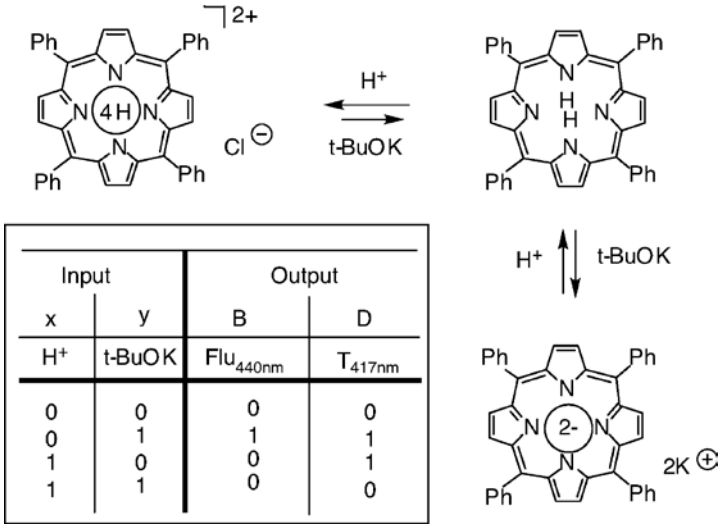

Input		Output	
x	y	B	D
H^+	t-BuOK	Flu_{440nm}	T_{417nm}
0	0	0	0
0	1	1	1
1	0	0	1
1	1	0	0

Figure 41. The first molecular half subtractor based on tetraphenylporphyrin[121]

H_4TPP^{2+} shows a strong emission at 405 nm while TPP^{2-} emits at 440 nm. When either acid or base is present in the media, a strong absorption at $\lambda > 425$ nm is monitored and this part corresponds to XOR gate. On the other hand, a strong emission is observed at the wavelengths of 405 or 440 nm only in the presence of one of the inputs (acid or base) and this part corresponds to INHIBIT gate. Coupling of XOR and INH gates in one molecule (tetraphenylporphyrin) using the same inputs and yielding different outputs (Figure 41) produces a molecular binary half subtractor.

2.10.2. Full-Adder and Full-Subtractor

Constructing a molecular full-adder is really a formidable challenge. It can add up three bits, which are In1, In2, and Carry in (C_{in}) coming from the previous addition. It composes two half adders and one OR gate and yields two-bit output upon full addition of three binary digits. The result of addition is resembled by the Carry output (C_{out}) and Sum output (S_{out}). Contrary to the half adder, a full-adder is capable of performing the addition of 1+1+1=3, giving the output of $C_{out}=S_{out}=1$.

In a similar fashion, full subtractor performs the subtraction of three one-bit numbers producing two-bit output, where the result of the subtraction is defined by the Borrow output (B_{out}) and Difference output (D_{out}). Arithmetic operations at highest complexity are accomplished by serial cascading of binary full adders and full subtractors.

Full Adder					Full Subtractor				
Inputs			Outputs		Inputs			Outputs	
A	B	C_{in}	S	C_{out}	A	B	B_{in}	D	B_{out}
0	0	0	0	0	0	0	0	0	0
0	0	1	1	0	0	0	1	1	1
0	1	0	1	0	0	1	0	1	1
0	1	1	0	1	0	1	1	0	1
1	0	0	1	0	1	0	0	1	0
1	0	1	0	1	1	0	1	0	0
1	1	0	0	1	1	1	0	0	0
1	1	1	1	1	1	1	1	1	1

Table 2. Truth tables for full-adder and full-subtractor

The first molecular system combining full-adder and full-subtractor in the same molecule was demonstrated by Margulies et al in 2006.[122] The molecular full adder/subtractor in this study relies on a simple fluorescein molecule. Acid and base are used as inputs, and changes in absorbance, transmittance and emission profiles are monitored as outputs. Protonation/deprotonation of fluorescein leads to changes in its absorption spectrum (Figure 42). 447 nm is chosen as the characteristic wavelength in the absorption spectrum for monocationic and monoanionic state of fluorescein while 474 nm is selected for monoanion and dianion form.

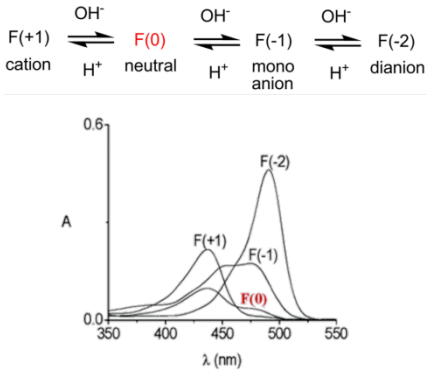

Figure 42. Absorption spectra for different forms of fluorescein[122]

The neutral form of fluorescein displays a weak absorption at both 447 and 474 nm. When the transmittance at 447 nm is selected as the Sum output, and absorption at 474 nm is assigned as the carry output, it will work in accordance with the full adder. This fluorescein based full adder works starting from the monocationic form, it corresponds to [0,0,0] set of inputs (each input is OH^- ion) and it results as Sum=0 (low transmittance at 447 nm) and Carry=0 (low absorbance at 474 nm). When one equivalent OH^- ion is added, produced neutral form exhibits high transmittance at 447 nm (Sum=1) and low absorbance at 474 nm (Carry=0). Addition of two equivalents of OH^- ion yields monoanionic form of fluorescein, which shows low transmittance at 447 nm (Sum=0) and high absorption at 474 nm (Carry=1). In the case of three equivalent of OH^- addition, dianion forms and it has a high transmittance at 447 nm and a high absorbance at 474 nm. In this case, both Sum and Carry is 1 (Figure 43).

	X	Y	C_{in}	C_{out}	S
a	0	0	0	0	0
b	0	OH^-	0	0	1
c	OH^-	0	0	0	1
d	OH^-	OH^-	0	1	0
e	0	0	OH^-	0	1
f	0	OH^-	OH^-	1	0
g	OH^-	0	OH^-	1	0
h	OH^-	OH^-	OH^-	1	1

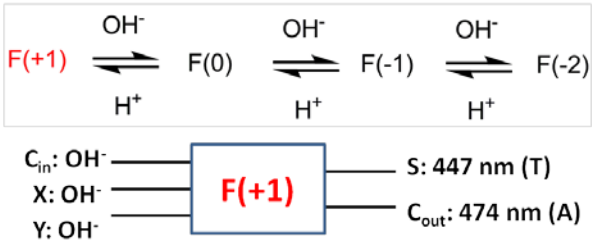

Figure 43. A full adder based on fluorescein molecule[122]

A full subtractor from the same molecule is achieved with the same system as well. In this case, absorbances at 447 nm and 474 nm are used as outputs whereas both acid and base are used as chemical inputs. Operation of this fluorescein based full subtractor begins with the neutral form, it corresponds to [0,0,0] set of inputs (Figure 44). The full subtractor, which is based on the half subtractor, also performs two-bits subtraction in the absence of additional B_{in} input so lines “a-d” in the truth table are naturally obtained (Figure 44).

	X	Y	B_{in}	B_{out}	D
a	0	0	0	0	0
b	0	OH^-	0	1	1
c	H^+	0	0	0	1
d	H^+	OH^-	0	0	0
e	0	0	OH^-	1	1
f	0	OH^-	OH^-	1	0
g	H^+	0	OH^-	0	0
h	H^+	OH^-	OH^-	1	1

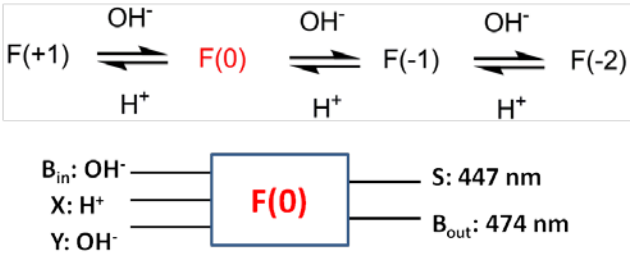

Figure 44. A full subtractor based on fluorescein molecule[122]

Furthermore, the set of chemical inputs in lines "d" and "g" produces the identical output signals (0,0) with the line "a" because of mutual annihilation of acid and base. In a similar way, set of inputs in lines "e" and "h" must give the same output signals (1,1) with the one in line "b". Only the set of inputs expressed in line "f" gives rise to a new chemical environment (di-anionic form) that has no corresponding analogy in the molecular half subtractor and it results the correct output signals (1,0) (Figure 44). As a consequence, this system results in a complete molecular full subtractor device.

2.10.3. Other Higher Functions

In the above subsections the molecular number processing devices (half-adder/subtractor, full-adder/subtractor) were discussed briefly. For clarity, some common examples for each case were demonstrated in details. However, there are some other higher functions of silicon based circuitry that have also been mimicked by molecular logic systems in the literature. Since they are out of the scope of this thesis, a quick look over them will be introduced within following paragraphs.

One of them is Multiplexer/Demultiplexer, which is a non-arithmetic function. It is a circuit analogous to a switch that combines various inputs into single output signal. Once several input signals are multiplexed into one output, they can be separated

again using a demultiplexer. Not so many molecular multiplexers/demultiplexers were reported in the literature.[123,124]

Another one is Encoder/Decoder, which is a device that compresses digital information for transmission or storage and converts information into a code while compressing it. For example, a single bit 4-to-2 encoder converts 4 bits of data to 2 bits. On the contrary, a decoder converts the compressed information back into the initial form. In a similar way, a 2-to-4 decoder converts 2 bits of information back to 4 bits using two inputs and producing 4 outputs.[125,126]

The above mentioned digital electronic devices, multiplexers and encoders, together with the number processing devices, adders and subtractors, are referred to as 'combinatorial' circuits. The output of these combinatorial circuits is exclusively a function of current inputs, meaning that history of inputs has no effect on device function. On the other hand, there are also 'sequential' circuits, the output of which is determined by the current state of the system that involves both previous and present inputs. Since such a circuit remembers information about the previous input, it functions as a memory element. Hence, this feature requires the use of feedback loops that connects the output of a logic gate back to one of its inputs (Figure 45). Sequential logic systems are used in memory devices and storage elements.[127,128,129]

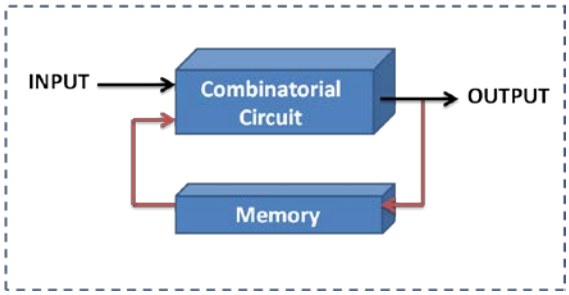

Figure 45. General representation for sequential logic circuit[131]

Van der Boom group have progressed in the area of molecular sequential logic, including the molecular random-access memory (RAM).[130] They have published a nice account on this topic, where some comments on combinatorial logic are also made. Readers should refer to this article for further details.[131]

2.11. Molecular Logic: Quo Vadis ?

Within the past 20 years, large number of molecules mimicking the silicon-based logic functions have been designed and characterized. Starting from the first reported rather simple yet influential 'molecular AND' gate, the molecular logic phenomena has upgraded to a more developed field, such that wide range of advanced logic functions of the conventional microprocessors can be performed on a unimolecular systems. Molecular equivalents for the most common complex logic devices were covered briefly in the previous section.

In silicon based circuitry these devices require a considerable degree of integration of simpler logic gates which is provided by wiring (concatenation) technology. On the other hand, molecular devices are capable of performing the same function without any concatenation which is one the most important advantages of molecular systems. It is done by rational selection of outputs at several channels (i.e. at different wavelengths) and then according to these produced outputs an integrated set of logic gates is suggested to be performing using the same inputs. More precisely, a unimolecular species represents the entire integrated logic circuit that constitutes various fundamental logic gates. Although this approach provides some important advantages, it does not truly solve the concatenation issue at the molecular level. Since that approach keeps postponing the main problem, now it is clear that physical integration of molecular (chemical) logic gates must be of great importance for the rational design and implementation for advanced molecular computing. Some novel approaches should be introduced in order to solve the concatenation problem.

Because of the aforementioned reason, there is neither a competitive molecular computer reported, nor a ready-to-use device developed so far. Perhaps, it will happen once the solid state platforms take the place of the solution-based chemistry where most of the molecular logic gates are described today. Nevertheless, the molecular logic phenomenon is a quite recent concept and despite all the improvements that took place, it is still in the 'proof-of-principle' stage.

CHAPTER 3

3. Cyanide Sensing via Metal Ion Removal From a Fluorogenic Bodipy Complex

This work is partially described in the following publication:

Guliyev, R.; Buyukcakir, O.; Sozmen, F.; Bozdemir, O.A. *Terahedron .Lett.* 2009, *50*, 5139-5141

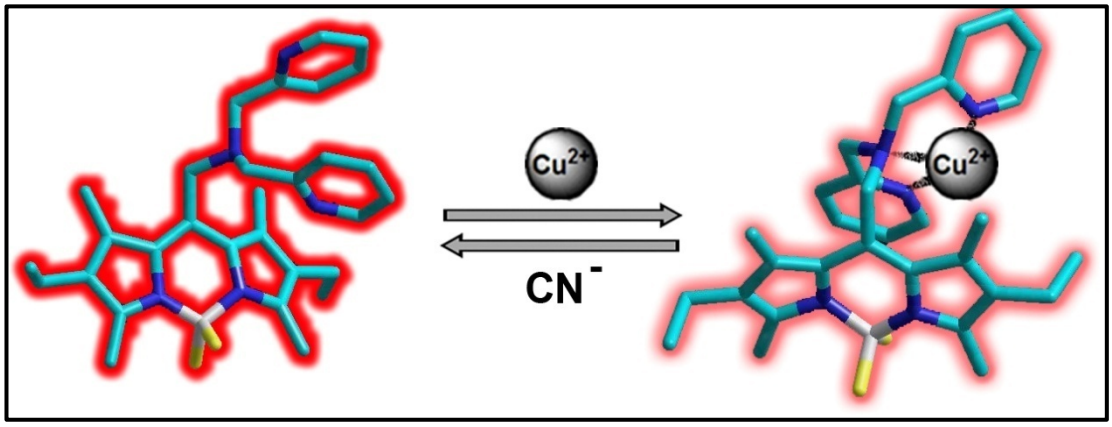

3.1. Objective

Bodipy dyes are very versatile chromophores in many applications, including fluorescent chemosensors. In this work, we are reporting highly selective and sensitive cyanide sensor operating in the "turn-off-on" mode *via* decomplexation of Cu(II) ion from a bright fluorescent boradiazaindacene derivative. The system described here can detect cyanide ion concentrations lower than 20.0 μM in water and this value is the lowest limit of the blood cyanide concentrations found in fire victims. We are confident that our system is an important member of cyanide sensors emerged in recent years.

3.2. Introduction

Fluorescent chemosensors capable of detecting toxic and lethal anionic species are of great interest in chemistry, biology, medicine and in relation to environmental issues.[132] Cyanide ion is one of the most lethal poisons known. The highest level of cyanide ion that is allowed in drinking water is lower than 1.9 µM.[133] As assessed by recent studies, victims of fire disasters have 20 to 30 µM blood cyanide levels.[134,135] Due to its widespread use in chemical industry in the synthesis of nitrile derivatives, nylon and acrylic polymers, electroplating and gold mining, development of highly selective chemosensors for detection of cyanide ion concentrations lower than 30 µM in water or water organic solvent mixtures is an important task for supramolecular photochemistry. There have been a number of fluorescent chemosensors and chemodosimeters reported for selective sensing of cyanide ion to date.[136,137,138] In addition to these coordination or covalent bond based sensors, there are a few systems utilizing strong affinity of cyanide ions towards transition metals.[139] In such systems complexation of cyanide ion with a transition metal cation, for example, results in a change in the photophysical properties of the dye and provides a method for detection. There are also some other analytical techniques that were adopted for the cyanide detection, however, they are usually disadvantageous considering longer procedures, less specificity and expensive instrumentation.

Boradiazaindacene (Bodipy) dyes, due to the emergence of new synthetic strategies for their derivatization, have received much attention in recent years. High quantum yields (typically 0.5-0.9), large extinction coefficients (60,000- 150,000 $M^{-1}cm^{-1}$), and photostability of these fluorophores ensure their diverse applications in the fields of chemosensors,[140] logic gates,[141] light harvesting systems,[95] energy transfer casettes,[142] photodynamic therapy,[93] and dye-sensitized solar cells.[92] 8-halomethyl-Bodipy dyes, among other members of this class, can be easily converted to new derivatives *via* a simple nucleophilic substitution reaction at the *meso* position. Based on these derivatives, several "turn- on" metal ion and pH sensors have been designed and studied in recent years.[143]

3.3. Results and Discussions

Herein, we report the design and synthesis of a new Bodipy derivative operating in "turn-off-on" mode for selective and sensitive detection of cyanide ion in a water-organic solvent mixture. The synthesis for our target molecule **28** is shown in figure 46, below. 4,4-difluoro-8-chloromethyl-1,3,5,7-tetramethyl-2,6-diethyl-4-bora-3a,4a-diaza-*s*-indacene **26** was obtained in 16 % yield by the reaction of 3-ethyl-2,4-dimethylpyrrole with chloroacetylchloride at room temperature in dichloromethane and subsequent addition of triethylamine and boron trifluoride diethyletherate.

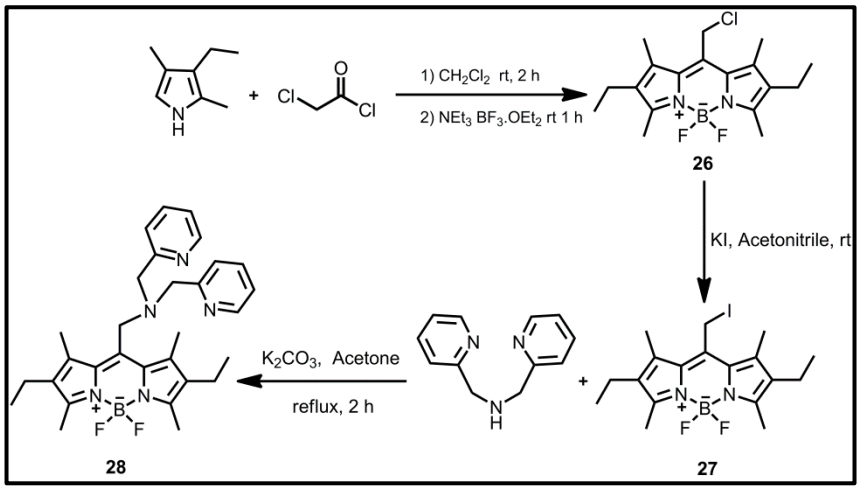

Figure 46. Synthesis of chemosensor **28**

The more reactive 8-iodomethyl-Bodipy **27** was prepared by treatment of compound **26** with KI in acetonitrile at room temperature. Compound **27** was then reacted with di-(2-picolyl)amine in the presence of K_2CO_3 in acetone at reflux temperatures to afford the target molecule **28** in 48% isolated yield. Structural characterizations of the synthesized molecules were done by ^{1}H NMR spectroscopy and Mass spectrometry (see experimental section).

Unlike related 8-aminomethyl-BODIPY derivatives, compound **28** is a fluorescent molecule having a relatively high quantum yield (ϕ_F=0.24). This new probe shows an absorption wavelength–ratiometric response to Cu(II) ions. Upon addition of Cu(II) ions (0.2 to 2 μM in THF) to the solution of **28** ($1.0x10^{-6}$ M in THF), absorption peak at 537 nm decreased and a new absorption peak appeared at 565 nm (Figure 47).

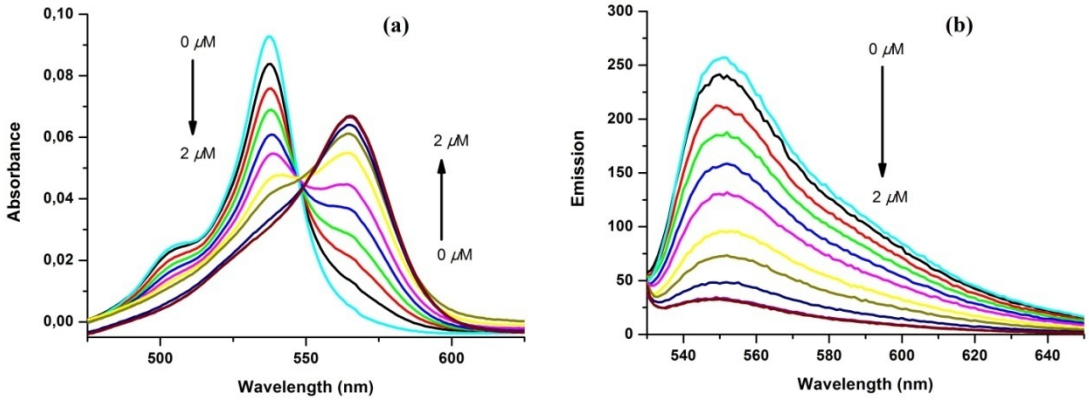

Figure 47. Absorbance (a) and emission (b) spectra of compound **28** in the presence of increasing Cu(II) concentrations (0.2, 0.4, 0.6, 0.8, 1.0, 1.2, 1.4, 1.6, 1.8, 2.0 μM)

This pronounced bathochromic shift is in accordance with previous literature, since electron withdrawing substituents at the 8-position (meso) of the Bodipy chromophore results in red shifts both in the absorption and emission spectra. The transformation of an electron donor aminomethyl substituent into a metal complexed amine substituent, possibly with electron withdrawing character, is expected to yield such a red shift. An isosbestic point shown at 548 nm clearly indicates the formation of single discrete species during the titration experiments. Complete quenching of the fluorescence takes place by the addition of Cu(II) ions (2 μM in THF) to the dye solution in THF (Figure 47). The observed quenching by Cu(II) ions is hardly

surprising, since Cu(II) is a redox-active, open-shell transition metal ion. The fact that the Bodipy derivative **28** having a bright fluorescence emission before metal-ion induced quenching may require an explanation. Photoinduced electron transfer process in Bodipy dyes was studied previously.[144] It appears that, substituents on the Bodipy core have very strong influence on the direction and magnitude of the PET process. We know that a Bodipy derivative which lacks ethyl substituents at 2 and 6 positions and otherwise identical to the compound **28**, shows a very strong PET quenching. Ethyl substituents not only cause a red shift of the absorption spectrum by 30 nm, but apparently do so by raising HOMO energy level significantly so that, there is no PET for the compound **28**.

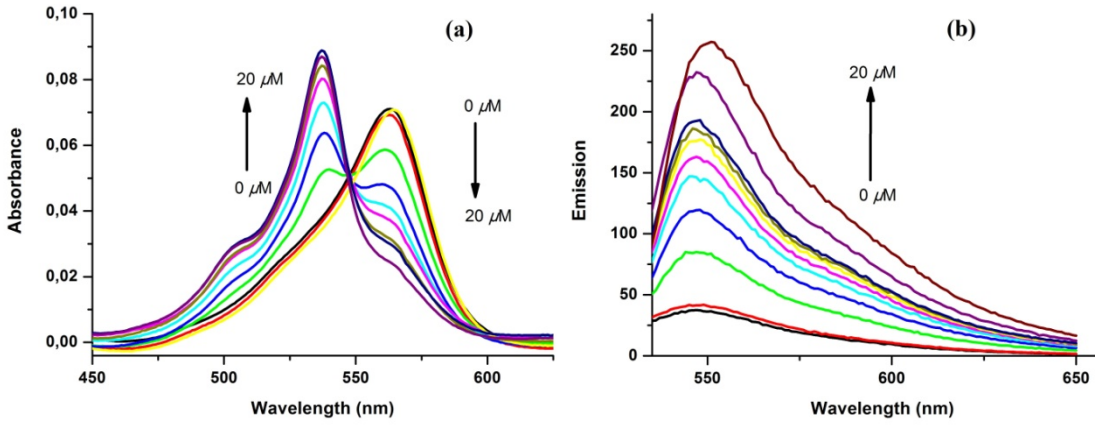

Figure 48. Absorbance (a) and emission (b) spectra of compound **28**+Cu(II) in the presence of increasing CN^- concentrations (0, 3.3, 6.7, 10.0, 11.7, 13.3, 15.0, 16.7, 18.3, 20.0 μM)

In the determination of its cyanide sensing ability, compound **28** was converted to its non-fluorescent "off-mode" by the addition of 2.0 μM Cu(II) ions (20.0 μL $3.0x10^{-4}$ M in THF, in the form of a perchlorate salt) to its solution (3.0 mL $1.0x10^{-6}$ M in THF) in a quartz cell. The solution of NaCN ($1.0x10^{-3}$ M in deionized water) was added in portions (total volume; 10.0 to 60.0 μL: 3.3 to 20.0 μM) and after each addition, absorbance and emission spectra (λ_{ex}: 530 nm) were recorded (Figure 48). As expected from the very high stability constant of tetracyanocuprate(II) complex ion, the addition of cyanide ion to the copper(II) complex form of **28** released the free, fluorescent "on-mode" of the chemosensor and absorption wavelength-ratiometric behaviour in the reverse direction was observed including the isosbestic

point at 549 nm (Figure 48a). While the absorption band at 565 nm decreased, an absorption band belonging to free form of **28** at 537 nm increased. To account for the quenching effect of the added water on the emission spectra during the titrations, we prepared a blank solution (3.0 mL $1.0x10^{-6}$ M) in THF containing 60.0 μL deionized water and obtained a reference emission spectrum (Figure 48b, top line).

Figure 48b indicates that starting from the very low concentrations of cyanide ion, an increase in the emission intensity occured with a small hypsochromic shift (5 nm). As compared to the reference emission intensity, nearly 90% of the emission was recovered upon addition of 20.0 μM cyanide ion and this result is the basis for the very sensitive "turn on" behaviour of our cyanide sensor at the lowest limit of the blood cyanide concentrations found in fire victims. In order to ascertain the selectivity of our **28**+Cu(II) complex system for cyanide ion, we repeated the titration experiments with other, potentially interfering anions, such as F^-, Cl^-, Br^-, I^-, AcO^-, NO_3^-, ClO_4^-, and HSO_4^- (Figure 49).

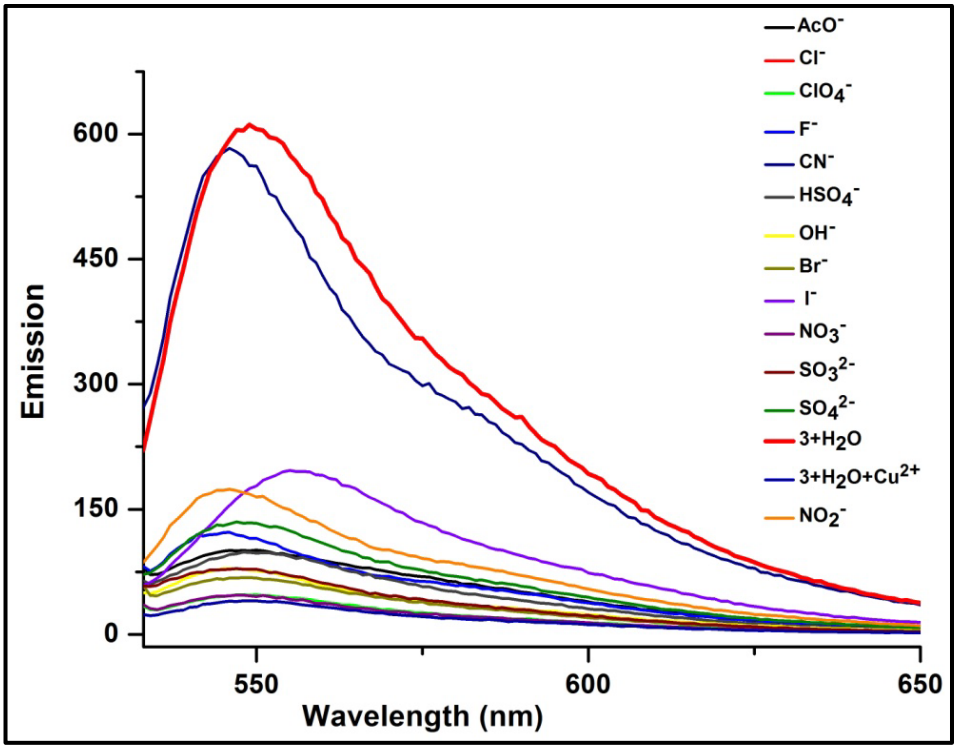

Figure 49. Emission spectra of compound **28**+Cu(II) in the presence of different anions (anion concentrations at 50 μM, λ_{ex} = 530 nm)

As indicated by the relative emission intensities (Figure 50), although the addition of I^- and NO_3^- resulted in some degree of emission recovery, they did not significantly interfere with the selective sensing of cyanide ion. Thus, in this study, we have successfully employed the "turn-off-on" sensing principle for the sensitive and selective probing of cyanide ions by using the ability of Cu(II) ions to quench the fluorescence of a novel BODIPY-dipicolylamine derivative. This simple system was shown to detect efficiently cyanide ion concentrations as low as 20.0 μM as an upper limit.

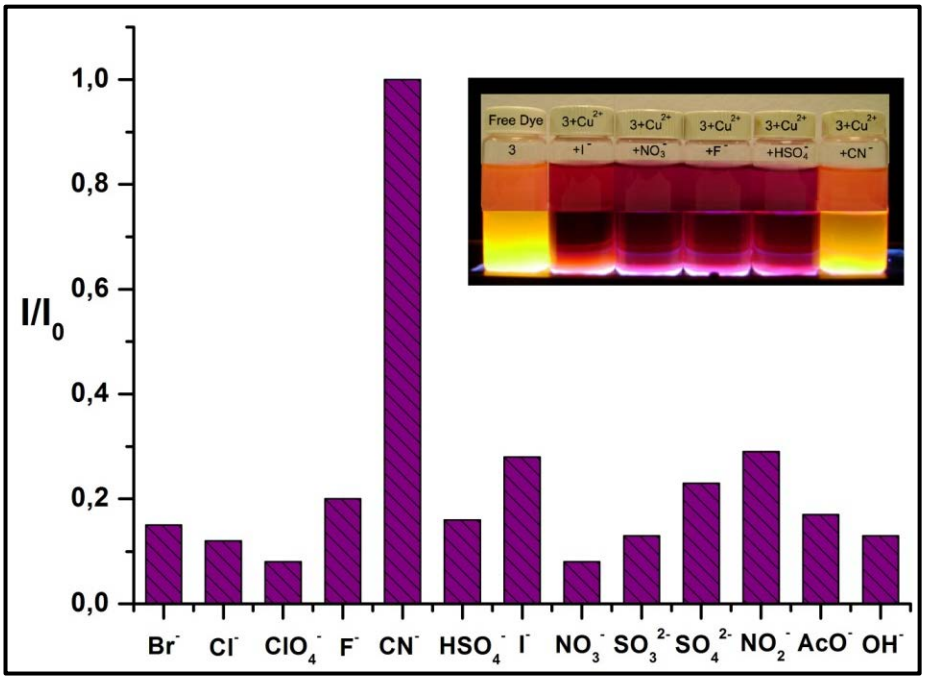

Figure 50. Emission ratios for the compound **28**+Cu(II) obtained in the presence of different anions. The chemosensor was excited at 530 nm and ratio of emission data at 547 nm was calculated. Inset shows the appearance of the indicated solutions under ambient light (top) and under hand-held UV-lamp (360 nm)

The sensor is reversible, as the emission signal originates from the dynamic equilibriation of dipicolylamine-Cu(II) and tetracyanocuprate complex ions. While the sensory system described here requires co-solvents (THF-deionized water), as a sensing method, it detects cyanide ions present in water. It is evident that the same sensing principle would be in effect in 100 % aqueous solutions as long as the dye component is also freely soluble in water.

3.4. Experimental Details

General: ^{1}H NMR and ^{13}C NMR spectra were recorded on Bruker DPX-400 (operating at 400 MHz for ^{1}H NMR and 100 MHz for ^{13}C NMR) in $CDCl_3$ and DMSO-d_6 solvents with tetramethylsilane as internal standard. All spectra were recorded at 25^{o}C and coupling constants (*J values*) are given in Hz. Chemical shifts are given in parts per million (ppm). Absorption spectra were performed by using a Varian Cary-100 spectrophotometer. Fluorescence measurements were conducted on a Varian Eclipse spectrofluometer. Mass spectra were recorded at the Ohio State University Mass Spectrometry and Proteomics Facility, Ohio, U.S.A. Reactions were monitored by thin layer chromatography using Merck TLC Silica gel 60 F_{254} Silica gel column chromatography was performed over Merck Silica gel 60 (particle size: 0.040-0.063 mm, 230-400 mesh ASTM). Quantum yield of compound **28** was determined in EtOH by using Rhodamine 6G as a reference dye.

3.4.1. UV-vis and Fluorescence Titration Experiments

Titrations of 28 with Cu(II) ion : 3 mL solution of 3 ($1x10^{-6}$ M) in THF was placed in a 10.0 mm quartz cell and to this solution was added $Cu(OTf)_2$ ($3x10^{-4}$ M in THF) in 2 μL portions (0, 0.2, 0.4, 0.6, 0.8, 1.0, 1.2, 1.4, 1.6, 1.8, 2.0 μM). After each addition, UV-vis absorption and fluorescence spectra were recorded at room temperature (λ_{ex}: 530 nm for **28**)

Titrations of 28 + Cu(II) with CN^- ion : A solution of NaCN ($1x10^{-3}$ M) in water was prepared in distilled water. 3 mL solution of **28** ($1x10^{-6}$ M) was placed in a 10.0 mm quartz cell and to this solution was added 20 μL of $Cu(OTf)_2$ ($3x10^{-4}$ M in THF) to quench the fluorescence of fluorophore. The solution of NaCN ($1x10^{-3}$ M) was added in portions (total volume ; 10,20,30,35,40,45,50,55,60 μL : 3.3, 6.7, 10, 11.7, 13.3, 15, 16.7, 18.3, 20 μM) and after each addition UV-vis absorption and fluorescence spectra were recorded at room temperature (λ_{ex}: 530 nm for **28**)

Fluorescence titrations of 28 + Cu(II) with other anions **:** 3 mL solution of **28** ($5x10^{-6}$ M) in THF was placed in a 10.0 mm quartz cell. 20 μL of $Cu(OTf)_2$ ($1.5x10^{-3}$ M in THF) was added to quench the fluorescence of the solution. 50 μL portion of the solution of different anions prepared in distilled water ($6x10^{-3}$ M) was introduced respectively and fluorescence spectra were recorded at room temperatıre (λ_{ex}: 530 nm for **28**)

3.4.2. Synthesis

8-(Chloromethyl)-Bodipy (26): To a 500 mL round-bottomed flask containing 250 mL argon-degassed CH_2Cl_2 were added 2,4-dimethyl-3-ethyl pyrrole (11.4 mmol, 1.5 g) and chloroacetyl chloride (5.7 mmol, 0.64 g) and the resulting mixture was stirred for 2 hours at room temperature. 8 mL of Et_3N and 10 mL of $BF_3.OEt_2$ were successively added and after 30 min, the reaction mixture was washed three times with water and carefully dried over anhydrous Na_2SO_4. The solvent was evaporated under vacuum at room temperature and the residue was purified by silica gel column chromatography using 3:1 Toluene : Hexanes as the eluant. Red solid (0.32 g, 16%).
^{1}H NMR (400 MHz, $CDCl_3$) δ_H 4.75 (2H, s, CH_2Cl), 2.46 (6H, s, CH_3), 2.39 (6H, s, CH_3), 2.32 (4H, q, J = 7.6 Hz, CH_2), 1.00 (6H, t, J = 7.6 Hz, CH_3).
^{13}C NMR (100 MHz, $CDCl_3$) δ_C 155.0, 136.3, 134.3, 133.5, 131.0, 37.9, 17.1, 14.7, 13.9, 12.6 ppm

8-{[Bis(pyridin-2-ylmethyl)amino]methyl}-Bodipy (28): To a solution of **(26)** (0.57 mmol, 0.2 g) in 200 mL acetonitrile was added KI (0.60 mmol, 0.10 g) and the resulting mixture was refluxed until TLC analysis indicated that all the starting material had been consumed. Solvent was evaporated and the reaction mixture was washed three times with water and chloroform. Organic phase was dried over anhydrous Na_2SO_4. Red solid obtained from the evaporation of the solvent was used in the next step without further purification. To a 250 mL round bottomed flask containing 100 mL acetone were added **(27) (**0.57 mmol, 0.25 g), di(2-picolyl)amine (0.57 mmol, 0.11 g) and potassium carbonate (0.57 mmol, 0.9 g) and the resulting

suspension was refluxed until TLC analysis indicated that **(27)** had been consumed. Reaction mixture was cooled to room temperature and solvent was removed by evaporation. Water was added and extracted with (3 x 100 mL) chloroform. Organic phase was dried over anhydrous Na_2SO_4 and evaporated. The residue was purified by silica gel column chromatography using Chloroform : Methanol (97 :3) as the eluent. Red solid (0.14 g, 48%).

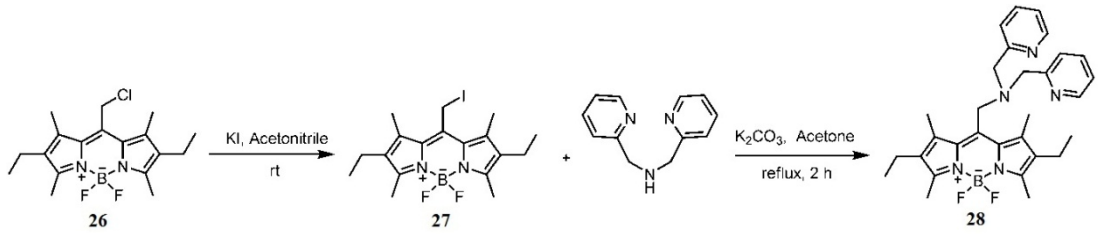

26 **27** **28**

^{1}H NMR (400 MHz, $CDCl_3$) δ_H 8.55 (2H, d, *J* = 4.8 Hz, ArH), 7.63 (2H, t, *J* = 6.8 Hz, ArH), 7.23 (2H, d, *J* = 7.8 Hz, ArH), 7.18 (2H, t, *J* = 6.2 Hz, ArH), 4.24 (2H, s, C*H*$_2$), 3.92 (4H, s, C*H*$_2$), 2.50 (6H, s, C*H*$_3$), 2.40 (4H, q, *J* = 7.6 Hz, C*H*$_2$), 2.35 (6H, s, C*H*$_3$), 1.05 (6H, t, *J* = 7.5 Hz, C*H*$_3$).

^{13}C NMR (100 MHz, $CDCl_3$) δ_C 158.2, 153.3, 148.8, 138.4, 137.3, 136.3, 133.1, 132.8, 124.1, 122.1, 57.2, 48.9, 17.2, 14.8, 13.7, 12.5 ppm

MS (TOF-MS-ES): m/z: : Calcd: 538.293 $[M+Na]^+$, Found: 538.291 $[M+Na]^+$ Δ=3.7 ppm.

CHAPTER 4

4. Expanded Bodipy Dyes: Anion Sensing Using a Bodipy Analog with an Additional Difluoroboron Bridge

This work is partially described in the following publication:

Guliyev, R.; Ozturk, S.; Sahin, E.; Akkaya, E.U. *Org. Lett*. **2012**, *14*, 1528-1531

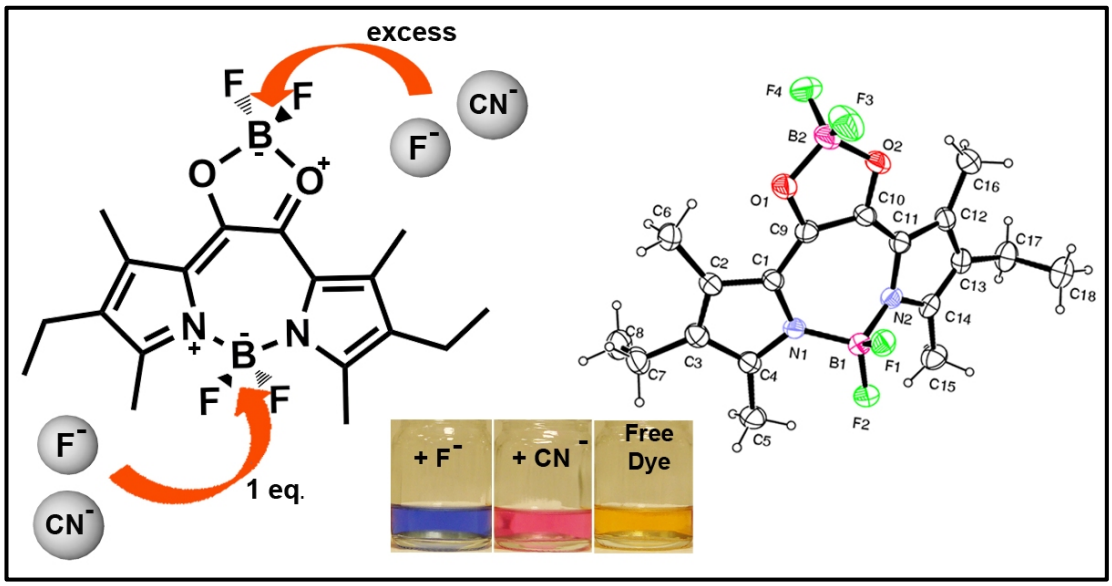

4.1. Objective

In this study, we present our work in the expansion of central Bodipy ring via a rational approach. Oxalyl-tethered pyrroles can be doubly bridged with two difluoroboron chelating units to yield bright orange dyes. Interestingly, in polar organic solvents, the addition of fluoride and cyanide anions result in reversible detachment of the otherwise stable difluoroboron bridges, displaying sharp changes in color. In other words, in this approach, the relief of distorted structure of boron bridges by fluoride/cyanide addition plays a key role in the recognition process. The structural characterization as well as sensing performance of this novel compound was investigated by ^{11}B NMR, absorption spectroscopic and mass spectrometric techniques.

4.2. Introduction

Within the last decade or so, Boron-dipyrrin (a.k.a., BODIPY, BDP, boradiazaindacene) dyes are having a *bona fide* renaissance after two decades of hiatus. This renewed interest is fueled by both new methodologies in derivatization and potential applications of these derivatives in ion sensing and signaling,[145] energy transfer and light harvesting,[146] photodynamic therapy,[147] dye-sensitized solar cells,[148] and non-linear optical properties,[149] to name just a few.

Once, just a class of fluorescent dyes limited by the repertoire of a single commercial supplier,[150] Boron-dipyrrins is now being compared to porphyrins in diversity, scope and function. The parent dye has been modified in many ways, including somewhat expanded versions; with pyridines instead of pyrroles were reported.[96] The central 6-membered ring however, was not altered in any of these constructs. As a part of our ongoing efforts to diversify boron-dipyrrin applications and find novel tactics of derivatization, we wanted to explore the effect of expanding the central chelate ring on absorption and fluorescence characteristics, in addition to potential signaling opportunities.

Designing a chemosensor selective to a specific anion is still a considerable challenge. A selective chemosensor for fluoride ion would be very relevant, since monitoring its concentration is important. Rapid assessment of fluoride ion concentration in drinking water, consumer products or in the environment is important, considering many detrimental health effects at elevated fluoride concentrations.[151,152] This challenge has been addressed using many strategies,[153,154] and colorimetric reagents are viable candidates for such analytic evaluations. One of the interesting sensing strategies for fluoride recognition is the usage of (Lewis acidic) boron compounds. Fluoride anion basically interacts with these molecules to form the corresponding fluoroborate species, and generates a signal.[155] Similarly, herein, we propose a modified Bodipy derivative as boron containing signaling unit.

4.3. Results and Discussions

In this study, an interesting and novel ethyl-extended Bodipy analog was synthesized. The relief of distorted structure of boron bridge on fluoride and/or cyanide addition, play a key role in the colorimetric responses, within the presented approach. Obtaining the seven-membered central ring, that was bridged by difluoroboron chelating unit, was the important step of the synthesis.

One promising path to an expanded central ring of the Boron-dipyrrin dyes was to tether two pyrroles with oxalyl chloride. To minimize any side reactions, we chose to start with a pyrrole with blocked reactive positions, i.e., 2,4-dimethyl-3-ethylpyrrole. The reaction with oxalyl chloride proceeded smoothly, and without isolating the intermediate, we added BF_3-etherate complex (Figure 51).

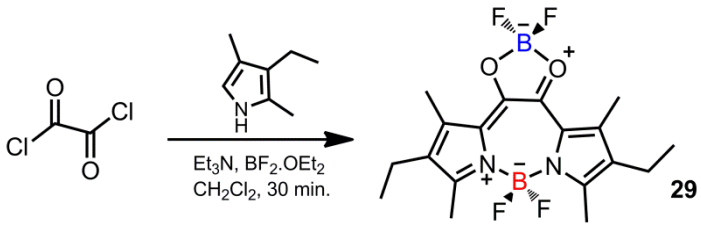

Figure 51. Synthesis of the target compound **29**

Following the usual work-up (details of the synthesis will be presented in the experimental section), the major product (**29**) turned out to be a non-fluorescent, bright red-orange product. While proton and carbon NMR spectra did not produce conclusive results regarding the exact chemical structure of the molecule, high resolution mass spectrometry (will be discussed within coming paragraphs) and finally X-ray crystallography provided definitive information about the structure. The product was indeed an expanded core Boron-dipyrrin dye (Figure 52).

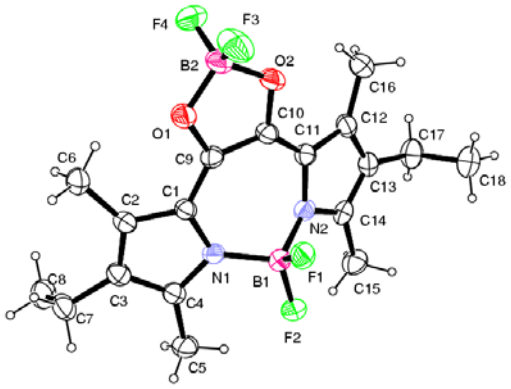

Figure 52. Ortep drawing of the compound **29**. The BF_2 bridge connecting two pyrroles is tilted out of planarity

Single crystals suitable for X-ray structure analysis were obtained by the slow evaporation of CH_2Cl_2 solutions at ambient temperature. The structure has some interesting features: both boron bridges display distorted tetrahedral geometry, with somewhat unequal B-F bond lengths and O-B-O bond angle of 103.4°. The molecule is not planar, with an approximate torsion angle of 25.3° for B_1-N_2-C_{11}-C_{10}. Thus, the expansion in the Bodipy ring tilts the BF_2 bridging two pyrrols above the plane defined by the rest of the molecule.

Apart from the X-ray analysis, ^{11}B-NMR was also highly informative. Boron atom has two isotopes, ^{10}B (I=3) and ^{11}B (I=3/2) with the 20% and 80% abundances, respectively. Both of them are NMR active nuclei ('I' is nonzero) and exhibit quadrupole moment. Due to this quadrupolar nature, usually broad signals are observed in their spectra. However, if the boron atom is located in the center of the highly symmetrical species (i.e. tetrahedral and/or octahedral), quadrupole moments

of ^{10}B and ^{11}B do not affect the spectra and the signals appear very sharp. Relatively small electric field gradient at the central boron nucleus makes this possible.[156]

In the ^{11}B NMR spectrum of **29**, two distinct boron nuclei at δ 1.68 ppm (internal reference BF_3-Et_2O) and 6.30 ppm are clearly identifiable. While one of the boron centers resonates as a triplet at 1.68 ppm, a broad peak at 6.30 ppm is observed for the other boron nucleus (Figure 53). The observed triplet originates from the coupling between ^{19}F (I=1/2) and ^{11}B (I=3/2). The B-F (^{11}B, ^{19}F) coupling constants highly depend on the ligands bound to the boron nuclei.[157,158]

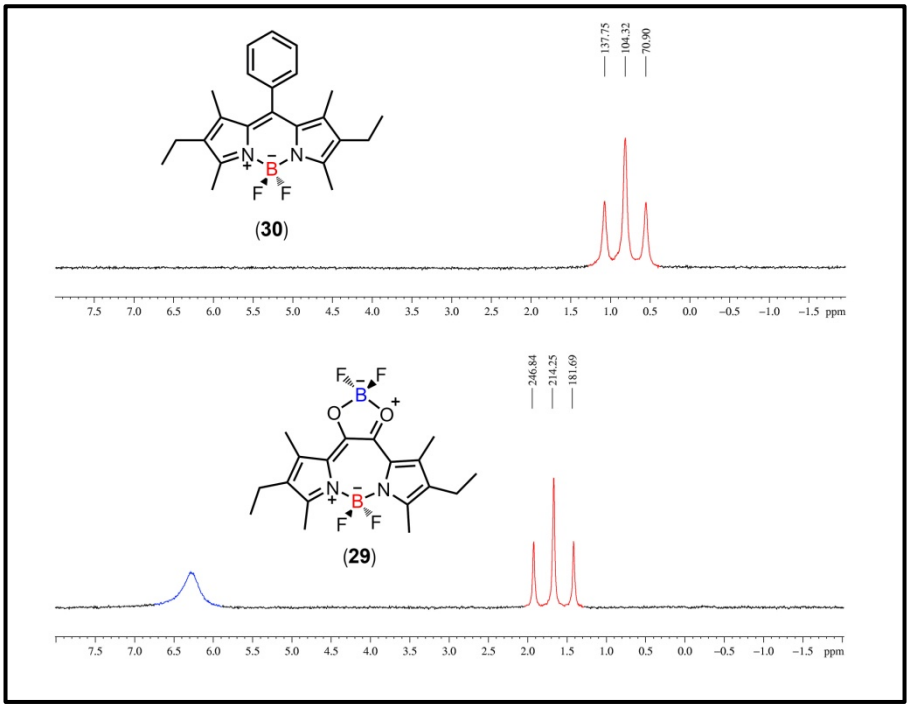

Figure 53. ^{11}B NMR spectra of the reference (**30**) and the target compound (**29**) recorded in $CDCl_3$ at room temperature. The expected triplet is observed which originates from the coupling between ^{19}F (I=1/2) and ^{11}B (I=3/2)

In comparison to a fairly typical Bodipy dye (compound **30**), which contains only one boron bridge, the peak which appears as a triplet, can be assigned to the boron nucleus connected to the two pyrrole nitrogens (Figure 53). B-F coupling constants for the expanded Bodipy **29** and the model compound **30** are very similar (32.6 Hz and 33.4 Hz, respectively), showing that they are more or less identical in terms of substituent groups.

^{19}F-NMR is also supportive of the ^{11}B-NMR peak assignment (Figure 54). ^{19}F is an NMR active nucleus with the nuclear spin value of 1/2. It is similar to the proton NMR which has the same nuclear spin (I=1/2). ^{19}F-NMR spectrum recorded for the target compound **29**, displays two sets of nonequivalent fluorine atoms, one of which is a standart quartet signal (at -132.5 ppm) that is also observed in the reference compound **30**. The other one is a singlet at -151.8 ppm, suggesting the presence of an oxygen atom adjacent to boron bridge.[159]

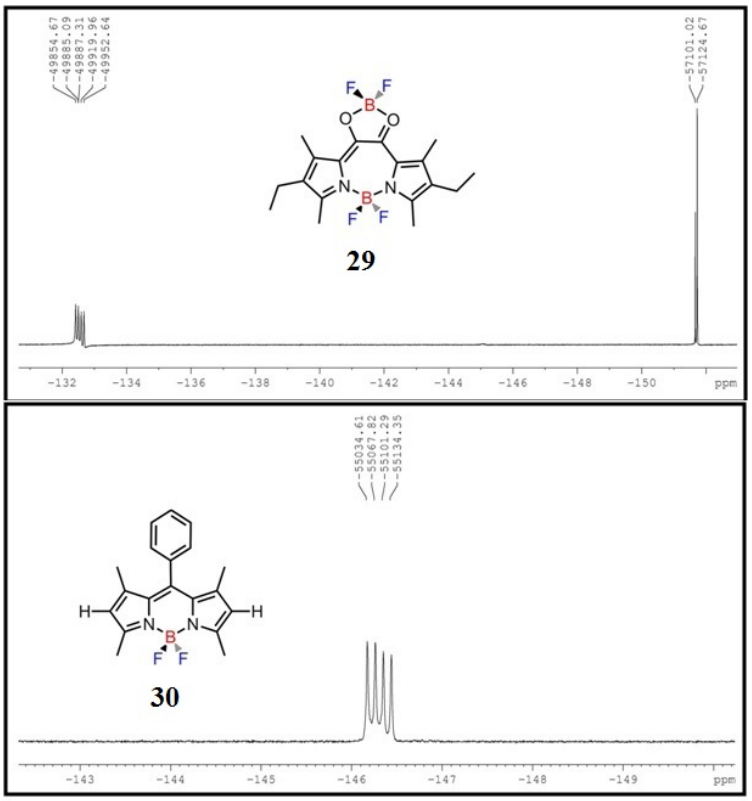

Figure 54. ^{19}F NMR spectrum of compound **29** and reference Bodipy compound (**30**) recorded in $CDCl_3$ at room temperature. The standart quartet is observed which originates from the coupling between ^{11}B (*I*=3/2) and ^{19}F

The other less intense singlet at -151.7 ppm is due to the less abundant NMR active ^{10}B isotope (20%). While for the 20% of molecules that contain ^{10}B, that ^{19}F nucleus resonates at -151.7 ppm, rest of the molecules that contain ^{11}B, resonance of the same nucleus is a little bit shifted upfield (-151.8). The isotope effect is also valid for the fluoride atoms resonating as a quartet signal (at -132.5 ppm). However, the septet originating from the ^{10}B (I=3) isotope coupling is obscured under the quartet peak.

The chemical shift and splitting pattern of the resonating fluoride nuclei bound to the boron atom depends on the neighboring ligands bound to the boron center. That's why while the fluoride nuclei, bound to boron atom bridging two pyrrole nitrogens, resonate as a quartet at -132.5 ppm, the other set of fluoride, bound to the boron center bridging two oxygens, appear as a singlet 151.8 ppm. In order to confirm the chemical shift of ^{19}F nucleus which is bound to the oxygen coordinated boron atom, we did the control experiment by measuring the ^{19}F NMR of the borontrifluoride diethyletherate (Figure 55). That molecule contains three equivalent fluorine atoms which resonate at -153 ppm as a broad singlet. This result is in accordance with our pick assignment that we made for compound **29**.

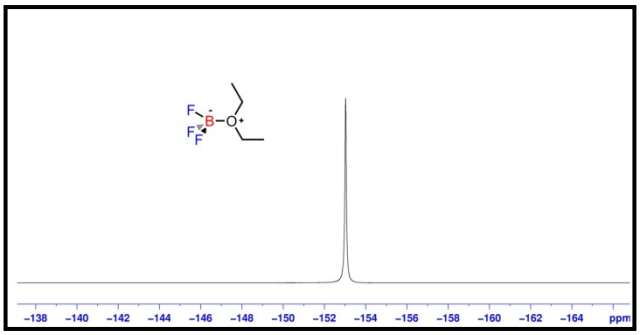

Figure 55. ^{19}F NMR spectrum of Boron trifluoride diethyl etherate recorded in $CDCl_3$ at room temperature

In hopes of creating a signal for the interaction of anions with the dye, we wanted to systematically study the spectral behavior of the solutions of **29** in the presence of selected anions. We suspected that one or both of the BF_2 bridges might be reversibly disconnected concomitant to a distinct spectral signature. We know that, in a regular Bodipy skeleton sp^3 hybridized boron atom is tetrahedrally bonded and is a member of six-membered ring, which makes it more stable. It is unlikely for a fluoride anion to disrupt that ring upon complexation with central boron atom. To do so, perhaps very high concentrations of anion is needed. This time in order to make the boron center more labile to fluoride binding, we expanded the central ring size to seven membered ring. As a result the shape (or structure) of boron center will be distorted tetrahedron. Thus, nucleophilic fluoride attack will be more feasible and hopefully colorimetric recognition of analyte will be achieved.

Before moving on to the absorption spectroscopy, compound **29** deserves a close-look in terms of fluorescence characteristics. Unfortunately, it is not a fluorescent compound. We know that, emission characteristic of any given molecule is dependent on a number of factors. For example, dipyrrins are not emissive, but when bridged with BF_2 units they become fluorescent. This is due to rigidification of the compound, which prohibits excited state rotation around the methine carbon. We might speculate that the out of plane BF_2 linkage in compound **29** may be more prone to vibrational deexcitation, and therefore become less emissive. On the other hand, reference compound **30** is emissive as most other Bodipy derivatives.

Coming back to the absorption experiments, a careful analysis of anion promoted changes were carried out, in order to explore ion response of the expanded Bodipy compound **29**.

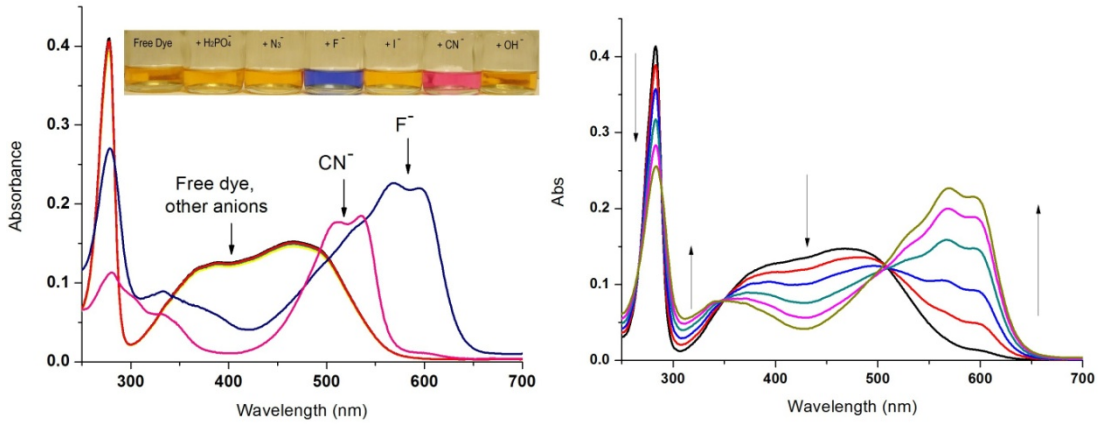

Figure 56. Absorbance spectra of target compound **29** (10.0 µM) in chloroform in the presence of several anions (left) and titration of it with the increasing fluoride (TBA salt) concentration (0-16.0 µM) in chloroform (right)

To do so, we added various anions in the form of TBA (tetrabutylammonium) salts into dilute chloroform solutions of **29** (10.0 µM). During the anion selectivity experiments (Figure 56, left) 16.0 µM fluoride ion and 40.0 µM of the other anions were used. Photograph of selected solutions under ambient light conditions in chloroform was set as inset picture in figure 56 (left). CN^- ions also showed spectral changes, but the most obvious change was obtained with fluoride anions, the solution immediately turns purple on the addition of fluoride. Fluoride seems to be unique in

generating such an intense spectral peak at the long wavelength region of the spectrum (at 600 nm). CN^- ions resulted in a less redshifted peak near 520 nm.

Titration with varying concentrations of F^- ions in the form of tetrabutylammonium salt in chloroform (Figure 56, right) clearly shows progressive decrease of the broad band with a peak at 465 nm. At the same time another set of peaks at longer wavelengths (565 and 600 nm) appear. Clean isosbestic point suggests a conversion between two distinct forms. The conversion is fast and reversible, addition of BF_3-Et_2O in chloroform reverses the process and the spectral features of compound **29** are restored. On closer inspection, we found out that excess F^- ion addition gradually resulted a similar absorption peak around 520 nm (as in the cyanide case) while the longer wavelength peak disappears (Figure 57).

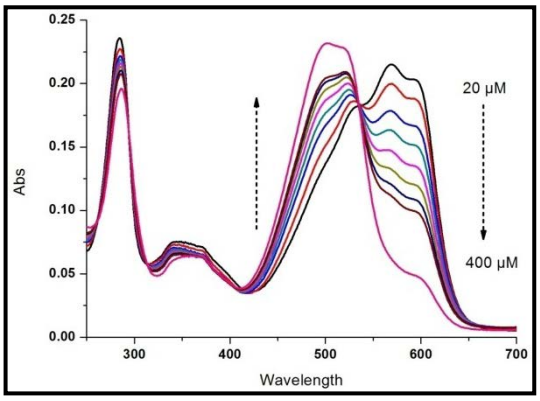

Figure 57. Titration of **29**+F^- (10.0 µM) with the increasing fluoride (TBA salt) concentration (20.0-400.0 µM) in chloroform

As it can be seen from the figure 57, elevated doses of fluoride resulted in a similar absorption profile as it was in the cyanide addition, suggesting the possible analogy between the final species of both cases. In order to understand the mechanism yielding this results, we performed some additional NMR and Mass spectometric analysis that will be briefly introduced within coming paragraphs.

First of all, a comparison between proposed compound **29** and the reference compound **30**, upon fluoride addition, was done in terms of ^{11}B NMR spectra. Reference compound **30**, a model Bodipy dye, showed no change in the ^{11}B-NMR spectrum upon addition of even 100 equivalents of fluoride anions (Figure 58).

Being a part of the six-membered ring makes the sp^3 hybridized boron center less prone to nucleophilic displacement. It is unlikely for fluoride anion to disrupt the ring through complexation with the central boron atom.

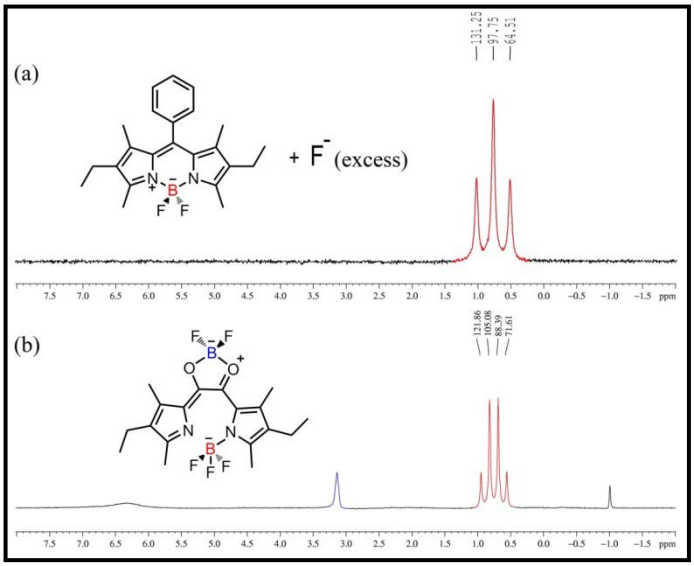

Figure 58. ^{11}B NMR spectra of the reference (**30**) and the target compound (**29**) after the addition of tetrabutyl ammonium fluoride are depicted (a and b)

However, expanded ring size (7-membered ring) distorts the perfect tetrahedral structure of the boron bridge, making it more labile to fluoride attack. As a result, gradual addition of fluoride ions lead to the decrease in the intensity of 6.3 ppm peak in ^{11}B NMR, with a concomitant increase of two new singlet peaks at approximately 3.1 and -1.0 ppm. Moreover, the triplet at 1.7 ppm is transformed into a quartet with the new chemical shift at about 0.8 ppm which can be assigned to partially coordinated BF_3 unit as shown in Figure 58.

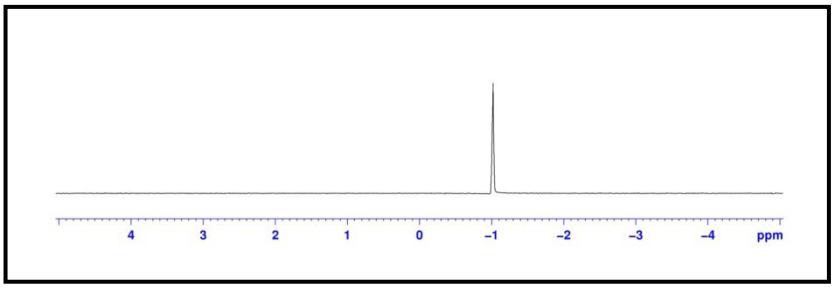

Figure 59. ^{11}B NMR spectrum of Tetrabutyl ammonium *Tetrafluoroborate* salt recorded in $CDCl_3$ at room temperature

The singlet peak at -1.0 ppm proves the formation of free BF_4^- anion in the solution. ^{11}B-NMR of the reference compound tetrabutylammonium tetrafluoroborate confirms that ^{11}B nucleus in the tetrafluoroborate anion resonates at -1.0 ppm without any splitting (Figure 59, previous page).

In order to understand the effect of added fluoride anion amounts, we carefully carried out NMR titration experiments observing the changes on the ^{11}B nuclei.

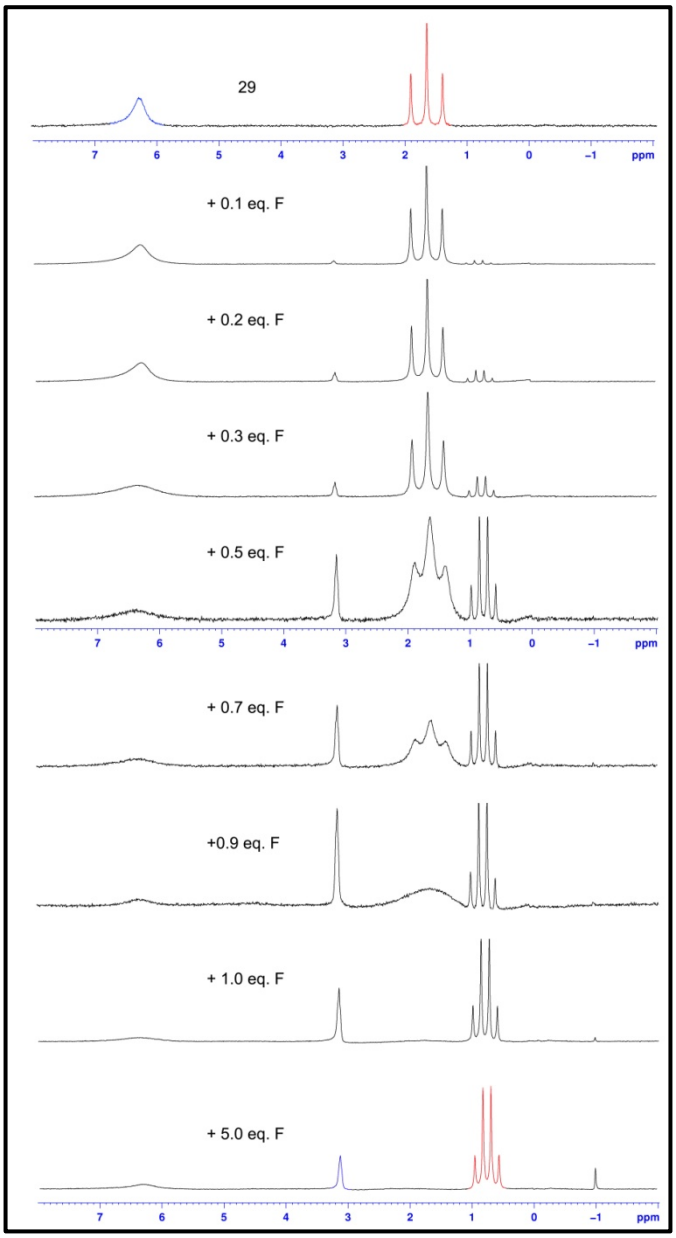

Figure 60. ^{11}B NMR spectra of **29** after the addition of increasing concentrations of TBAF (recorded in $CDCl_3$ at room temperature). The concentration of **29** is 12.6 mM

Analysis of NMR titration data illustrated above (Figure 60) suggests that at lower concentrations of F^- ions, initially, BF_2 unit bridging two pyrroles is detached. We claim so, because after addition of the 1.0 equivalent of fluoride, the triplet peak is fully converted to the quartet. Conversion of the triplet signal (at 1.7 ppm) to the corresponding quartet indicates the three neighboring fluorine nuclei splitting the boron peak into a quartet (at 0.8 ppm), and proposed intermediate species was depicted in Figure 61. Clear observation of the coupling constants suggests the existence of a covalent bond between boron and one of the pyrrole nitrogens. At higher concentrations, a new singlet appeared at -1 ppm, which is probably resulted from the removal of the second BF_2 unit in the form of BF_4^- anion. Since the excess fluoride ions detaches the second BF_2 bridge, a clean saturation point is not observed in the absorption spectra at lower concentrations (Figures 56 and 57).

Moreover, the broad signal at 6.3 ppm is shifted to 3.1 ppm as the concentration of the fluoride anion increased during the titration experiments, and this new broad singlet at 3.1 ppm indicates the existence of the boron atom that is covalently attached at least to one of the oxygens in the molecule (Figure 61). Since the triplet peak at 1.7 ppm is transformed to quartet upon 1.0 eq. addition of TBAF, we proposed that the above mentioned broad signal shifting occurs due to the structural change originating from the cleavage of one of the N-B bonds.

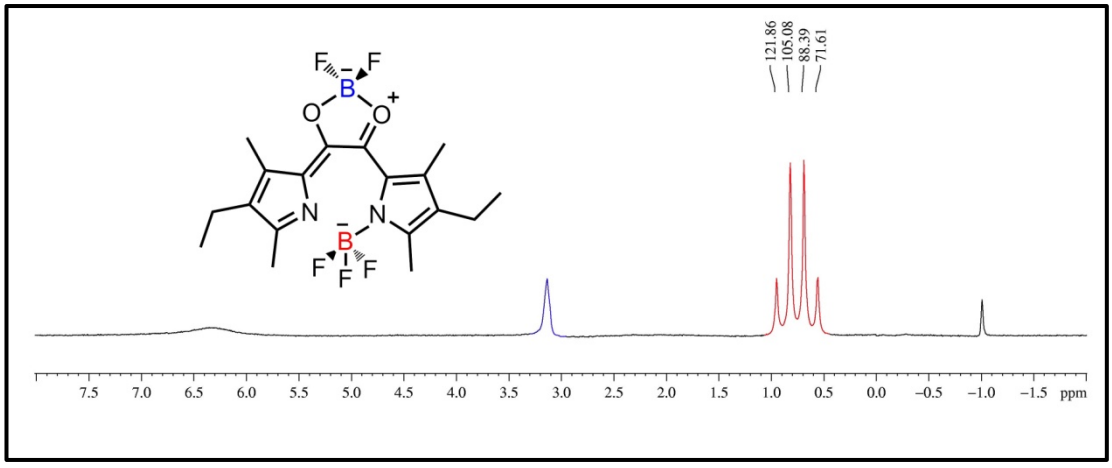

Figure 61. ^{11}B NMR spectra of the target compound (**29**) after the addition of tetrabutyl ammonium fluoride

Cyanide ions on the other hand, do not discriminate between the two bridges; both linkages are attacked with comparable rates resulting in a red solution (520 nm). The same aborption peak and color formed only with excess fluoride ions. Thus, both NMR spectra and absorption spectroscopy demonstrate that the differential reactivities of CN^- and F^- with two different boron centers is the reason for different absorbance signals.

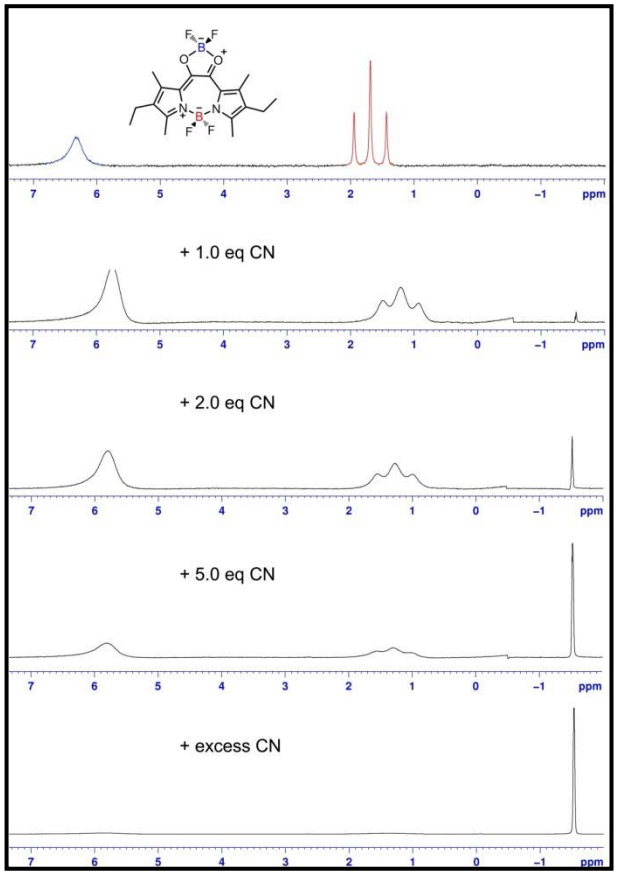

Figure 62. ^{11}B NMR spectra of **29** after the addition of increasing concentrations of TBACN (recorded in $CDCl_3$ at room temperature). The concentration of **29** is 12.6 mM (3.0 mg in 0.6 mL of $CDCl_3$)

The NMR titration experiments were also done for the cyanide ions. This time simultaneous decrease in the intensities of the regular peaks of **29**, and new emerging singlet peak at -1.5 ppm was observed. At higher concentrations of cyanide ions, both triplet and broad singlet peaks has disappeared, only the singlet peak has remained in the spectrum, which is most probably a cyanofluoroborate type anionic species (Figure 62).

Considering all the evidences above, we propose that, during the fluoride titration, one of the boron bridges (bridging two pyrroles) is forming a borate complex as an intermediate during titration. As the concentration of the analyte increases, attack to the second the boron nucleus takes place and simultaneously boron bridges start to cleave off of the compound **29** in the form of tetrafluoroborate anion. Poor solubility of the intermediate species prevented further analysis by ^{11}B NMR spectra at higher fluoride concentrations, and made us to seek some extra evidence via Mass spectroscopy analysis (Figure 63).

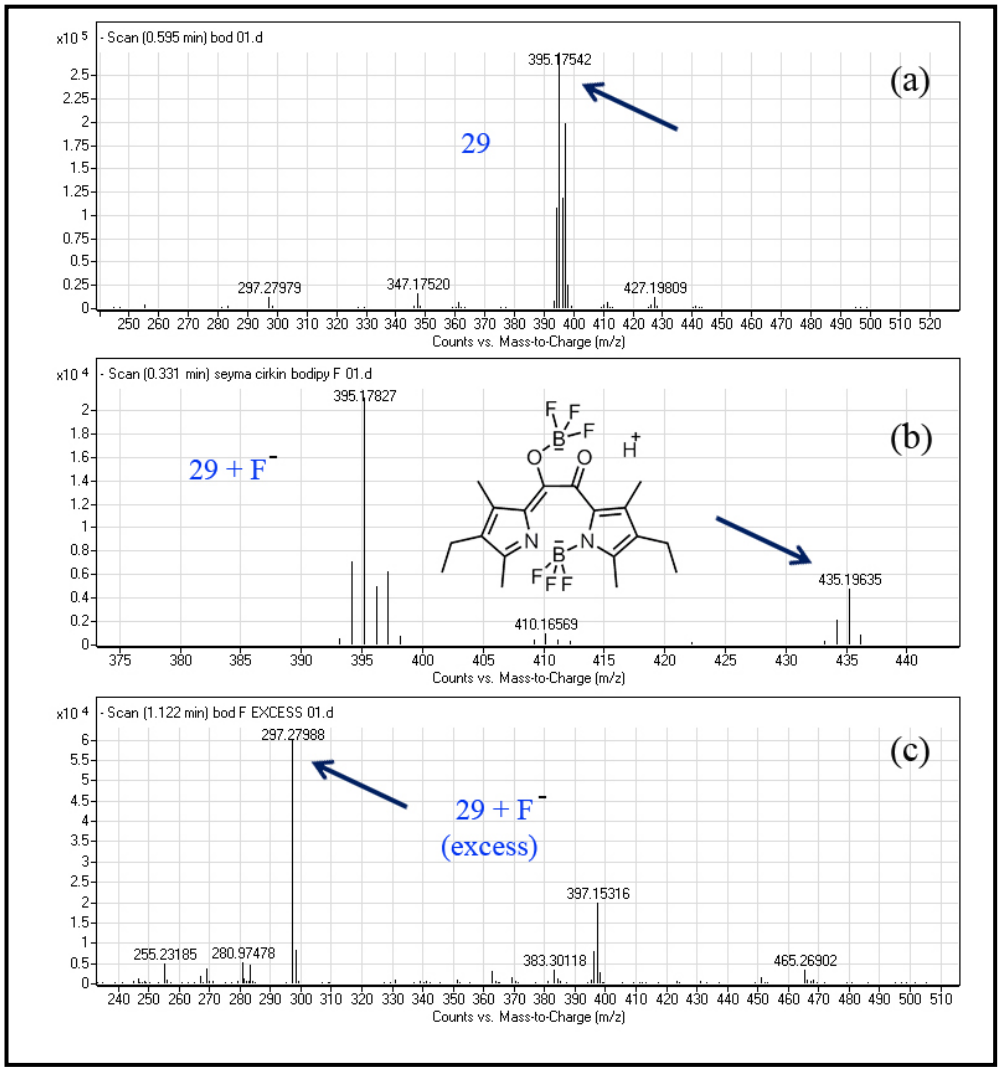

Figure 63. (a) MS (TOF - ESI) of compound **29**: Calcd: 396.1804, Found: 395.17542 $[M-H]^-$, Δ=7.1 ppm (b) MS (TOF - ESI) of compound **29**+4eq F: Calcd: 435.1855, Found: 435.1963$[M+H]^-$, Δ=15.7 ppm (c) MS (TOF - ESI) of compound **29**+excess TBAF

Same mechanism is also valid for the cyanide titration (supporting information). While higher concentrations are required for the response in the case of cyanide anion, the cleavage of the boron bridges is much faster compared to that of the fluoride case. In other words, cyanide anion follows the same mechanism as fluoride with one difference, faster rate in both detachment reactions, which results in higher detection limit. Unfortunately, we couldn't grow single crystals of the intermediate species that are suitable for x-ray analysis and the intermediate complexes formed after the addition of analytes (fluoride and cyanide) do not show any emission properties.

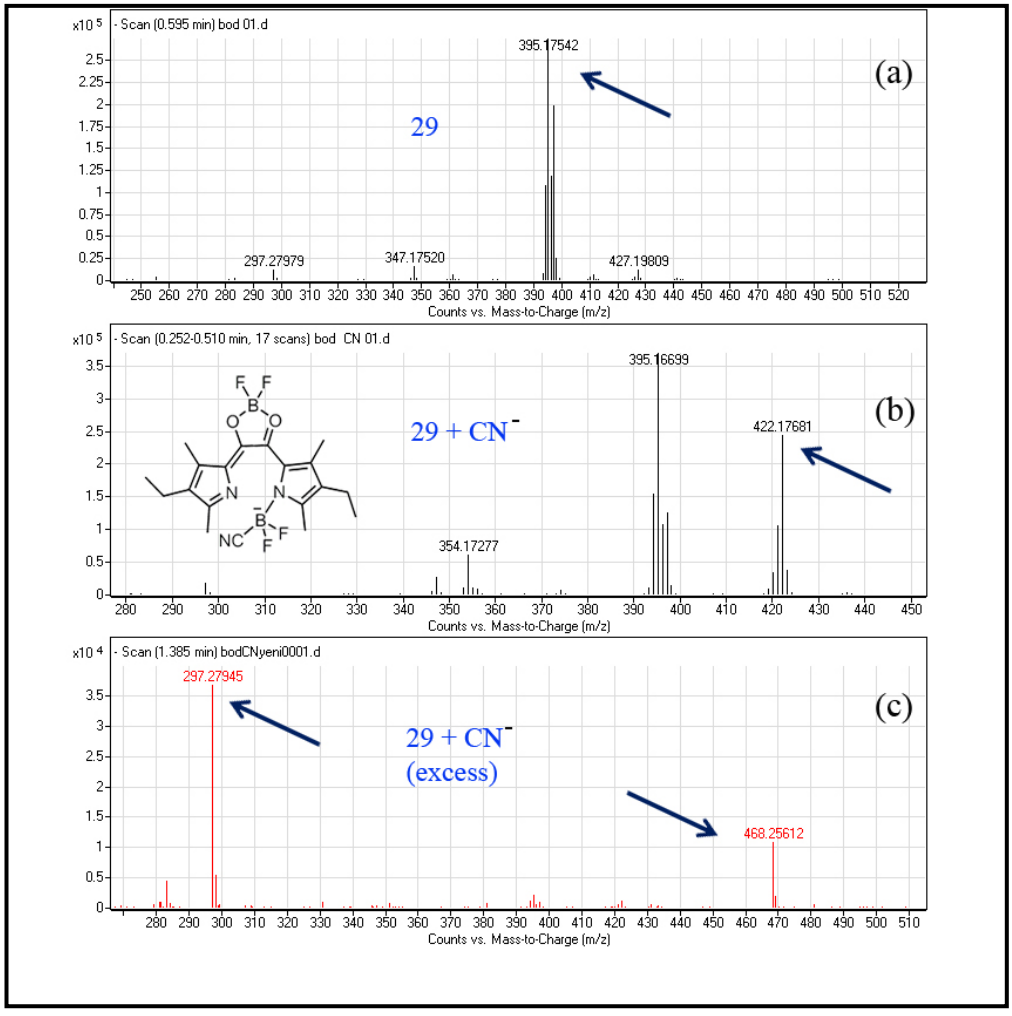

Figure 64. (a) MS (TOF - ESI) of compound **29**: Calcd: 396.1804, Found: 395.17542 $[M-H]^-$, Δ=7.1 ppm (b) MS (TOF - ESI) of compound **29**+4eq CN: Calcd: 423.1913, Found: 422.17681 $[M-H]^-$, Δ=15.7 ppm (c) MS (TOF - ESI) of compound **29**+excess TBA**CN**

In order to provide more evidence, we also tried to prove the formation of intermediate species (after the addition of fluoride and/or cyanide anions, Figures 63 and 64 respectively) by mass spectroscopy. For the cyanide case, we were able to identify the peak belonging to the [1+CN]. For the fluoride reaction, we were able to detect [1+2F] at 435 m/e. When excess analyte was added, we were able to observe [1-2H-2BF2] at 297 m/e (both for CN and F cases).

4.4. Experimental Details

General: ^{1}H NMR, ^{13}C NMR, ^{11}B NMR and ^{19}F NMR spectra were recorded on Bruker DPX-400 multiprobe NMR (operating at 400 MHz for ^{1}H NMR, 100 MHz for ^{13}C NMR, 128 MHz for ^{11}B NMR and 376 MHz for ^{19}F NMR) in $CDCl_3$ with tetramethylsilane and borontrifluoride as internal standards. All spectra were recorded at 25 ^{o}C and coupling constants (*J* values) were given in Hz. Chemical shifts were given in parts per million (ppm). Splitting patterns are designated as s (singlet), d (doublet), t (triplet), q (quartet), m (multiplet), and p (pentet). All the ^{13}C spectra were recorded with simultaneous decoupling of proton nuclei. Quartz NMR tubes were used while measuring the ^{11}B nucleus. Mass spectra were recorded on Agilent Technologies 6530 Accurate-Mass Q-TOF LC/MS. UV-Vis Absorption spectra were performed by using a Varian Cary-100 spectrophotometer. Reactions were monitored by thin layer chromatography using Merck TLC Silica gel 60 F_{254}. Silica gel column chromatography was performed over Merck Silica gel 60 (particle size: 0.040-0.063 mm, 230-400 mesh ASTM). All other reagents and solvents were purchased from Aldrich and used without further purification.

NMR Titration Experiment: The concentration of the compound **29** used in the NMR experiments is 12.6 mM (3.0 mg in 0.6 mL of $CDCl_3$). During the fluoride titration we gradually increased the concentration of the fluoride anion from 0.1 eq. to 1.0 equivalent. For the titrations with cyanide ions, the guest concentration is increased from 1.0 eq. to 5.0 equivalents.

4.4.1. Synthesis

Synthesis of Compound 29: To a 250 mL round-bottomed flask containing 100 mL argon-degassed CH_2Cl_2 were added 2,4-dimethyl 3-ethyl pyrrole (7.0 mmol, 0.86 g), and oxalyl chloride (3.5 mmol, 0.44 g) dropwise. Attained red color of the solution got darker with time. The reaction was stirred under N_2 at room temperature for 30 min. After that 5 mL of Et_3N and 5 mL of $BF_3.OEt_2$ were successively added and stirred for another 30 min. Then the reaction mixture was washed with water (3 x 300 mL) and dried over anhydrous Na_2SO_4. The solvent was evaporated and the residue was purified by silica gel column chromatography using EtOAc : Hexane (2 : 1) as the eluent, yielding the nonemissive compound as a red solid. (0.45 g, 33%).

^{1}H NMR (400 MHz, $CDCl_3$): δH 2.63 (6H, m, upper 2xCH3), 2.48 (4H, q, J = 6.9 Hz, 2xCH2), 2.44 (6H, s, 2xCH3), 1.10 (6H, t, J = 7.6 Hz, 2xCH3) ppm.

^{13}C NMR (100 MHz, $CDCl_3$): δC 167.8, 159.0, 148.3, 137.8, 129.1, 18.2, 15.1, 14.9 ppm

MS (TOF - ESI): m/z: Calcd: 396.1804 [M]+, Found: 395.17542 $[M-H]^-$, Δ=7.1ppm

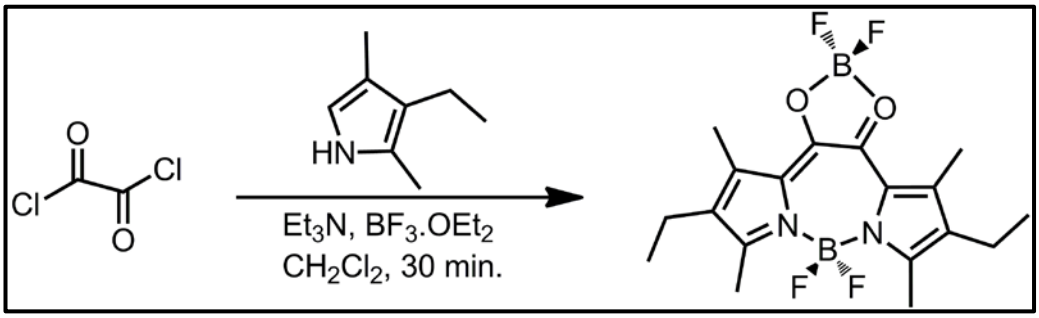

4.5. Conclusion

Our study has considerable number of features which would make this a valuable and broadly interesting work for readers. Successful use of heteronuclear NMR to elucidate the signaling mechanism in a chemosensor is very rare. In addition, Bodipy dyes are at the focus of considerable attention in recent years, straightforward access into ring expanded derivatives would be of interest just as a result of because of this. In addition, we unequivocally demonstrated that the compound **29** is a selective and sensitive chromogenic molecular sensor.

Considering the need for simple colorimetric reagents for anion sensing, the novel expanded Bodipy dye described here, is highly promising. The color changes are vivid, clearly distinguishing fluoride and cyanide ions in the presence of competing ions. Embedded to the polymeric matrix, this compound or a derivative is likely to find applications as anion sensors. In addition, further substitution on the Bodipy core is likely to broaden the palette of colors available in anion sensing. Our work in that direction is in progress.

CHAPTER 5

5. Selective Manipulation of ICT and PET Processes in Styryl-Bodipy Derivatives: Applications in Molecular Logic and Fluorescence Sensing of Multiple Metal Ions

This work is partially described in the following publication which was featured on the front cover of JACS:

Bozdemir, O.A.; **Guliyev, R**.; Buyukcakir, O.; Selcuk, S.; Kolemen, S.; Gulseren, G.; Nalbantoglu, T.; Boyaci, H.; Akkaya, E.U. *J. Am. Chem. Soc.* **2010**, *132*, 8029

5.1. Objective

Bodipy dyes allow straightforward derivatization to place both ICT and PET modulators on a single fluorophore. These modulators can then be selectively addressed by exploiting selective metal ion/ligand interactions, resulting in signal changes which can be separately associated with ICT or PET processes. In addition, such designed systems eliminate the need for self-annihilating "inputs", the use of which in retrospect, look very crafty. In this work, we demonstrate that with a prior knowledge of respective binding affinities of metal ions for various ligands, it should be possible to design molecular logic gates using different metal ions as inputs. Styryl-modifications of Bodipy proved to be a useful reaction. In the three examples presented, this modification allowed us to place ICT donor functionalities at strategically important positions. The result is straightforward syntheses of the target molecules, with responses compatible with 3-input AND logic and, a molecular half-adder with non-annihilating inputs. Outputs compatible with XOR logic has been difficult to attain without the use of self-annihilating (such as acids and bases, either Lewis or Bronsted-Lowry) inputs, but in the half-adder described in this work, this is done by the differential selective interactions between the ligands and the metal ions selected. Keeping the logic gate correlation apart, our approach is offering an enticing potential for multianalyte chemosensors.

5.2. Introduction

Molecular logic research today is built on an initial recognition by de Silva[110] that fluorescence signals obtained in response to cations, could be considered to be analogous to the digital responses in electronic logic gates. Molecules can undergo changes in the ground or excited states, in response to modulators which can be other molecules, ions, or light of a certain wavelength. In most cases, these changes could then be signaled by changes in the emission intensity or wavelength and can be related to the operation of logic gates, *via* the familiar Boolean logic.[160] In addition, it has become apparent that logic gate design using molecules may not necessarily be

subject to the same limitations as the silicon-based analogs. One can design a single molecule which can simultaneously behave as two (or more) distinct logic gates, depending on the exact choice or definition of outputs.[161] On the other hand, while functional integration is possible within single molecule, at least partly because of input-output heterogeneity, integration of logic gates to implement more complex functions is far from being straight-forward. Nevertheless, molecular logic gates represent a true bottom-up approach for information processing at the molecular level. Strongest aspect of molecular logic gates is the fresh new look, which provides a novel mental platform to build new ideas.

More recently, the logic gates research is perhaps being redefined as of late, with an eye on the applications, most interesting targets being the small spaces such the inside of a cell, where silicon-based analogs are not expected to get in.[141] Among the possible signal modalities, changes in absorption or emission spectra are the most common one. Photoinduced electron transfer (PET) process was particularly useful in this regard, as the signal, depending on the special circumstances, was either an "on-off" or "off-on" type, resulting in a well-defined "digital" response. PET produces very sharp changes in the signal intensity, while keeping the emission wavelength unchanged.[162] Intramolecular charge transfer (ICT, a.k.a., PCT: photoinduced charge transfer) on the other hand, can be modulated in such a way to generate changes in the absorption or emission wavelengths, which proved to be very useful for superposed logic gates, sometimes referred to as wavelength-reconfigurable logic gates.[163]

The first contribution of Akkaya group to molecular logic gates in the year 2000,[164] broke the near monopoly of PET processes in the logic gate design. Molecular interactions, including cation binding were known to produce shifts in the absorption and emission peaks, but it was this article which first presented an explicit use of spectral shifts to harvest two distinct superposed logic gates out of a single molecular recognition phenomenon. This was simply done by choosing two different observation wavelengths, i.e. two different channels. Naturally, by finer adjustment of the parameters, more than two logic gates can be obtained.

ICT processes are of course, highly desirable for this kind of a design, as very large spectral shifts are the norm rather than exception in ICT-fluorophores with electron donor (or acceptor) ligands as integral parts of the π-systems. To increase signal diversity, it is possible to include both PET and ICT process on a single fluorophore. They have demonstrated an example of that approach a few years ago,[165] and it is a very straightforward path to molecular "half-subtractor" once the inputs were chosen to be self-annihilating. In that article, we also restated the obvious; which is the fact that the assignment of "1" to high signal and "0" to low signal is arbitrary both in molecular and silicon-based information processing. The reverse is equally acceptable, and known as "negative logic" in electronics. Annihilating inputs on the other hand, are quite convenient, when one needs to produce an XOR gate, but the use of such inputs (like a strong acid and strong base) in logic gates would have quite a limited value, with any consideration of "practicality". Especially in aqueous solutions, H^+ and OH^- are not independent variables. It must be self-evident that the inputs in a logic gate have to independent variables. With that kind of a perspective, it made a lot of sense for us to go back to the drawing board and find new designs for simple logic elements, with potential for integration and independently variable inputs. The key may be selectivity. Metal ions, with their inherent selectivities for ligands have been used as chemical inputs in many molecular logic gates. Metal ions are Lewis acids, and it is possible to make use of them as non-selective agents, just like ydrogen ions. However, accumulated knowledge of ligand design, and available quantitative data on metal-ligand affinities, should allow one to propose selective interactions in a mixture of metal ions with a molecule containing multiple ligating sites.[166] Selective targeting of different modulation sites within a fluorophore could be important for practical sensing applications as well.

The fluoroionophores of choice in this work is Bodipy-derived (Figure 65). Bodipy dyes have become a rising star of fluorophores in the fluorescent chemosensor community due to their remarkable properties such a high quantum yield and large extinction coefficients. But more importantly, these dyes are open to derivatization in a multitude of ways through recently expanding "Bodipy chemistry". Part of this versatile chemistry allowed us to design new Bodipy-based fluorescent molecules

with different ligands attached at locations where the modulation of ICT and PET processes can be achieved independently. This is not an easy synthetic task for most other fluorophores. But, with Bodipy dyes, it is just couple of well coordinated sequence of transformations.

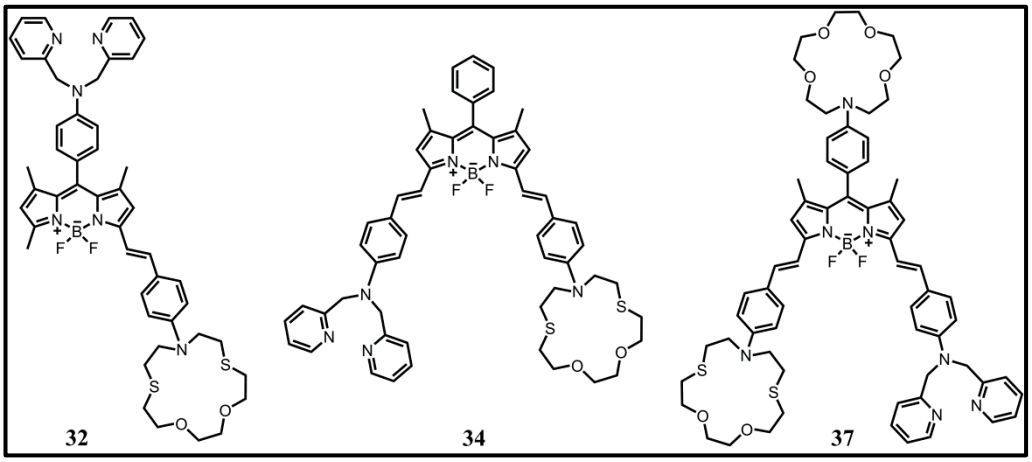

Figure 65. Target structures for two-input AND logic **32**, Half-Adder **34**, and three-input AND logic **37**

5.3. Synthesis

We targeted three different styryl-Bodipy derivatives **32**, **34**, and **37** (Figure 65). In designing these compounds, we kept in mind that the *meso*-substituents are more likely to interfere with the excited state processes only, partly because of the orthogonal arrangement of *meso*-(8)-phenyl moiety under the steric influence of the neighboring (1,7) methyl groups, and partly due to the fact that in the HOMO of the Bodipy chromophore, C8 position is a nodal point. Therefore, right chosen substituents at the *meso* position are expected to alter the efficiency of photoinduced electron transfer process (PET), but not intramolecular charge transfer (ICT). Because, ICT requires a conjugation between substituent and the dye molecule.

With this consideration, in the design for compound **32** (Figure 66) the dipicolylamine ligand which is known to be selective for Zn(II)[167] ions was placed at the 8-position (*meso*) of the Bodipy core.

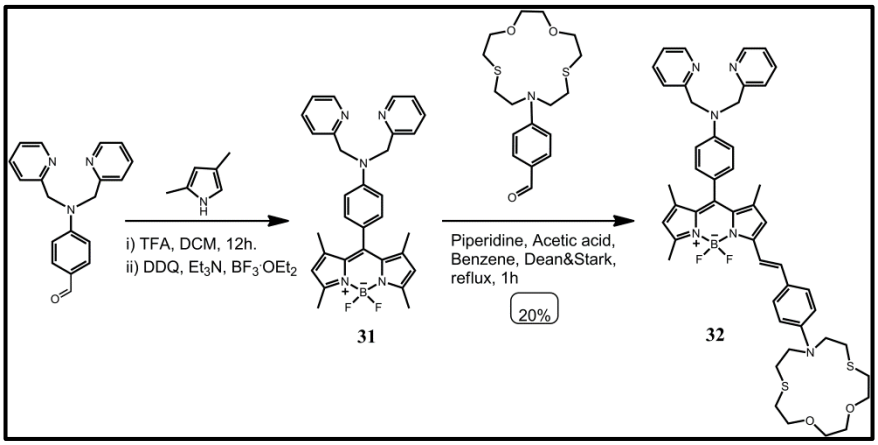

Figure 66. Synthesis of target compound **32**

This is easily accomplished by the reaction of dipicolylamine-substituted benzaldehyde, which was synthesized according to the literature procedure,[168] with 2,4-dimethylpyrrole under the usual conditions for Bodipy synthesis. The isolated Bodipy dye **31** was then reacted with the known thiazacrown-tethered benzaldehyde[169] under Knoevenagel conditions, thus placing a strong ICT donor in full conjugation to the Bodipy core. The binucleating monostyryl-Bodipy (**32**) obtained in this way, was purified by column chromatography.

The synthesis for the second target compound started with the known Bodipy dye, 4,4-difluoro-8-phenyl-1,3,5,7-tetramethyl-4-bora-3a,4a-diaza-s-indacene (Figure 67).

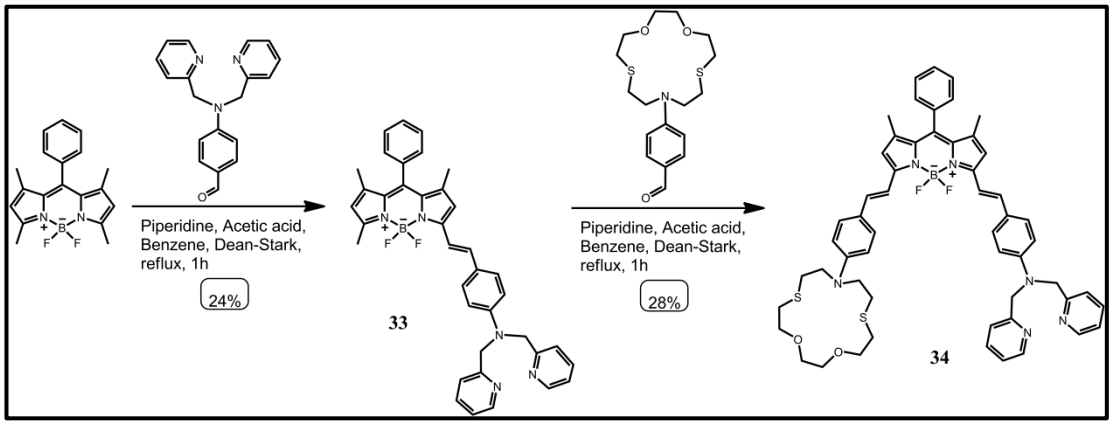

Figure 67. Synthesis of target compound **34**

Consecutive Knoevenagel condensation reactions of the starting material with the two aromatic aldehydes mentioned above yielded first compound **33** and then **34** (Figure **67**). In this way, two ICT donors which can be modulated with two different metal ion modulators were installed on the fluorophore in full conjugation.

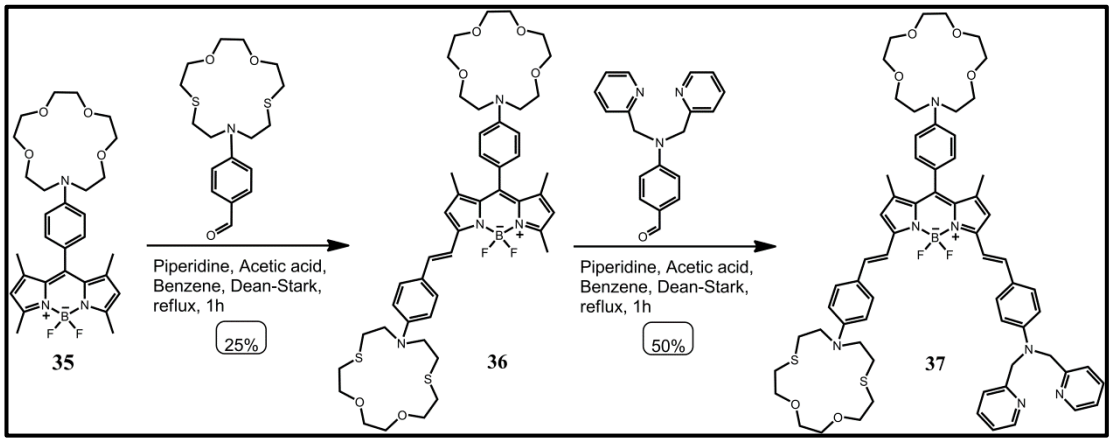

Figure 68. Synthesis of target compound **37**

The synthetic pathway for the third target molecule **37** is shown in Figure 68. First, crown ether appended Bodipy dye **35** was synthesized starting with N-phenylaza[15]crown-5 where the phenylazacrown moiety is chosen as a PET modulator. Vilsmeier formylation, followed by standard Bodipy synthesis procedure, resulted in the desired compound, a phenylazacrown-tethered *meso*-phenyl-Bodipy **35**. Consecutive styryl modifications are illustrated in Figure 68. The ICT modulators were then added one after the other, using thiaazacrown-benzaldehyde, followed by dipicolylaminobenzaldehye, isolating the intermediate **36** during the two step synthesis. The Knoevenagel condensations were driven by the continuous removal of the water formed using a Dean-Stark apparatus. Thus, compound **37** was obtained and purified by silica gel column chromatography. The azacrown ether has a larger affinity for harder alkaline and alkaline-earth cations.[170] Dithiaazacrown ligand is known to have selectivity for Hg^{2+} over many other metal ions.[171] The dipicolylamine ligand is known to be highly selective for Zn(II) in many literature examples.[140] Thus, three target molecules having ligands of different affinities, organized in diverse arrangements were synthesized.

5.4. Results and Discussions

Precise control of PET and ICT Processes: The emission spectra of binucleating monostyryl-Bodipy **32** in the presence of added metal ion modulators are shown in Figure 69. The emission spectrum of the dye has a broad peak, with a maximum at 679 nm. It is interesting to note that the addition of Zn(II) ions in the form of a perchlorate salt has a minimal effect with very small changes in the emission intensity or peak maximum, apparently ICT donor dialkylaminophenyl group in full conjugation with the Bodipy core determines the spectrum, since Zn(II) at the applied concentration (1.67 μM) has much lower affinity for the thiazacrown moiety and charge transfer is not altered to any extent.

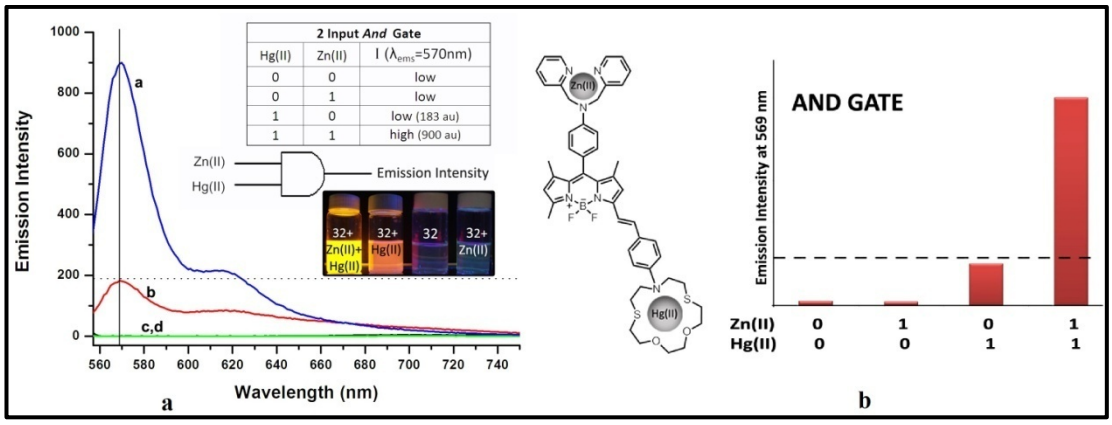

Figure 69. Emission spectra of **32** (1.67 μM) in acetonitrile in the presence of Hg(II) and Zn(II) (6.68 and 1.67 μM, respectively). Inset shows truth table for AND gate (λex= 555 nm)

In addition, PET is known to be less significant in the longer wavelength region of the spectrum (*vide infra*). On the other hand, the addition of Hg(II) (6.68 μM) alone, leads to an entirely different outcome: the softer Hg(II) ions prefer the thiaazacrown ligand, causing a blue shift of 109 nm. This is due to reduced charge transfer on metal ion binding, increasing the HOMO-LUMO gap. However, PET from the *meso* substituent become more pronounced, since the Hg^{2+} does not have particularly high affinity for the azacrown, thus the emission intensity at the peak (570 nm) stays low. When both ions were added at the concentrations above, finally the PET from the dipicolylamine substituent is blocked and in addition the large spectral shift, we now

have an impressive enhancement of emission at 570 nm. The inset picture shows the colorful signaling which is in accordance with the AND logic when the emission is recorded at 570 nm.

The experimental results obtained here is in accordance with a theoretical model for a Bodipy system with both PET and ICT active groups. MO calculations for compound **32** at DFT (B3LYP/6-31G) level reveals a number of frontier orbitals centered at the fluorophore or ligands (Figure 70), and using this data and protonation of the donor amino nitrogen as a reasonable model for metal ion binding, following MO description of the signals can be obtained:

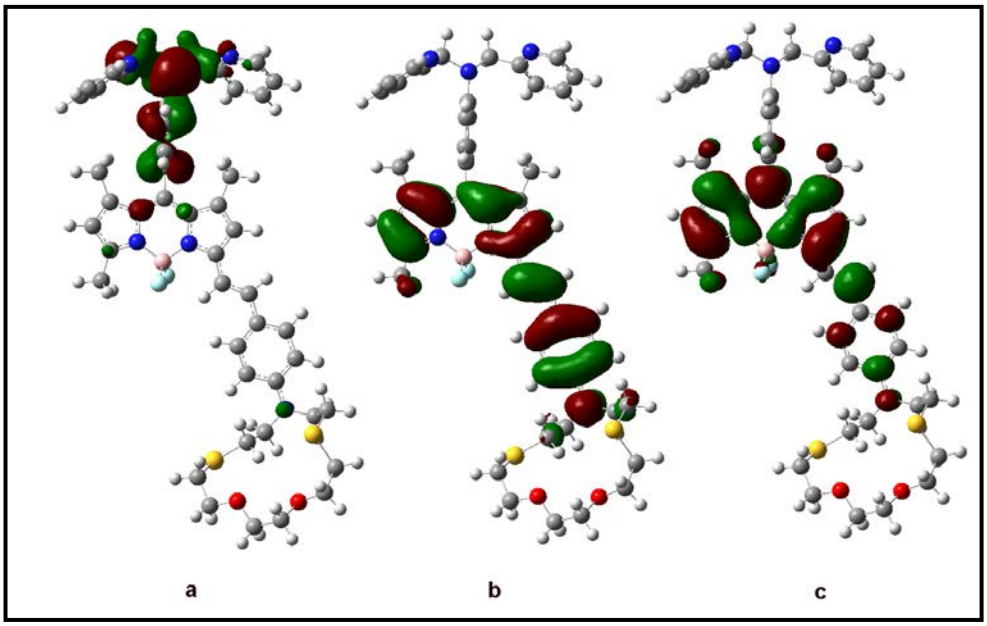

Figure 70. Schematic representation of the frontier orbitals (**a**: HOMO-1, **b**: HOMO, **c**: LUMO) of compound **32** computed at B3LYP/6-31G level of theory. The surfaces are generated with isovalue 0.02. As seen in the figure, for free dye, both HOMO and LUMO are primarily comprised of the π framework of Bodipy, dye is PeT inactive. To find the relative order of orbitals upon Hg(II) binding, protonated form of the azadithiacrown moity at nitrogen atom was used as a reasonable model

(i)- The major transition is always from the Bodipy centered orbital (HOMO or HOMO-1) to the LUMO, which is again invariably dye centered (DC in Figure 71).
(ii)- PET activity is linked to the presence of a ligand centered HOMO (here ligand refers specifically to the dipicolylamine ligand) above a dye-centered orbital, to the energy gap between this HOMO orbital and the dye-centered HOMO-1. The

magnitude of this gap is related to the thermodynamic driving force for PET and thus the rate of PET. PET is non-existent or slow for compound **32** alone. However, the emission is still low due to a polar excited state, since the measurements were performed in a polar solvent.

Dyes	**Occupied**		**Unoccupied**
	LC (eV)	DC (eV)	LUMO (eV)
32	-5.31	-4.46	-2.29
32 + H^+ [Hg(II)]	-6.64	-7.24	-4.73
32 + H^+ [Zn(II)]	-9.74	-6.15	-4.24
32 + $2H^+$ [Zn(II) + Hg(II)]	-11.70	-9.09	-6.69

Table 3. Energy levels obtained for dye **32** and various metal complexes as modeled by protonation of the primary donor atom (N-bonded to phenyl rings)

In addition, non-radiative decay is faster for longer wavelength transitions. When Hg(II) is added, since it is highly selective for the thiaazacrown unit, but not the dipicolyamine ligand, thus the energy level of the potential PET donor is not significantly affected. The dye centered orbital is now HOMO and it will be an efficient PET donor. This is why when Hg(II) ions were added, there is a blue shift, but no increase in the emission intensity. In 1:1 complex of **32**-Hg(II), PET is expected to be more effective.

When only Zn(II) ions were added, the relative positions of the dye centered HOMO and the ligand centered LUMO is not changed, but the ligand centered orbital is highly stabilized. This actually translates as little or no change in the emission character as the HOMO-LUMO gap is moderately affected.

However, when both ions were added, the stabilizion of dye centered HOMO (larger gap for the major transition), and large stabilization of the ligand-centered (dipicolyamine) orbitals (blocking of PET) were in effect. The net result is a blue shift with significant increase in the emission intensity.

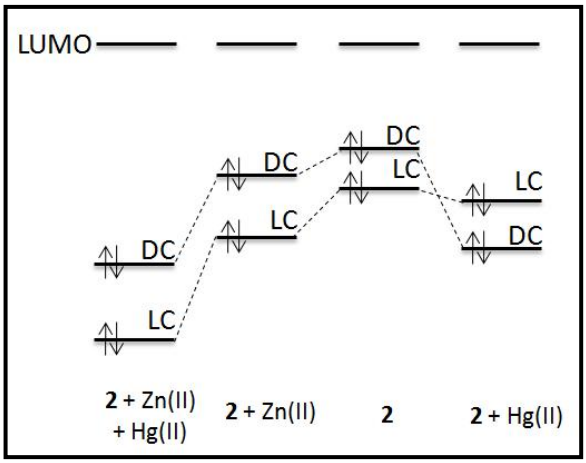

Figure 71. Qualitative assessment of relative energy levels of frontier molecular orbitals in metal ion-2 interactions. DC refers to dye (2) centered molecular orbitals confined essentially to the Bodipy core. LC refers to the ligand centered orbitals which are potential electron donors at the excited state. These are invariably located at the *meso*-tethered dipicolylamine unit. LUMO's were adjusted arbitrarily to the same level for clarity

Half-adder in the absorption mode: The distyryl compound **34**, on the other hand, has two different ligands attached to the Bodipy core as ICT donors. The spectral changes are the direct consequences of relative affinities of these ligands to Hg(II) and Zn(II).[172] A dilute solution (3.2 μM) of the distyryl-Bodipy dye **34** in acetonitrile has an absorbance peak at 698 nm (Figure 72).

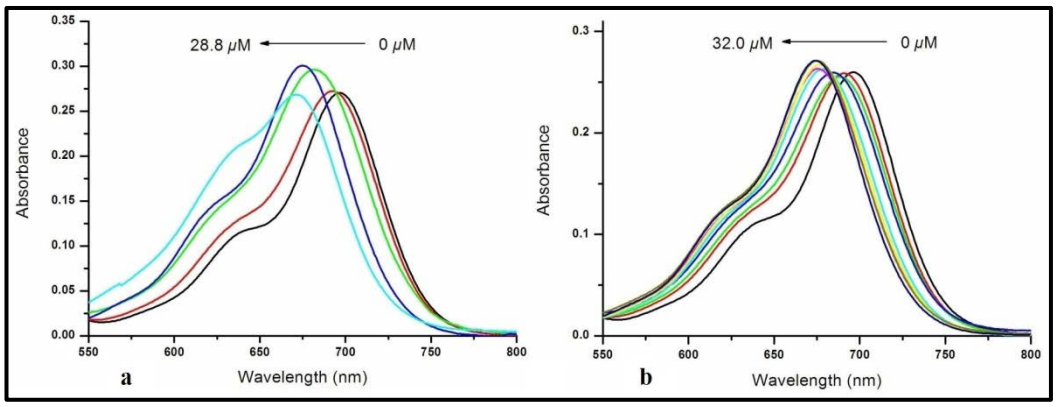

Figure 72. Absorbance spectra of compound **34** in acetonitrile in the presence of increasing (a) Hg(II) concentrations (0, 6.4, 25.6, 28.8, 32.0 μM) (b) Zn(II) concentrations (0, 3.2, 6.4, 9.6, 12.8, 16.0, 19.2, 25.6, 32.0 μM)

When Zn(II) ions were added in the form of perchlorate salt, there is a small blue shift to 675 nm. A similar shift takes place when Hg(II) alone was added. It is clear that even excess of these ions target essentially just one of the ligands, and thus blocking ICT only partially.

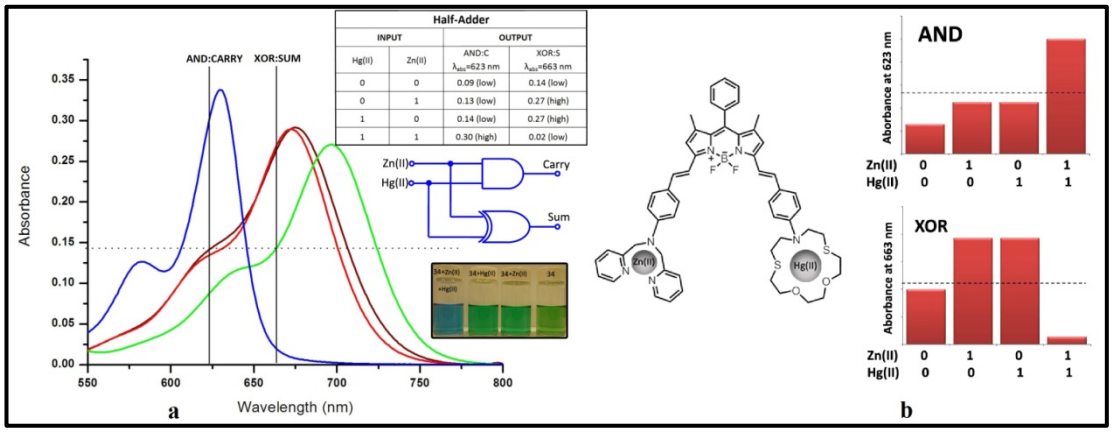

Figure 73. Absorption spectra of compound **34** (3.2 μM) in acetonitrile in the presence of Hg(II) and Zn(II) ions (28.8 and 32.0 μM, respectively). Inset shows truth table for half-adder

However, when both ions were added, the peak shifts further towards shorter wavelengths, the new metal-bound complex absorbs maximally at 630 nm. When the absorbance is recorded at 623 nm, the data is in accordance with AND logic. Absorbance data collected near the longer wavelength peak, however, results in an XOR logic. These two gates operated in parallel, a half-adder is obtained. The relevant spectra and the truth table for the two logic gates are shown Figure 73.

A three-input AND Gate: Compound **37** is a ternucleating (tritopic) compound that constitutes three different receptors. Two of them which are selective to Zn^{2+} and Hg^{2+} are attached to the Bodipy core as ICT donors, the other one, which is selective to Ca^{2+} cations, is placed at the *meso* position altering the efficiency of photoinduced electron transfer (PET). Before moving on to the photophysical experiments done with ternucleating compound **37**, we wanted to assure that the azacrown-phenyl moiety at the meso position of the regular Bodipy dye (compound **35**), recognizes Ca^{2+} selectively following the classical PET mechanism.

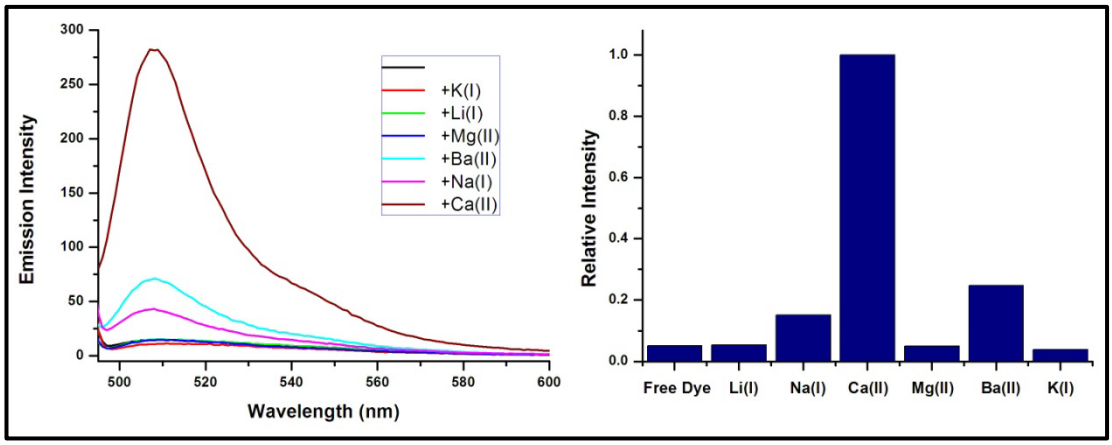

Figure 74. Emission spectra of compound **35** (1.67 μM) in acetonitrile in the presence of various cations (cation concentrations are 1.67 mM). (λ_{ex}=495 nm)

Compound **35** is a PET-type quenched molecule, and among several alkali and alkali earth metals only Ca^{2+} cations has prevented PET efficiently, resulting in the bright fluorescence at 510 nm (Figure 74, left). A bar graph showing relative emission ratios for compound **35** obtained in the presence of different cations is also illustrated in Figure 74 (right). Samples were excited at 495 nm and the normalized emission intensity values at 510 nm are shown on the y-axis.

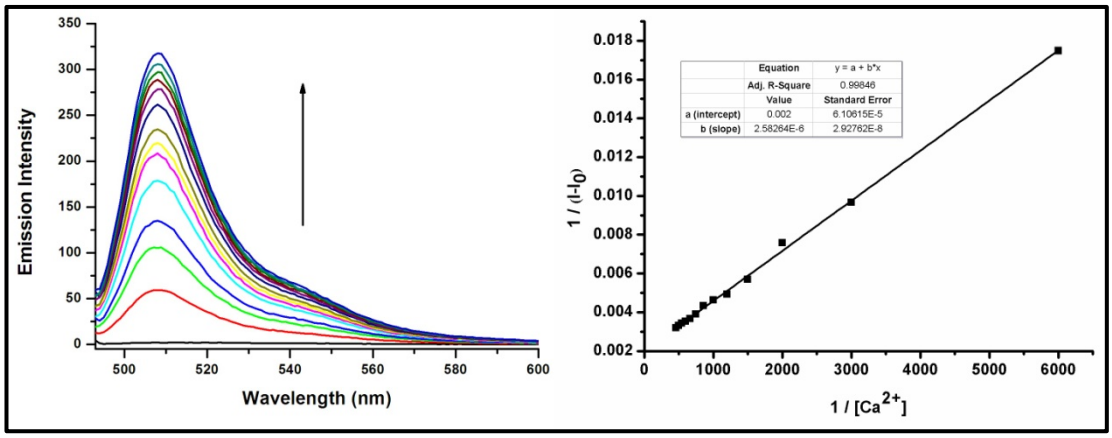

Figure 75. Leftside is the emission specta of compound **35** (1.67 μM) in acetonitrile in the presence of increasing Ca(II) concentrations (0.0, 0.17, 0.33 0.5, 0.67, 0.83, 1.0, 1.17, 1.33, 1.5, 1.67, 1.83, 2.0, 2.17 mM)

We also ran some titrations experiments for compound **35**. It is shown in the Figure 75 (left) above. From that fluorimetric Ca(II) titration data, we carried out Benesi-Hildebrand analysis for compound **35**. The plot yields a K_a of 680 M^{-1}.

Absorption spectrum of the ternucleating (tritopic) compound **37** is presented in Figure 76, and the effects of added metal ions (Ca^{2+}, Zn^{2+} and Hg^{2+}) are apparent. It is clear that the metal ions separately or together, have different affinities (or regioselectivities). Harder Ca(II) ions prefer to interact with harder azacrown ligand at the *meso* position of the Bodipy dye. This interaction is not expected to alter the absorption spectrum, but since it has to be added at a larger concentration (1.0 mM) than the other metal ions, a minor 25 nm blue shift is nevertheless observed, indicating some interference at the ICT donor ligands. Compared to free fluoroionophore, approximately 25 nm blue shift was observed in the following combinations: Ca(II), Zn(II), Ca(II)+Zn(II).

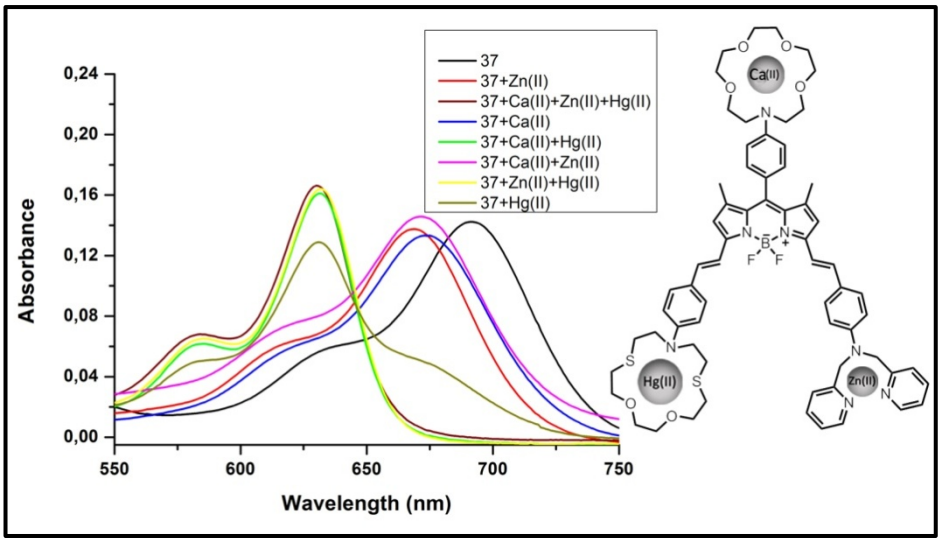

Figure 76. Absorption specta of compound **37** (2.0 μM) in acetonitrile solutions, in the presence of Hg(II), Zn(II) and Ca(II) ions (20.0 μM, 20.0 μM, and 1.0 mM respectively)

Hg(II) is particularly effective, and in all input scenarios including Hg(II), there is large 70 nm hypsochromic shift. Nevertheless, it is obvious that absorbance changes seem far too complicated to be of much use in logic gate design. However, the emission changes (Figure 77) result in a better picture for this purpose. At the concentrations used in the present work (Hg(II) and Zn(II) at 20.0 μM and Ca(II) at 1.0 mM), only when all three cations were added as inputs, emission is significantly enhanced above the threshold.

The three cations separately, or in other binary combinations, do not induce an enhanced and blue shifted emission from the compound **37**. Thus, all three metal ion inputs are required simultaneously for the large emission increase at 656 nm, this behavior is in accordance with an AND logic gate.

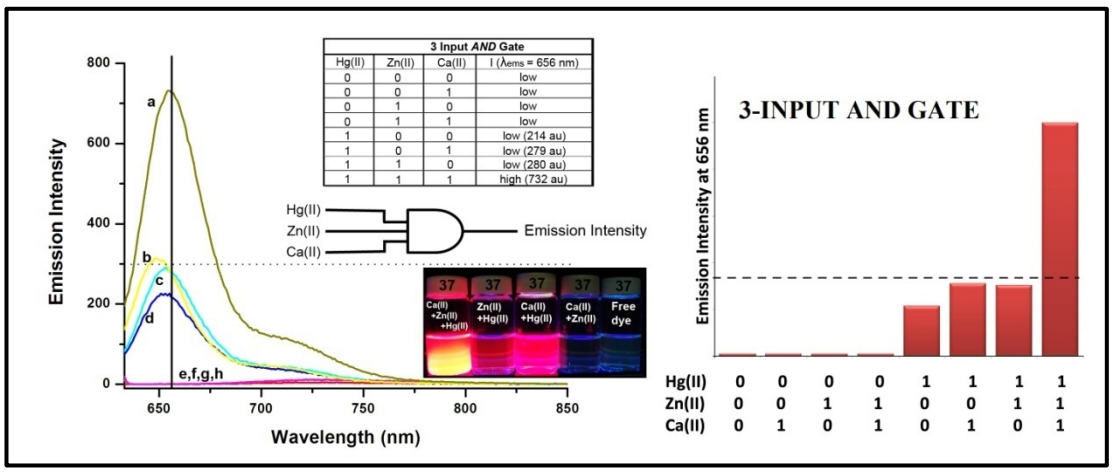

Figure 77. Emission spectra of **37** (2.0 μM) in acetonitrile in the presence of Hg(II), Zn(II), and Ca(II) (20.0 μM, 20.0 μM, and 1.0 mM respectively). Inset shows truth table for **3**-input-AND gate. (a): **37**+Ca(II)+Zn(II)+Hg(II) (b): **37**+Ca(II)+Hg(II) (c): **37**+Zn(II)+Hg(II) (d): **37**+Hg(II) (e): **37** (f): **37**+Ca(II)+Zn(II) (g): **37**+Ca(II) (h): **37**+Zn(II). Excitation wavelength is 620 nm.

One can envision a scenario, where elevated concentrations of three different molecular or ionic species may indicate a particular disease state (lab-on-a molecule, as elaborated previously by de Silva), thus a non-zero AND logic response, could be a positive identification of that particular state. The use of multiple photophysical processes for eliciting an AND response is highly relevant, as it would minimize false positives, since for example in this case, both a blue shift and large enhancement of emission signal should be expected.

In addition, simultaneous sensing is also possible: PET and ICT processes can clearly be addressed separately, for shorter wavelength emitting fluorophores, PET processes can be effective, and be separately blocked by an appropriate metal ion, resulting signal enhancement, regardless of the ICT modulating ions. On the other hand, ICT donor ligand will result in spectral shift which can be correlated to the

concentration of the analyte targeting that particular ligand. The spectral data for all three target compounds and their metal complexes were tabulated in Table **4**.

Compounds	λ_{max} (nm)	Abs (nm)[a]	ε_{max} ($M^{-1}cm^{-1}$)	fwhm (cm^{-1})	Φ[b]
32	600	0.135	80000	1540	0.10
32+Zn(II)	602	0.132	79000	1640	0.16
32+Hg(II)	560	0.075	53000	2460	0.19
32+Zn(II)+Hg(II)	560	0.153	92000	900	0.43
34	697	0.259	81000	1420	0.11
34+Zn(II)	673	0.288	90000	1440	0.33
34+Hg(II)	674	0.294	92000	1640	0.28
34+Zn(II)+Hg(II)	630	0.34	106000	840	0.78
35	497	0.101	60600	960	0.012
35+Ca(II)	498	0.095	57000	870	0.592
37	692	0.142	71000	1280	0.038
37+Ca(II)+Zn(II)+Hg(II)	626	0.122	61000	1240	0.266

Table 4. Spectroscopic data for compounds **32**, **34**, **35**, **37** and their metal complexes [a] Peak absorption values at the specific concentrations of the study, [b] Quantum yields for compounds **32**, **34**, and **37** were determined in reference to Sulforhodamine 101 (0.90 in ethanol) and for compound **35** Rhodamine 6G (0.95 in ethanol) was used as a reference

Binding Constants: Isothermal titration calorimetry (ITC) was useful in determining the binding constants of Hg(II) and Zn(II) (Table **5**). Before discussing the obtained results, a few words regarding the instrumentation and followed protocols should be noted: Isothermal titration calorimetry experiments were performed on a *iTC-200 microcalorimete* (Microcal Inc., Northampton, MA). All solutions were prepared in spectroscopic grade acetonitrile. For a typical ITC run, the instrument chamber (200 μL) contained a solution of a ligand (0.1 – 0.5 mM) while a 1.0 – 5.0 mM solution of $Zn(ClO_4)_2$ or $Hg(ClO_4)_2$ was taken up in a 40 μL injection syringe. The syringe was assembled into the chamber for equilibration while stirring at 1000 rpm. The chamber temperature was set to 25 °C. The injections were programmed at 1 μL each, added over 2 sec and spaced 2 min apart. Association enthalpy (ΔH° in cal/mol), "number of sites" (N), and association constant (K in M^{-1}) were obtained by fitting the titration data using the "One (Two) Set of Sites model" algorithm provided

in the MicroCal Origin Software package (version 7.0). Association entropy (ΔS in cal/mol/K) is calculated from fitted values of ΔH° and K.

Titration	K (M^{-1})	Δ***H*** (kcal/mol)	Δ***S*** cal/(mol.K)	model
Compound **31** (1:1) binding-Zn(II)	$(4.8 \pm 0.4) \times 10^7$	-7.5 ± 1.6	5.99	two sets of sites
Compound **31** (1:2) binding-Zn(II)[a]	$(5.9 \pm 0.8) \times 10^6$	-11.4 ± 0.4	-2.95	two sets of sites
Reference[b] dithiaazacrown-Hg(II)	$(3.4 \pm 0.8) \times 10^6$	-11.6 ± 0.08	-9.27	one set of sites
Compound **31**-Hg(II)	$(9.1 \pm 0.5) \times 10^6$	-15.3 ± 0.02	-19.3	one set of sites
Half adder **34**-Zn(II)	$(6.7 \pm 0.6) \times 10^5$	-14.9 ± 0.1	-23.2	one set of sites
Half adder **34**-Hg(II)	$(8.0 \pm 2.6) \times 10^7$	-39.4 ± 0.3	-95.6	two sets of sites
Half adder **34**-Hg(II), 2nd binding	$(1.1 \pm 0.2) \times 10^5$	-1.1 ± 0.2	-41.1	two sets of sites
AND Gate **32**-Zn(II)	$(1.8 \pm 0.8) \times 10^6$	-6.8 ± 0.2	5.7	one set of sites
AND Gate **32**-Hg(II)	$(1.3 \pm 0.9) \times 10^8$	-12.0 ± 0.1	-3.18	two sets of sites
AND Gate **32**-Hg(II), 2nd binding	$(7.7 \pm 1.2) \times 10^4$	-8.1 ± 0.2	-4.74	two sets of sites

Table 5. Binding constants determined by isothermal titration calorimetry (ITC) for the relevant binding events. [a] Compound **31** shows a clear 1:2 (two Bodipy-ligands-one Zn(II) at high concentrations of **31**. Similar interaction is not observed when the dipicolylamine ligand is tethered with a styryl group to 3 (or 5) position of Bodipy, which can be understood in terms of steric demands of 1:2 interaction. [b] The reference compound used here is N-(4-formylphenyl)-1-aza-4,13-dithia-[15]crown-5

Experimentally determined binding affinities confirm the working principle of the proposed molecular logic gates. For example, half-adder molecule **34** when titrated with Zn(II) ions shows just one binding with the binding constant of 6.7×10^5 M^{-1}, indicating an affinity for the picolylamine ligand, but not for the dithiaazacrown ligand (Figure 78). The two-input AND logic (compound **32**) titration with Zn(II) ions also shows just one binding event (1.8×10^6 M^{-1}). Compared to that of Hg(II) ions, larger affinity of Zn(II) ions for dipicolylamine ligand apparent in the separate titration studies (Figure 79) done with these two cations and the reference compound **31 (**4.8×10^7 M^{-1} for Zn(II) and 9.1×10^6 M^{-1} for Hg(II)).

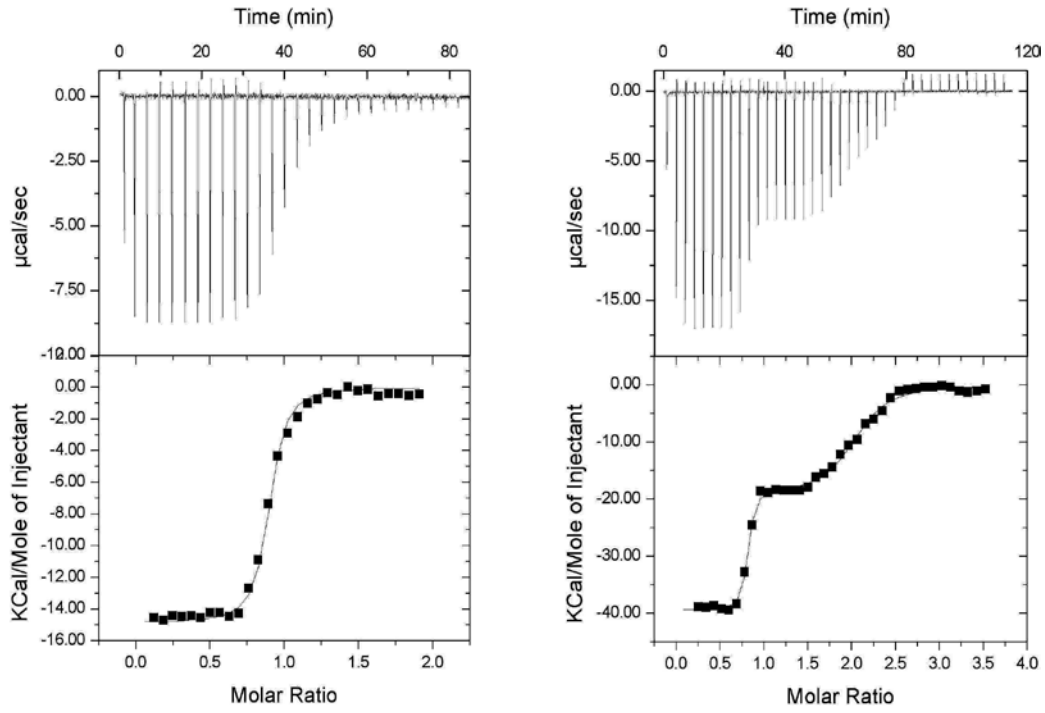

Figure 78. ITC titration curves of compound **34** in acetonitrile. Left: 0.4 mM **34** titrated with 5.0 mM $Zn(ClO_4)_2$, Right: b) 0.3 mM **34** titrated with 5.0 mM $Hg(ClO_4)_2$

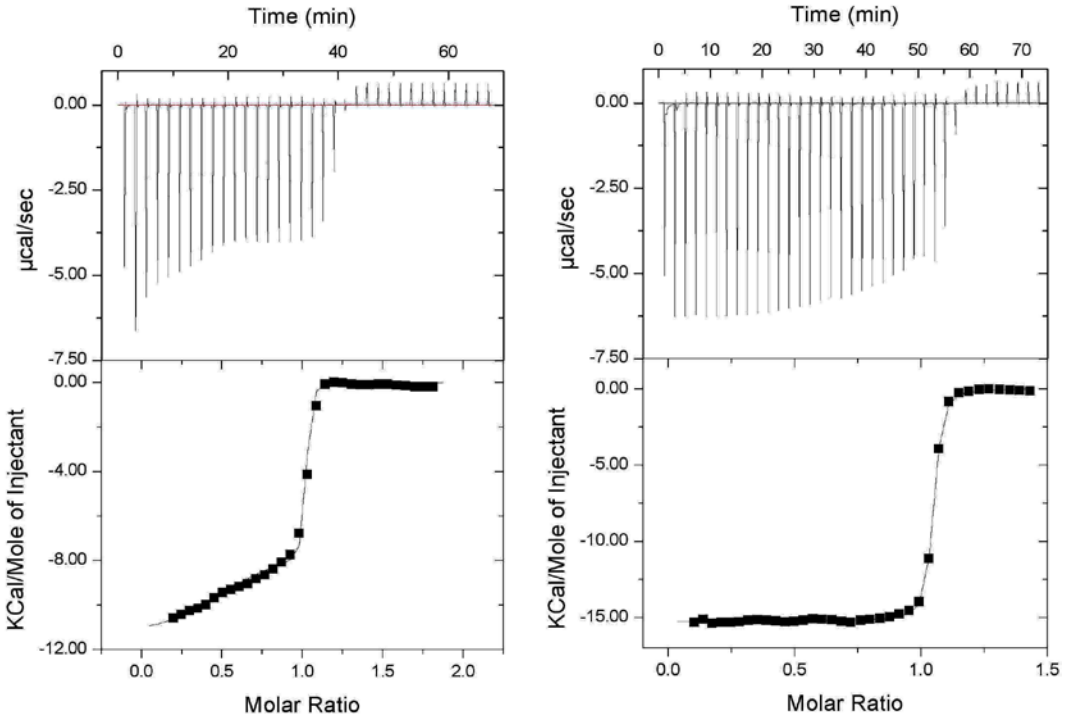

Figure 79. ITC titration curves of reference compound **31** in acetonitrile. Left: 0.5 mM **31** titrated with 5.0 mM $Zn(ClO_4)_2$, Right: b) 0.5 mM **31** titrated with 4.0 mM $Hg(ClO_4)_2$

Titration of ditopic compounds with Hg(II) ions revealed that, Hg(II) have strong affinities for both dipicolylamine and the dithiaazacrown ligands, and at larger concentrations both ligands would be engaged. But at the selected concentrations of Zn(II) and Hg(II) as inputs, dynamic nature of the binding events dictate that Zn(II) ions with no affinity to dithiaazacrown ligand and larger affinity for dipicolyl ligand will preferentially occupy dipicolylamin ligand. This order of affinity will be in place for all three logic gates designs.

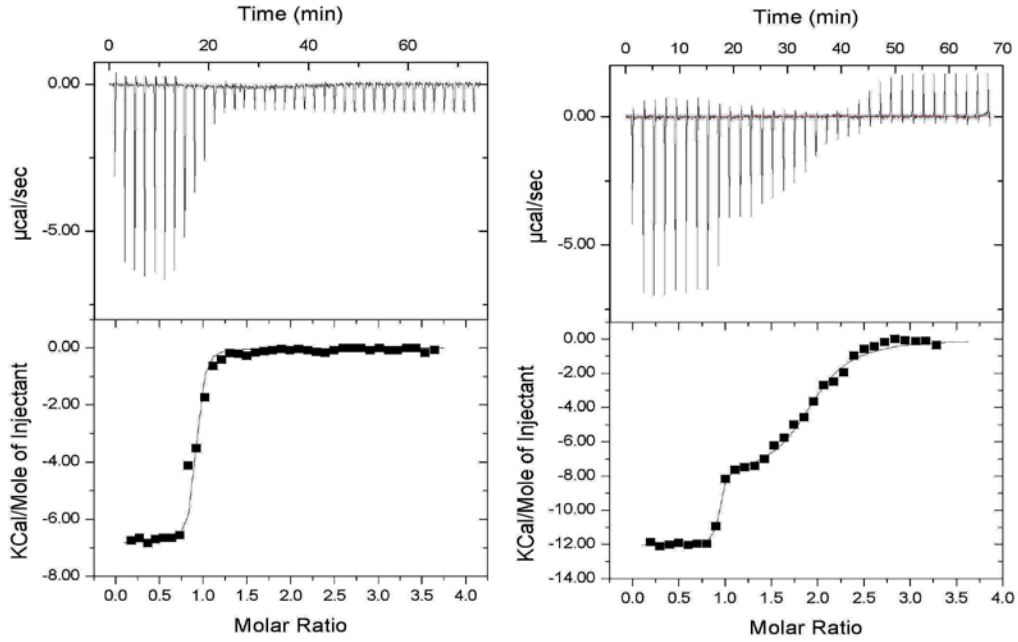

Figure 80. ITC titration curves of compound **32** in acetonitrile. Left: 0.3 mM **32** titrated with 5.5 mM $Zn(ClO_4)_2$, Right: b) 0.3 mM **32** titrated with 5mM $Hg(ClO_4)_2$

On the other hand, binding affinity of Ca(II) ions were significantly smaller, therefore relavant binding constant in the interaction of these ions with three-input logic gate molecule **37** were determined by spectrofluorometry. The value obtained for K is 680 M^{-1} (supporting information) suggest that at higher input concentrations of Ca(II) ions, the crown ether moiety will be engaged by this cation.

In this study, remarkably versatile chemistry of Bodipy dyes allows the design and straightforward synthesis of multivalent-multitopic derivatives, which with judicious

selection of metal ion-ligand pairs based on known affinities, affords control and manipulation of PET and ICT processes as desired. We have demonstrated that metal ions acting as modulators (or inputs, in digital design parlance), can generate absorbance changes in accordance with the operation of a half-adder. In addition, an AND logic gate in the emission mode was delivered using a different binucleating arrangement of ligands. A molecular equivalent of a three-input AND logic gate was also obtained exploiting differential binding affinities of metal ions for different ligands. The results suggest that different metal ions can be used as non-annihilating inputs, selectively targeting various ligands incorporated within a single fluorophore, and with careful design, diverse photophysical processes can be selectively modulated, resulting in a range of signals, useful in molecular logic design, and offering an enticing potential for multianalyte chemosensors.

5.5. Experimental Details

General: ^{1}H NMR and ^{13}C NMR spectra were recorded on Bruker DPX-400 (operating at 400 MHz for ^{1}H NMR and 100 MHz for ^{13}C NMR) in $CDCl_3$ with tetramethylsilane as internal standard. All spectra were recorded at 25 ^{o}C and coupling constants (*J* values) are given in Hz. Chemical shifts are given in parts per million (ppm). All the ^{13}C spectra were recorded with simultaneous decoupling of proton nuclei. Mass spectroscopy data were acquired using Bruker Autoflex-III (smartbeam) MALDI TOF/TOF system at IYTE Chemistry Department, Izmir, Turkey. Absorption spectra were performed by using a Varian Cary-100 spectrophotometer. Fluorescence measurements were conducted on a Varian Eclipse spectrofluorometer. Reactions were monitored by thin layer chromatography using Merck TLC Silica gel 60 F_{254}. Silica gel column chromatography was performed over Merck Silica gel 60 (particle size: 0.040-0.063 mm, 230-400 mesh ASTM). All other reagents and solvents were purchased from Aldrich and used without further purification. Phenyl Bodipy[173] and 4-(1,4-dioxa-7,13-dithia-10-azacyclopentadecan-10-yl) benzaldehyde[169] were synthesized according to literature reports.

5.5.1. UV-Vis Titration Experiments

*Titrations of **34** with Zn(II) ion* : 100 μL portions of 0.16 mM stock solution of **34** were diluted to 2 mL by adding Acetonitrile (3.2×10^{-6} M) and to these solutions were added aliquots of $Zn(OTf)_2$ solutions (0.1 mM) in Acetonitrile (0, 160, 320, 480, 640, 800, 960, 1120, 1280, 1600 μL). Volumes of these solutions were adjusted to 5 mL. UV-vis absorption spectra were recorded at room temperature.

*Titrations of **34** with Hg(II) ion* : 100 μL portions of 0.16 mM stock solution of **34** were diluted to 2 mL by adding Acetonitrile (3.2×10^{-6} M) and to these solutions were added aliquots of $Hg(ClO_4)_2$ solutions (0.1 mM) in Acetonitrile (0, 320, 1280, 1440, 1600 μL). Volumes of these solutions were adjusted to 5 mL. UV-vis absorption spectra were recorded at room temperature.

5.5.2. Reaction Procedures

Synthesis of molecular Two-Input-AND gate (32)

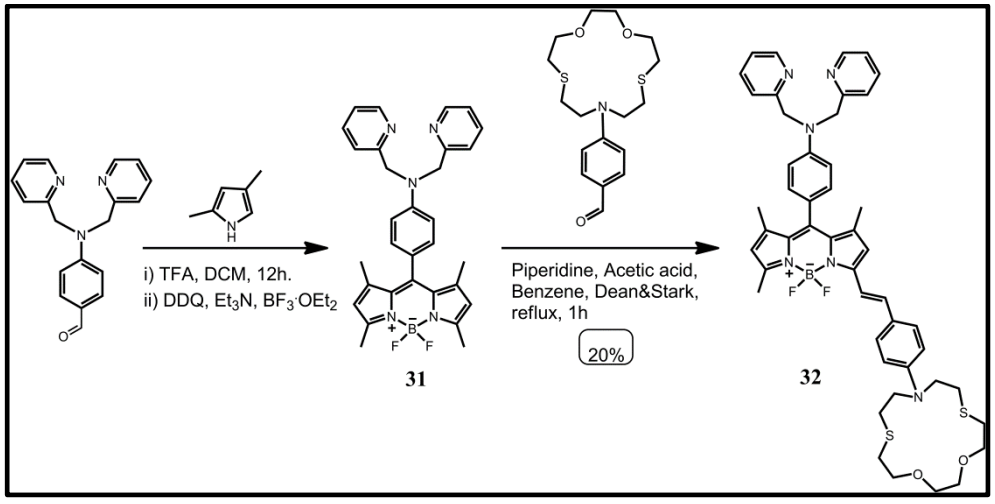

***Synthesis of Compound 31*:** To a 1.0 L round-bottomed flask containing 400 mL argon-degassed CH_2Cl_2 were added 2,4-dimethyl pyrrole (4.4 mmol, 0.4 g), 4-(*N*,*N*-di-(pyridine-2-ylmethyl)amino) benzaldehyde (1.98 mmol, 0.6 g) and one drop of trifluoroacetic acid. The solution was stirred under N_2 at room temperature for 1d.

After addition of a solution of DDQ (1.98 mmol, 0.45 g) in 100 mL of CH_2Cl_2 to the reaction mixture, stirring was continued for 30 min. 6 mL of Et_3N and 5 mL of $BF_3.OEt_2$ were successively added and after 30 min, the reaction mixture was washed with water (3 x 300 mL) and dried over anhydrous Na_2SO_4. The solvent was evaporated and the residue was purified by silica gel column chromatography using $CHCl_3$: Methanol (97 : 5) as the eluant. Orange solid (0.25 g, 23%).

^{1}H NMR (400 MHz, $CDCl_3$): δ_H 8.60 (2H, d, *J* = 6.48 Hz, ArH), 7.62 (2H, t, *J* = 7.71 Hz, ArH), 7.22 (2H, d, *J* = 7.84 Hz, ArH), 7.18 (2H, t, *J* = 6.58 Hz, ArH), 6.98 (2H, d, *J* = 8.80, ArH), 6.80 (2H, d, *J* = 8.80, ArH), 5.95 (2H, s, ArH), 4.87 (4H, s, C*H*$_2$), 2.52 (6H, s, C*H*$_3$), 1.45 (6H, s, C*H*$_3$);

^{13}C NMR (100 MHz, $CDCl_3$): δ_C 158.3, 154.8, 149.8, 149.7, 148.8, 143.1, 136.7, 128.9, 123.3, 122.2, 120.9, 113.2, 57.4, 14.5 ppm.

Anal. Calcd. for $C_{31}H_{30}BF_2N_5$: C 71.41, H 5.80, N 13.43. Found: C 71.33, H 5.89, N 13.12 %.

***Synthesis of Compound 32*:** In a 100 mL round-bottomed flask equipped with a Dean-Stark trap and a reflux condenser were added 40 mL of benzene, **31** (0.15 mmol, 80 mg), 4-(1,4-dioxa-7,13-dithia-10-azacyclopentadecan-10-yl) benzaldehyde (0.15 mmol, 54 mg), acetic acid (0.2 mL), and piperidine (0.2 mL). The reaction mixture was stirred at reflux temperature and concentrated nearly to dryness. Progress of the reaction was monitored by TLC (1:1 Hexanes : Acetone). When all the starting material had been consumed, water (100 mL) was added and mixture was extracted into $CHCl_3$. The organic layer was dried on Na_2SO_4 and evaporated. Column chromatographic separation (silica gel, 1:1 Hexanes : Acetone) of the residue yielded the desired product as a dark blue solid. (25 mg, 20%).

^{1}H NMR (400 MHz, $CDCl_3$): δ_H 8.62 (2H, d, *J* = 5.72 Hz, ArH), 7.65 (2H, t, *J* = 8.54 Hz, ArH), 7.50-7.43 (3H, m: 2H, ArH; 1H, C*H*), 7.26-7.15 (5H, m: 4H, ArH; 1H, C*H*), 7.03 (2H, d, *J* = 8.60 Hz, ArH), 6.80 (2H, d, *J* = 8.68 Hz, ArH), 6.62 (2H, d, *J* = 8.96, ArH), 6.58 (1H, s, ArH), 5.90 (1H, s, ArH), 4.88 (4H, s, C*H*$_2$), 3.82 (4H, t, *J* = 4.98 Hz, OC*H*$_2$CH$_2$S), 3.70-3.62 (8H, m, 4H, NC*H*$_2$CH$_2$S, 4H, OC*H*$_2$C*H*$_2$O), 2.90 (4H, t, *J* = 7.86 Hz, OCH$_2$C*H*$_2$S), 2.78 (4H, t, *J* = 5.05 Hz, NCH$_2$C*H*$_2$S), 2.58 (6H, s, C*H*$_3$), 1.48 (3H, s, C*H*$_3$), 1.44 (3H, s, C*H*$_3$)

^{13}C NMR (100 MHz, $CDCl_3$): δ_C 158.4, 153.0, 149.8, 149.0, 148.7, 139.0, 136.7, 129.5, 129.3, 126.0, 125.2, 122.1, 120.9, 120.7, 117.0, 115.0, 113.1, 111.8, 74.3, 70.7, 57.5, 51.9, 31.3, 29.6, 14.8, 14.7 ppm.

Anal. Calcd. for $C_{48}H_{53}BF_2N_6O_2S_2$: C 67.12, H 6.22, N 9.78 %. Found: C 66.98, H 6.34, N 9.70 %.

MS (MALDI-TOF): m/z: Calcd. for $C_{48}H_{53}BF_2N_6O_2S_2$: 858.4 [$M^+$], Found: 858.1[$M^+$]

Synthesis of molecular Half adder (34)

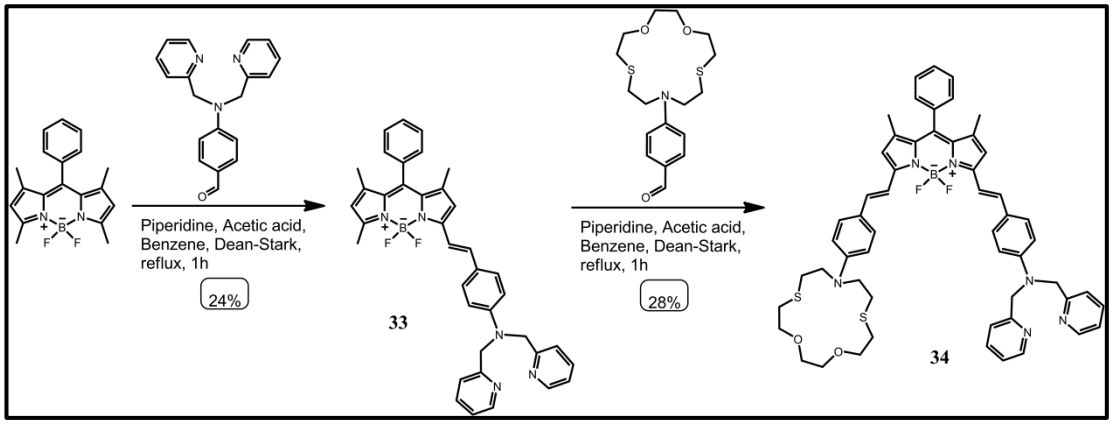

***Synthesis of Compound 33*:** In a 100 mL round-bottomed flask equipped with a Dean-Stark trap and a reflux condenser were added 40 mL of benzene, 4,4-difluoro-8-phenyl-1,3,5,7-tetramethyl-4-bora-3a,4a-diaza-*s*-indacene (0.37 mmol, 0.12 g), 4-(*N*,*N*-di-(pyridine-2-ylmethyl)amino) benzaldehyde (0.37 mmol, 0.11 g), acetic acid (0.2 mL), and piperidine (0.2 mL). The reaction mixture was stirred at reflux temperature and concentrated nearly to dryness. Progress of the reaction was monitored by TLC (Ethyl acetate : Methanol ; 97 : 3). When all the starting material had been consumed, water (100 mL) was added and mixture was extracted into $CHCl_3$. The organic layer was dried on Na_2SO_4 and evaporated. Column chromatographic separation (silica gel, Ethyl acetate : Methanol ; 97 : 3) of the residue yielded desired product as a dark blue solid (53mg, 24%). ^{1}H NMR (400 MHz, $CDCl_3$): δ_H 8.61 (2H, d, *J* = 5.72 Hz, ArH), 7.65 (2H, t, *J* = 8.48 Hz, ArH), 7.50-7.40 (6H, m: 3H, ArH; 2H, ArH; 1H, C*H*), 7.30-7.22 (4H, m: 2H, ArH; 2H, ArH), 7.20-7.12 (3H, m: 2H, ArH; 1H, C*H*), 6.72 (2H, d, *J* = 8.21 Hz, ArH), 6.57

(1H, s, ArH), 5.95 (1H, s, ArH), 4.88 (4H, s, C*H*$_2$), 2.55 (6H, s, C*H*$_3$), 1.41 (3H, s, C*H*$_3$), 1.39 (3H, s, C*H*$_3$);

^{13}C NMR (100 MHz, $CDCl_3$): δ_C 158.9, 158.2, 154.3, 153.5, 149.8, 149.7, 142.7, 141.3, 139.2, 136.9, 136.8, 135.3, 129.2, 129.0, 128.8, 125.9, 122.2, 122.0, 120.8, 117.6, 117.2, 115.3, 112.7, 57.3, 14.6, 14.5, 14.2 ppm.

Anal. Calcd. for $C_{38}H_{34}BF_2N_5$: C 74.88, H 6.62, N 11.49 %. Found: C 74.91, H 6.73, N 11.40 %.

MS (MALDI-TOF): m/z: Calcd. for $C_{38}H_{34}BF_2N_5$: 609.3 [M^+], Found: 608.9 [M^+]

***Synthesis of Compound 34*:** In a 100 mL round-bottomed flask equipped with a Dean-Stark trap and a reflux condenser were added 40 mL of benzene, **33** (0.08 mmol, 50 mg), 4-(1,4-dioxa-7,13-dithia-10-azacyclopentadecan-10-yl) benzaldehyde (0.08 mmol, 28.4 mg), acetic acid (0.2 mL), and piperidine (0.2 mL). The reaction mixture was stirred at reflux temperature and concentrated nearly to dryness. Progress of the reaction was monitored by TLC (Ethyl acetate : Methanol ; 95 : 5). When all the starting material had been consumed, water (100 mL) was added and mixture was extracted into $CHCl_3$. The organic layer was dried on Na_2SO_4 and evaporated. Column chromatographic separation (silica gel, Ethyl acetate : Methanol ; 95 : 5) of the residue yielded the desired product as a green solid. (25 mg, 28%). ^{1}H NMR (400 MHz, $CDCl_3$): δ_H 8.63 (2H, d, *J* = 3.16 Hz, ArH), 7.67 (2H, t, *J* = 7.26 Hz, ArH), 7.58-7.44 (9H, m: 3H, ArH; 2H, ArH; 2H, ArH; 2H, C*H*), 7.35-7.28 (3H, m: 2H, ArH; 1H, C*H*), 7.24-7.13 (4H, m: 2H, ArH; 2H, ArH), 7.05 (1H, d, *J* = 15.3 Hz, C*H*), 6.74 (2H, d, *J* = 8.40 Hz, ArH), 6.65 (2H, d, *J* = 8.45, ArH), 6.59 (1H, s, ArH), 6.57 (1H, s, ArH), 4.90 (4H, s, C*H*$_2$), 3.74 (4H, t, *J* = 4.62 Hz, OC*H*$_2$CH$_2$S), 3.75-3.62 (8H, m, 4H, NC*H*$_2$CH$_2$S, 4H, OC*H*$_2$C*H*$_2$O), 2.92 (4H, t, *J* = 3.88 Hz, OCH$_2$C*H*$_2$S), 2.78 (4H, t, *J* = 4.50 Hz, NCH$_2$C*H*$_2$S), 2.58 (6H, s, C*H*$_3$), 1.42 (6H, s, C*H*$_3$);

^{13}C NMR (100 MHz, $CDCl_3$): δ_C 158.3, 153.1, 152.3, 149.9, 149.7, 148.7, 147.6, 141.2, 140.8, 136.9, 136.5, 136.3, 135.6, 135.5, 129.4, 129.1, 128.9, 128.6, 126.3, 125.2, 124.8, 122.6, 122.2, 122.9, 117.3, 117.1, 115.8, 115.0, 112.7, 112.0, 111.8, 74.3, 70.7, 57.3, 52.0, 31.3, 29.7, 14.6, 14.5 ppm.

Anal. Calcd. for $C_{55}H_{57}BF_2N_6O_2S_2$: C 69.75, H 6.07, N 8.87 %. Found: C 69.68, H 6.15, N 8.79 %.

MS (MALDI-TOF): m/z: Calcd. for $C_{55}H_{57}BF_2N_6O_2S_2$: 946.4 [$M^+$], Found: 946.2 [$M^+$]

Synthesis of molecular Three-Input-AND Logic (37)

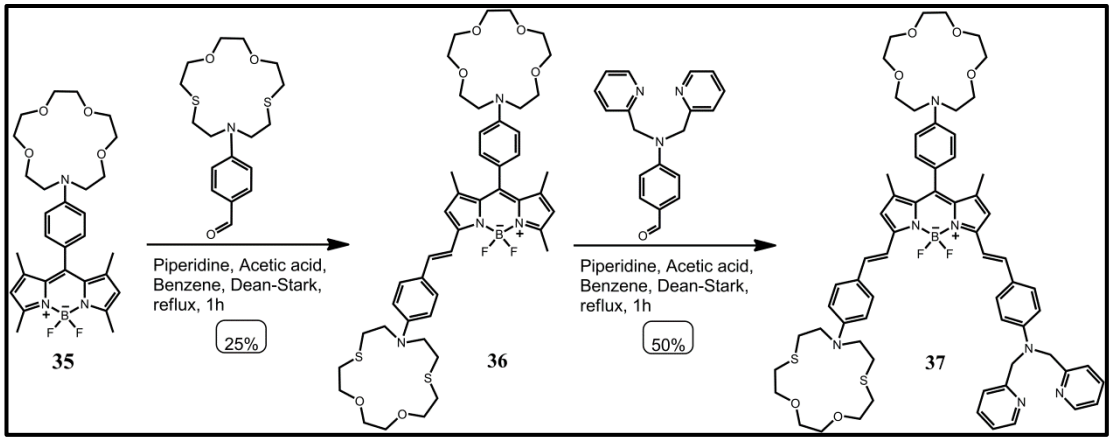

***Synthesis of 4-(1,4,7,10-tetraoxa-13-azacyclopentadecan-13-yl)benzaldehyd*e:** To a cooled (0°C) solution of anhydrous DMF (10mL), was added $POCl_3$ (4 mmol, 0.615 g) within 5 min. The mixture was stirred for 30 min at room temperature, then 13-phenyl-1,4,7,10-tetraoxa-13-azacyclopentadecane[174] (3.4 mmol, 1 g) was added and the resulting mixture was heated for 5h at 80°C. The dark brown solution was slowly added cold water and then neutralized with K_2CO_3. The product was extracted with CH_2Cl_2 and dried over anhydrous Na_2SO_4. The solvent was evaporated and the residue was purified by silica gel column chromatography using $CHCl_3$: Methanol (95: 5) as the eluant. Yellowish viscous liquid (0.7 g, 64%).

^{1}H NMR (400 MHz, $CDCl_3$): δ_H 9.72 (1H, s), 8.78 (2H, d, *J* = 8.84 Hz, ArH), 6.80 (2H, d, *J* = 8.96 Hz, ArH), 3.83 (4H, t, *J*=6.16), 3.70-3.56 (16H, m)

^{13}C NMR (100 MHz, $CDCl_3$): δ_C 190.0, 152.4, 132.0, 125.2, 111.0, 71.2, 70.3, 70.0, 68.1, 52.8 ppm.

Anal. Calcd. for $C_{17}H_{25}NO_5$: C 63.14, H 7.79, N 4.33 %. Found: C 63.18, H 7.85, N 4.19 %.

***Synthesis of Compound 35*:** To a 1L round-bottomed flask containing 400 mL argon-degassed CH_2Cl_2 were added 2,4-dimethyl pyrrole (3.41 mmol, 0.324 g), 4-(1,4,7,10-tetraoxa-13-azacyclopentadecan-13-yl)benzaldehyde (1.55 mmol, 0.5 g) and one drop of trifluoroacetic acid. The solution was stirred under N_2 at room temperature for 1d. After addition of a solution of DDQ (1.60 mmol, 0.363 g) in 100 mL of CH_2Cl_2 to the reaction mixture, stirring was continued for 30 min. 6 mL of Et_3N and 5 mL of $BF_3.OEt_2$ were successively added and after 30 min, the reaction mixture was washed with water (3 x 300 mL) and dried over anhydrous Na_2SO_4. The solvent was evaporated and the residue was purified by silica gel column chromatography using $CHCl_3$: Methanol (95 : 5) as the eluant. Orange solid (0.225 g, 27%).

^{1}H NMR (400 MHz, $CDCl_3$): δ_H 7.01 (2H, d, *J* = 7.92 Hz, ArH), 6.73 (2H, d, *J* = 8.12 Hz, ArH), 6.94 (2H, s, ArH), 3.80 (4H, t, *J*=5.64), 3.73-3.60 (16H, m) 2.52 (6H, s, C*H*$_3$), 1.50 (6H, s, C*H*$_3$);

^{13}C NMR (100 MHz, $CDCl_3$): δ_C 154,7, 148.2, 143.2, 132.2, 130.7, 128.9, 121.8, 120.8, 111.6, 110.7, 71.3, 70.2, 70.0, 68.5, 52.6, 14.8, 14.5 ppm.

Anal. Calcd. for $C_{29}H_{38}BF_2N_3O_4$: C 64.33, H 7.07, N 7.76 %. Found: C 64.28, H 7.16, N 7.70 %.

MS (MALDI-TOF): m/z: Calcd. for $C_{29}H_{38}BF_2N_3O_4$: 541.3 [M^+], Found: 541.9 [M^+]

Synthesis of Compound 36: In a 100 mL round-bottomed flask equipped with a Dean-Stark trap and a reflux condenser were added 40 mL of benzene, **35** (0.37 mmol, 200 mg), 4-(1,4-dioxa-7,13-dithia-10-azacyclopentadecan-10-yl)-benzaldehyde (0.33 mmol, 118 mg), acetic acid (0.2 mL), and piperidine (0.2 mL). The reaction mixture was stirred at reflux temperature and concentrated nearly to dryness. Progress of the reaction was monitored by TLC (eluent: Ethyl acetate). When all the starting material has been consumed, water (100 mL) was added and mixture was extracted into $CHCl_3$. The organic layer was dried on Na_2SO_4 and evaporated. Column chromatographic separation (silica gel, eluent: Ethyl acetate) of the residue yielded the desired product as a dark blue solid. (80 mg, 25%).

^{1}H NMR (400 MHz, $CDCl_3$): δ_H 7.54-7.42 (3H, m: 2H, ArH; 1H, C*H*), 7.18 (1H, d, *J* = 16.10 Hz, CH), 7.05 (2H, d, *J* = 8.60 Hz, Ar*H*), 6.75 (2H, d, *J* = 8.70 Hz, C*H*),

6.62 (2H, d, *J* = 8.90 Hz, ArH), 6.10 (1H, s, ArH), 5.95 (1H, s, ArH), 3.85-3.75 (8H, m), 3.72-3.59 (24H, m), 2.91 (4H, t, *J* =7.80 Hz), 2.78 (4H, t, *J* = 4.90 Hz), 2.57 (3H, s), 1.54 (3H, s), 1.50 (3H, s); ^{13}C NMR (100 MHz, $CDCl_3$):

δ_C 154.0, 148.0, 147.6, 142.9, 140.5, 136.7, 130.9, 130.8, 129.7, 129.4, 129.3, 125.0, 123,5 122.2, 120.2, 117.2, 114.8, 111,8, 111.6, 74.2, 71.3, 70.7, 70.2, 70.0, 68.5, 52.6, 51.9, 31.6, 31.3, 30.3, 29.6, 15.1, 14.7 ppm.

Anal. Calcd. for $C_{46}H_{61}BF_2N_4O_6S_2$: C 62.86, H 7.00, N 6.37 %. Found: C 63.01, H 7.14, N 6.40 %.

MS (MALDI-TOF): m/z: Calcd. for $C_{46}H_{61}BF_2N_4O_6S_2$: 878.4 [$M^+$], Found: 878.2 [$M^+$]

Synthesis of Compound 37: In a 100 mL round-bottomed flask equipped with a Dean-Stark trap and a reflux condenser were added 40 mL of benzene, **36** (0.06 mmol, 50 mg), 4-(*N*,*N*-di-(pyridine-2-ylmethyl)amino)benzaldehyde (0.12 mmol, 36.40 mg), acetic acid (0.2 mL), and piperidine (0.2 mL). The reaction mixture was stirred at reflux temperature and concentrated nearly to dryness. Progress of the reaction was monitored by TLC (Ethyl acetate : Methanol ; 90 : 10). When all the starting material had been consumed, water (100 mL) was added and mixture was extracted into $CHCl_3$. The organic layer was dried on Na_2SO_4 and evaporated. Column chromatographic separation (silica gel, Ethyl acetate : Methanol ; 90 : 10) of the residue yielded the desired product as a green solid. (33 mg, 50%).

^{1}H NMR (400 MHz, $CDCl_3$): δ_H 8.61 (2H, d, *J* = 5.68 Hz, ArH), 7.67 (2H, t, *J* = 3.89 Hz, ArH), 7.57-7.47 (4H, m: 2H, ArH; 2H, C*H*), 7.46 (2H, d, *J* = 8.80 Hz, ArH), 7.28 (2H, d, *J* = 8.67 Hz, ArH), 7.24-7.15 (3H, m: 2H Ar*H;* 1*H* C*H*), 7.12 (1H, d, *J* = 15.90 Hz, ArH), 7.06 (2H, d, *J* = 8.54, ArH), 6.76-6.70 (4H, m, ArH), 6.65 (2H, d, *J* = 9.00 Hz, ArH), 6.59 (1H, s, Ar*H*), 6.56 (1H, s, Ar*H*), 4.89 (4H, s), 3.85-3.76 (8H, m), 3.72-3.58 (24H, m), 2.92 (4H, t, *J* = 7.92 Hz), 2.76 (4H, t, *J* = 4.94 Hz), 1.52 (6H, s);

^{13}C NMR (100 MHz, $CDCl_3$): δ_C 158.3, 149.8, 149.7, 147.4, 136.9, 135.7, 129.6, 129.3, 129.0, 126.5, 125.3, 122.2, 122.0, 120.9, 112.7, 111.8, 111.5, 74.3, 71.3, 70.7, 70.2, 70.0, 68.6, 57.3, 52.6, 51.9, 38.7, 31.6, 31.3, 30.3, 29.6, 28.9, 15.0, 14.9 ppm.

Anal. Calcd. for $C_{65}H_{76}BF_2N_7O_6S_2$: C 67.05, H 6.58, N 8.42 %. Found: C 66.91, H 6.64, N 8.33 %.

MS (MALDI-TOF): m/z: Calcd. for $C_{65}H_{76}BF_2N_7O_6S_2$: 1163.5 [$M^+$], Found: 1163.3 [$M^+$]

5.6. Conclusion

We demonstrated that with a prior knowledge of respective binding affinities of metal ions for various ligands, it should be possible to design molecular logic gates using different metal ions as inputs. Bodipy chemistry is particularly useful in this regard, because it allows straightforward placement of ICT and PET donors on the same molecule, and that increases signal diversity to a great extent. Styryl-modifications of Bodipy proved to be a useful reaction. In the three examples presented, this modification allowed us to place ICT donor functionalities at strategically important positions. The result is straightforward syntheses of the target molecules, with responses compatible with AND logic and, a molecular half-adder with non-annihilating inputs. Outputs compatible with XOR logic has been difficult to attain without the use of self-annihilating (such as acids and bases, either Lewis or Bronsted-Lowry) inputs, but in the half-adder described in this work, this is done by the differential selective interactions between the ligands and the metal ions selected. Using signals obtained by exploiting relative selectivity of inputs for different ligands/chelators, more challenging molecular logic operations should be within reach.

CHAPTER 6

6. From Virtual to Physical : Integration of Chemical Logic Gates

This work is partially described in the following publication which was highlighted in the Frontispiece of Angewandte Chemie.

Guliyev, R.; Ozturk, S.; Kostereli, Z.; Akkaya, E.U. *Angew. Chem. Int. Ed*. **2011**, *50*, 9826

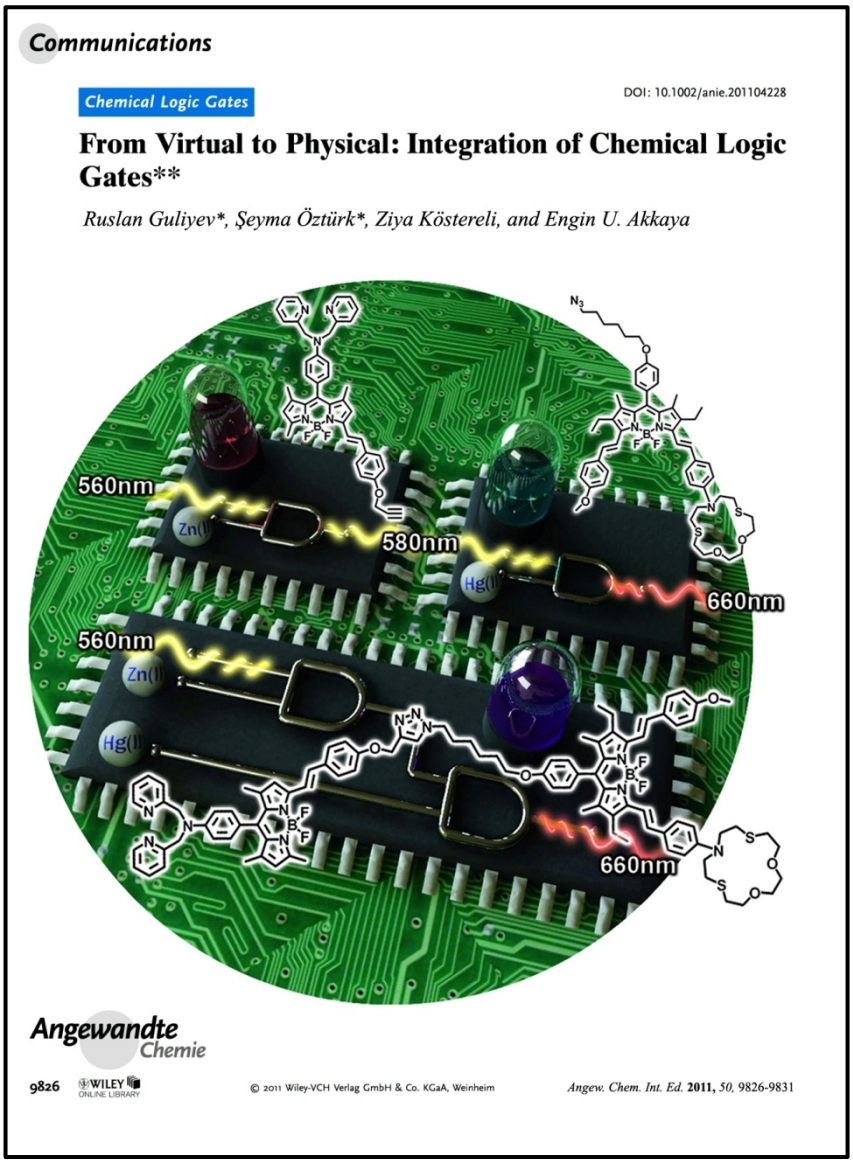

6.1. Objective

For a rational design and implementation towards a sophisticated molecular computing, physical integration/concatenation of molecular (chemical) logic gates should also be provided, like in all other digital devices. Since assuring communication between species is a very difficult task at the molecular level, their physical integration still is one of the foremost problems remaining in the field of molecular logic gates. However, in order to make some further significant advances in this field, there is no doubt that this is the right time for the new methodologies to be developed or put forward as an idea, suggesting alternative solutions to the aforementioned issue. Realizing this emergency, we are reporting a study where two possible methodologies for concatenating two separately functioning molecular logic gates which are energy transfer and modulation of inner filter effect, is proposed. We provide Bodipy- based molecular systems to illustrate these approaches. Particularly, we have synthesized a few derivatives of the well known fluorophore, Bodipy, and in one instance we were able to couple a photochromicity based logic gate to an ion responsive Bodipy based logic gate. In the second example two independent ion responsive logic gates were concatenated by a click reaction as a straightforward example of chemical integration. Details of our work along these lines will be presented within the coming sections.

6.2. Introduction

Logic gates are fundamental building blocks of silicon circuitry. Current technology used in integrated circuit design is fast approaching its physical limits and this "impending doom" scenario[175] led many to consider potential alternatives in information processing. Bottom-up approaches, including molecular mimicry of logic gates with ion responsive molecules received considerable attention since 1993, following the pioneering work of A. P. de Silva.[110] In nearly two decades, all 16 fundamental logic gates and higher functions such as half-adder/subtractor, multiplexer, password protection, encoder/ decoder, sequential logic, etc. were

demonstrated. These higher functions require considerable degrees of integration or concatenation between logic gates, if they were to be implemented using standard practice of semiconductor technology. We also appreciate the fact molecular logic need not be confined with the reigning paradigms of silicon-based information processing. Nevertheless, physical integration of chemical (molecular) logic gates is especially important for rational design and implementation towards advanced molecular scale computing. However, with chemical logic gates, almost all of the integration or concatenation is "functional". In other words, the outputs at various channels (for example, at different wavelengths) are typically analyzed, and a concatenated set of logic gates is then proposed to be acting on the inputs to generate the apparent output sequence. A more fitting term for this class of integration might be "virtual". While this approach is highly convenient and reconfigurable/superposed logic gates can be quite useful, it is nevertheless obvious that, at some point, there has to be simple and general methodologies for physically (as opposed to virtually) bringing together independently working molecular logic gates to function together as concatenated/integrated logic gates.

Despite the adversity of physical integration/wiring of chemical logic gates, there has to be some simple methods, at least to connect a couple of independently working chemical logic gates in a physical way, such that the output of one gate must be the input of the other gate. Obviously, this would not solve the whole issue, yet it should be noted that, even longer marathons are starting with the smaller steps.

Previous work toward concatenated logic gates were often based on enzymatically coupled systems.[176,177,178] While these are interesting reinterpretations and/or rewiring of enzymatic pathways and other biomolecular interactions, we will need to have more general and broadly applicable methodologies for *de novo* concatenation on the way to more capable integrated systems.

In recent years, a few examples of chemical cascading, or integration schemes were proposed.[179,180] In a promising recent report[181] by Raymo and Credi groups, a spiropyran derivative photochemically producing hydrogen ions was linked to a ruthenium complex, resulting in a serial connection between two logic operations.

However, clear demonstration (with non-additive inputs, and large digital-on-off changes) of independently existing and functional logic gates, physically coupled together and thus functioning in an integrated fashion remained elusive.

Herein, we propose two possible ways of achieving integration of independently functioning chemical logic gates: one approach makes use of inner filter effect (IFE) which is modulated photochromically, and the other one is based on increased efficiency of Förster type intramolecular energy transfer (FRET) compared to the intermolecular energy transfer (other factors remaining unchanged).

6.3. Results and Discussions

First approach - Inner filter effect (IFE): Utility of IFE in molecular logic was shown earlier,[182] in that work distinct compartmentalization of the logic molecules was needed and this was done at macroscopic level by placing them in separate cuvettes. More precisely, they had the cuvettes containing spiropyran solutions and each cell mimicking the NOT gate (they took only UV-light as an input). By aligning two and/or three cells in series, and assigning the UV light as an input, and taking the advantage of 'filter effect' they come up with 2-input NOR gate, and 3-input NOR gate respectively. To conclude, the idea of concatenation, is neither "applied" in that article, nor suggested, nor implied. However, in our IFE based approach, we coupled a photochromic molecular AND logic gate to an ion responsive Bodipy based AND logic gate. For this purpose, we chose thionine as the photochromic agent (Figure 81). Thionine, although not utilized in any logic gate design so far, could be highly useful in optical concatenation of logic gates.

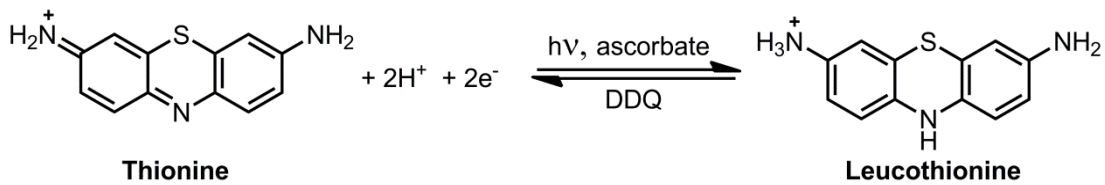

Figure 81. Reversible photochemical conversion of thionine into leucothionine form

The intense blue colored solution of thionine (absorption maximum at 590 nm) can be photochemically reduced to colorless *leuco* form in the presence of intense broadband Uv-Vis light together with any mild reducing agents, such as sodium ascorbate. The reduction of thionine into leucothionine occurs in a very short time, and the leuco form in turn can be converted back into the thionine form in the absence of light or in the presence of any oxidizing agents, such as DDQ.

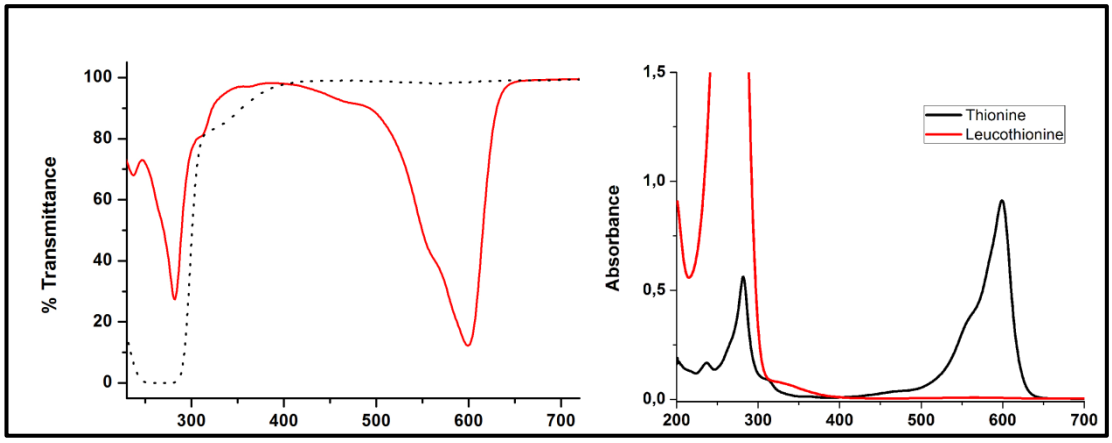

Figure 82. Transmission and absorption spectra of thionine (red curve) and leucothionine (black, dashed) 12.5 µM in methanol. The leuco form was obtained by exposing the thionine solution to broadband white light in the presence of sodium ascorbate as a reducing agent

The clear solution with a higher transmittance (Figure 82), will allow sufficient intensity of light at another wavelength (560 nm) to interrogate the second logic gate (and serve as an input) present in the same solution.

Here, the first independent AND logic gate is the thionine molecule: the output is the transmitted monochromatic light at 560 nm. Both inputs are photonic; one of them is monochromatic light at 560 nm while the other one is broadband white light. When none of the inputs are introduced obviously, no output will be monitored. When thionine solution is irradiated only with the light at 560 nm, it will be absorbed by the thionine molecules (filter effect), resulting in the very little amount of transmitted light at 560 nm. The same situation will be observed when thionine solution is only irradiated with broadband white light, such that thionine absorbs all the light, yielding no transmitted light at 560 nm. The output will be ‘High’ only if both photonic inputs, broadband white light and 560 nm light are introduced to the

system. In this case, thionine will be converted into the leucothionine form with white light and the clear leucothionine solution with a higher transmittance (Figure 48) will allow 560 nm light to be transmitted. Schematic representation of this AND gate with the truth table is shown in Figure 83.

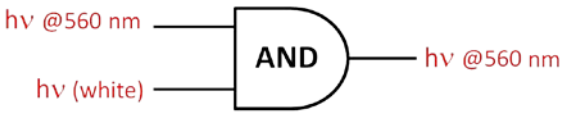

In 1 (white light)	In 2 (560 nm light)	Out (560 nm light)
0	0	0
1	0	0
0	1	0
1	1	1

Figure 83. Schematic representation of first independent AND gate with the truth table

The other AND logic gate we propose here is an ion responsive Bodipy derivative, compound **44**, with the absorption maxima at 560 nm (Figure 87). It is a styryl-Bodipy derivative with a dipicolylamine (DPA) group tethered at the *meso*-(8) position. Its fluorescence is quenched through an efficient PET (photoinduced electron transfer) process, but high emission intensity is recovered, when certain metal ions such as Zn(II) are added. Both inputs (light at 560 nm and Zn(II) ions) need to be HIGH for output, which is the emission intensity at 580 nm, to be HIGH (1), these are. Naturally, this second AND gate works independently as well (Figure 84).

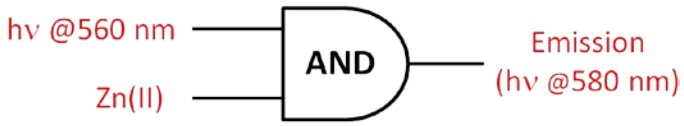

In 1 (560 nm light)	In 2 (Zn(II) ion)	Out (ems at 580 nm light)
0	0	0
1	0	0
0	1	0
1	1	1

Figure 84. Schematic representation of second independent AND gate with the truth table

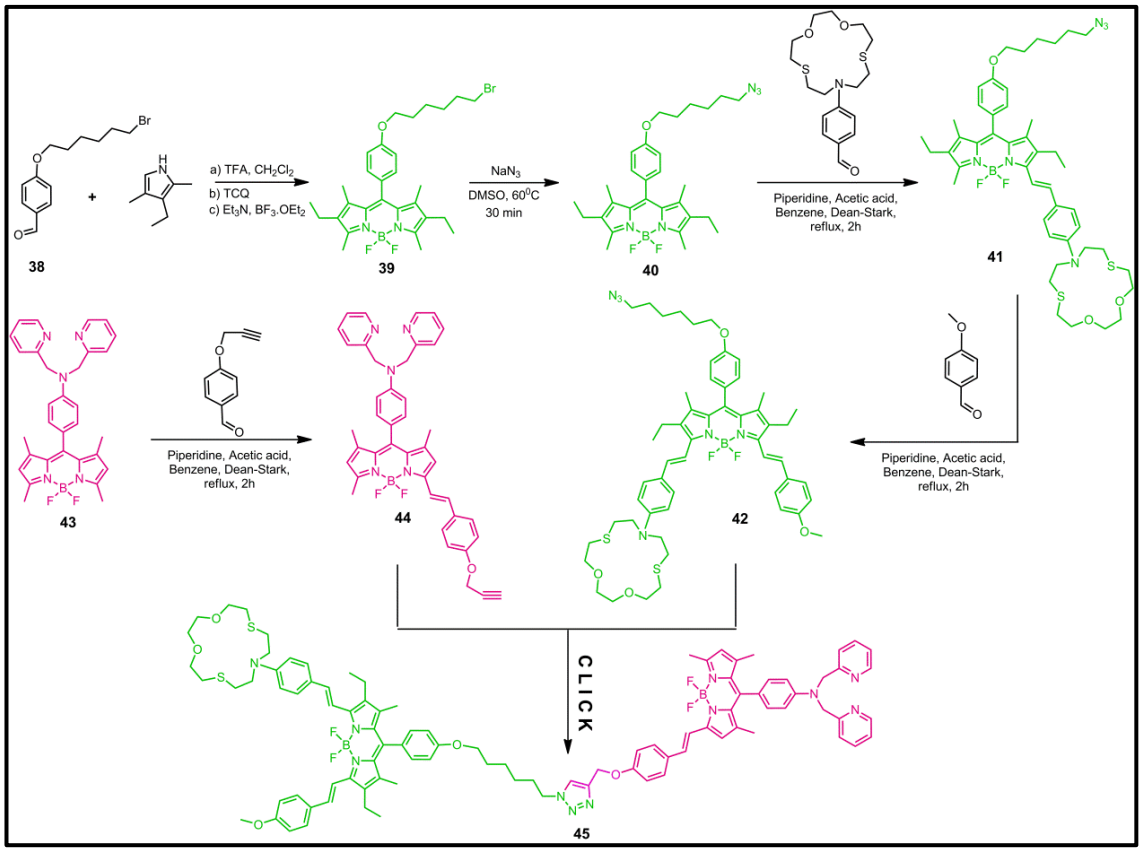

Figure 85. Synthesis of logic gate modules and the final click reaction for the integrated logic compound **45**

When we bring together these two gates in solution, the output of the first gate (thionine) will be one of the inputs of the second AND gate **44**. When the solution of thionine (12.5 μM) and compound **44** (2.2 μM) together in methanol was irradiated with both white light and 560 nm light, thionine will first absorb the white light and will be converted to colorless leucothionine form.

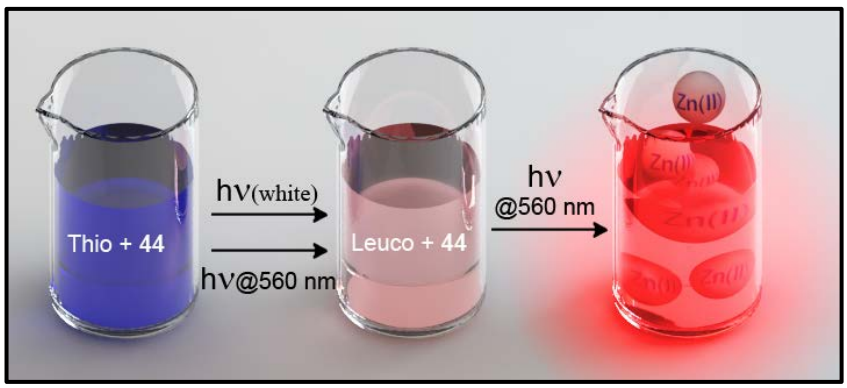

Figure 86. A representation of the operation of the coupled AND logic gates

This colorless form will allow 560 nm light to be transmitted through and used by compound **44**. Then, by the subsequent addition of Zn^{2+} ions to the solution (in addition to 560 nm light) compound **44** would exhibit a strong emission at 580 nm. This is the way, how two separetely functioning AND gates are concatenated through photochemical modulation of the inner filter effect. A representation for the operation of the coupled two AND logic gates is shown in Figure 86.

The operation of integrated logic gates is confirmed by observing the emission behavior of compound **44** (2.2 μM) in the presence of thionine/leucothionine (12.5 μM) in methanol (Figure 87). As demonstrated in the emission spectra, compound **44** has a strong emission in the presence of Zn^{2+} ions while normally it has a very low emission (a and b). The presence of thionine filters the emission of compound **44** in any cases, the emission intensities of both **44** and **44**+Zn(II) is lowered when thionine is present in the solution (c and e compared to a and b).

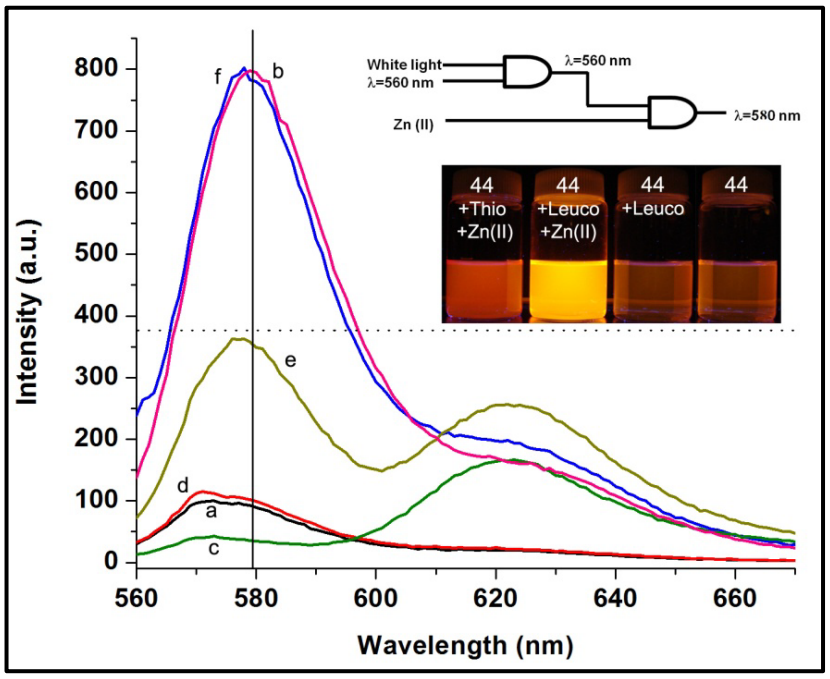

Figure 87. Operation of the integrated logic gates (IFE) as demonstrated by the emission spectra: Emission spectra of compound **44** (2.2 µM) in the presence of thionine/leucothionine (12.5 µM) in methanol. a) 44 alone, b) 44 + Zn(II), c) **44** + thionine, d) **44** + leucothionine (c + white light), e) **44** + thionine + Zn(II), f) **44** + leucothionine + Zn(II) (e +white light). Zn(II) ions were added in the form of perchlorate salt at 22.0 µM concentration. λ_{ex}=560 nm, slit width=5 nm.

When thionine is reduced to leucothionine, its filtering capability is prohibited and thus, the high emission intensity of **44**+Zn(II) is recovered (f compared to e). As a result, high intensity emission (@580 nm) for compound **44** is monitored as the output of the integrated system, only when Zn^{2+} ions and leucothionine are present in the media.

Reversibility of the photochromic response was clearly demonstrated (Figure 88). It is also important to show that with broadband white light alone, the emission from the gate **44** (styryl-Bodipy) has to be low, and that has been demonstrated as well. On standing at room temperature in the presence of excess ascorbate, the oxidized form can be accessed by the addition of DDQ or by air oxidation. It is interesting to note that, DDQ and ascorbate do not react directly, under the conditions of the study. To sum it up, two independent AND logic gates can be coerced to work in an integrated fashion by simply mixing in solution.

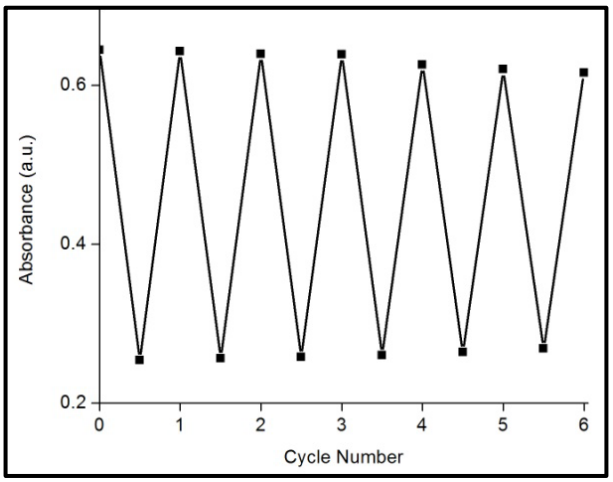

Figure 88. Reversibility of the thionine photochromic response. Reduced *leuco* from of thionine (12.5 μM) which is produced by the photochemical reduction can be transformed back to the original chromophore by DDQ oxidation. The reduction-oxidation cycling can be repeated many times in the presence of the second logic compound **44** (2.2 μM)

To sum up, in our study, we have only one solution, containing two different molecules in it. By taking the advantage of photochromic nature of the thionine molecule, and considering the ion-responsive property of the modified Bodipy molecule, we are proposing the concatenation of two molecules, each mimicking the AND gate separately.

Second approach - Modulation of Intramolecular energy transfer: The idea of using excitation energy transfer for the integration of logic gates was put forward previously by Levine in a conjectural article, in 2001.[183] That article is a 'proposal paper' since there is no experimental section to back this up. In addition, it's a very specific example illustrating the concatenation of two 'virtual' Half Adders to get a full adder. We call that 'virtual', because there are not any two independent molecular half adders to concatenate. They simply think that two dyes (rhodamine and azulene), having detectable one-photon and two-photon absorption, in a solution can be excited at three different wavelengths (three inputs), such that the energy transfer (ET) represents the 'mid-sum'. As this one was the proposal paper, there were no spectroscopic evidences to grasp the proposed idea much better.

In 2006, Speiser et al published nearly the same concept with a very small alteration, covalently attachment of the dyes, with very little experimental work.[184] They called their system as the first single molecule operating in accordance with the full adder. This time they defined ET as the Carry input (Carry-In). Again, there are no separately working logic elements, no spectroscopic data demonstrating the role of ET during concatenation, even output signals were not reported clearly. Regardless of other deficiencies, this article is just another example of virtual integration (or concatenation).

Of course criticizing the previous publications is beyond the scope of this thesis. We are trying to explain that, they have nothing to do with our arguments. They are just any other logic gate system with 'virtual' logic gates, supposedly coming together to generate the output scheme compatible with a full adder, and they may have used ET within their context. To conclude, the above papers, does not contain any concatenation of independently operating/working logic elements, which happens to be the one of the major points of our paper.

However, in our energy transfer (EET) based approach, two chemical gates were again, designed to act separately and independently as two distinct AND gates, without interference and/or cross-talk. The design of these chemical logic gate molecules includes "clickable" azide and terminal alkyne units.

The concatenation was achieved in one “clicked” molecule (Figure 89), which is an ion-modulated energy transfer cassette.

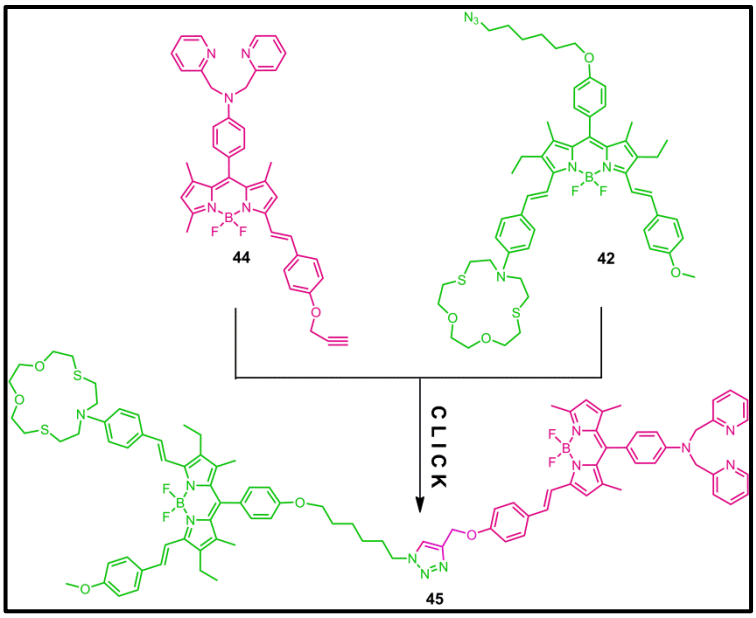

Figure 89. The “clicked” molecule **45**, used in the energy transfer based integration

The first AND gate is the same as the second one used in the previous scheme, compound **44**. The other one is also mono-styryl derivative (**42**), but since it has an azathiacrown moiety attached through its amine nitrogen (essentially a dialkylamino group), increased charge transfer characteristics lead to a longer wavelength absorption and emission (Figure 90).

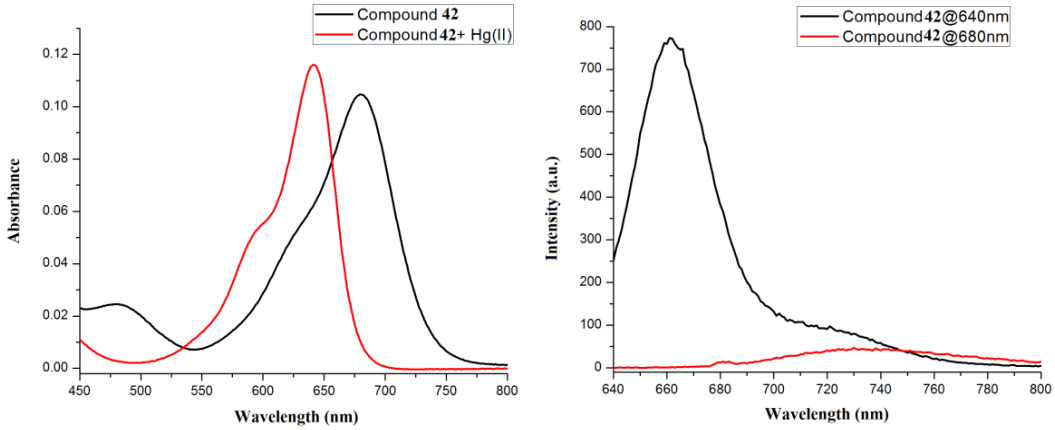

Figure 90. Absorbance and emission spectra of compound **42** (2 μM) in Acetonitrile in the presence of Hg(II) (40 µM)

When Hg^{2+} ions bind to the crown moiety of **42**, a blue shift is monitored in the absorption and emission spectra of the molecule such that the absorption maximum shifts to 640 nm in the presence of Hg^{2+} ions (Figure 90). Compound **42** also acts as an AND gate, with a photonic (light at 580 nm) and ionic (Hg^{2+} ion) inputs. Only when both inputs are present, strong red emission at 660 nm is produced. When compound **42** is excited with 680 nm light, very little emission is monitored. However, when the compound in the presence of Hg^{2+} is excited with 640 nm light (absorption maximum of **42**+Hg^{2+} is at 640 nm) or 580 nm light, a strong red emission at 660 nm is monitored.

When compounds **44** and **42** are "clicked" together with Huisgen cycloaddition, the product obtained (**45**) is in fact, an ion modulated energy transfer cassette with two chromophores, which is designed to couple those two distinct AND gates in one molecule such that the output of the first gate would be the input of the second one.

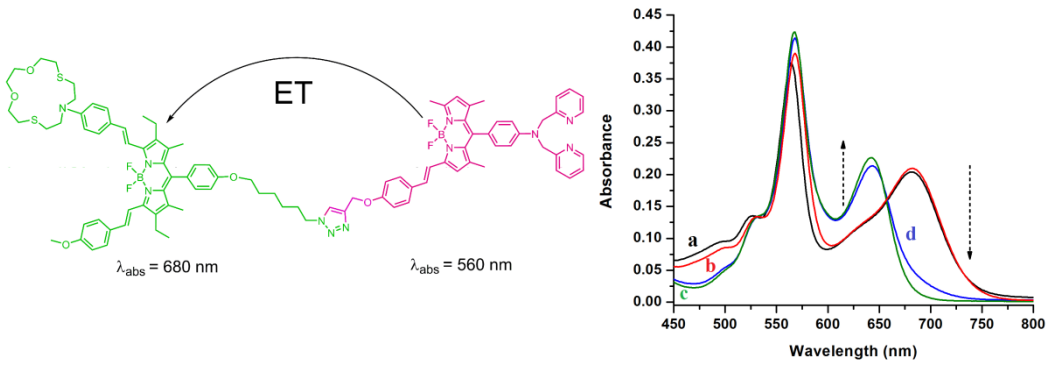

Figure 91. Absorbance spectra of Compound **45** (3.0 µM) in acetonitrile in the presence of Zn(II) and Hg(II) cations (20.0 µM and 10 µM, respectively) a) **45**, b) **45**+Zn(II), c) **45**+Hg(II), d) **45**+Zn(II)+Hg(II)

In this molecule, the photonic output at 660 nm is only generated when all three inputs (hv@560, Zn(II) and Hg(II)) nm are present (HIGH). In all other combinations, the emission at 660 nm is low (Figure 92). Considering compound **45**, the donor chromophore does not emit light (at 580 nm) when irradiated with 560 nm even in the presence of Zn(II) ions, because of the energy transfer occurring from donor to acceptor. The emission at the red channel is dependent on the PeT efficiency of the module derived from the first logic gate (**44**).

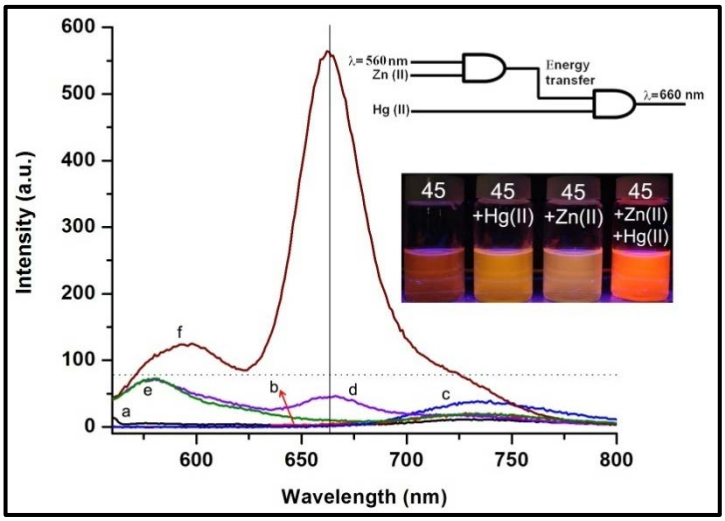

Figure 92. Operation of the integrated logic gates as demonstrated by the emission spectra: Emission spectra of compound **45** (3.0 µM) in acetonitrile in the presence of Zn(II) and Hg(II) cations (20.0 µM and 10 µM, respectively). (λ_{ex}=560 nm, slit width=5-2.5) a) **45**@560 nm, b) **45**@640 nm; c) **45**@680 nm; d) **45**+Hg(II)@560 nm; e) **45**+Zn(II)@560 nm; f) **45**+Hg(II)+Zn(II)@560 nm.

The excitation of compound **45** at 560 nm results in excitation of donor unit. When **45** is irradiated with 560 nm monochromatic light in the absence of Zn^{2+} ion, the efficiency of energy transfer is drastically reduced, because of PET process (Figure 93). Since almost no energy transfer happens from donor to acceptor, a strong red emission at 660 nm cannot be monitored, corresponding to Output=0.

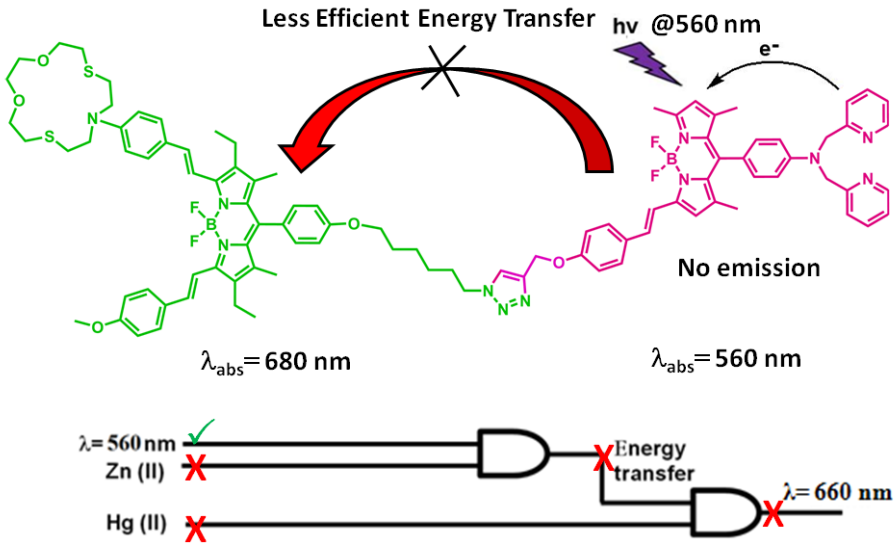

Figure 93. Effect of PET on compound **45**

When Zn^{2+} ions are present in the media, the PET is quenched. Excitation of the molecule with 560 nm light in the presence of Zn^{2+}, results in the very weak emission at 580 nm. It is because of the energy transfer occurring from donor to acceptor, however, it is not sufficient enough to yield the strong red emission at 660 nm. As a result, a strong red emission cannot be observed (Figure 94).

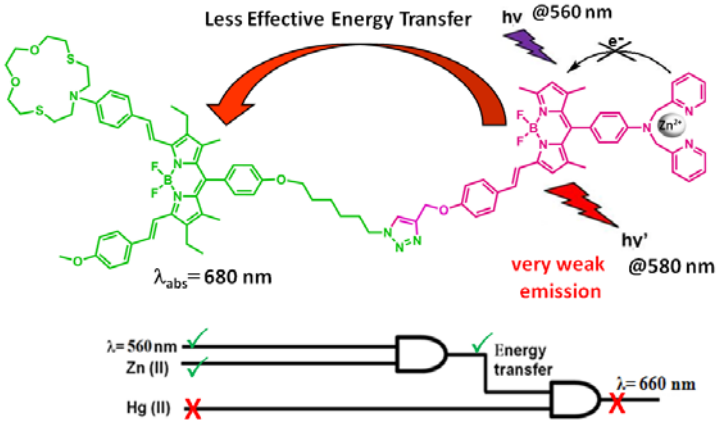

Figure 94. Less effective ET because of the inadequate spectral overlap

As stated before, absorption maximum of **45** is blue shifted from 680 nm to 640 nm in the presence of Hg^{2+} ions. In this case, due to the increased spectral overlap between donor emission and acceptor absorption, the efficiency of energy transfer is improved. As a result, when **45** is irradiated with 560 nm light while both Zn^{2+} and Hg^{2+} ions are present, strong red emission at 660 nm can be monitored (Figure 95).

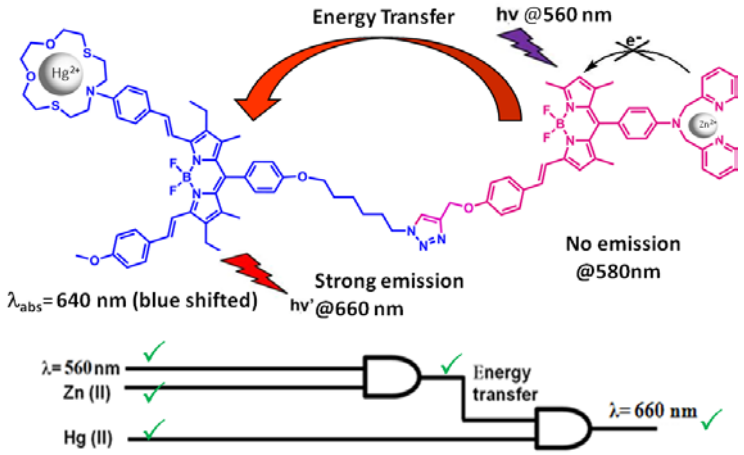

Figure 95. Output is high (1) when all the inputs exist at the same time

This energy transfer is evidenced both by quantum yield (**44** vs **45**, the donor data) and lifetime changes (Table 6). The emission quantum yield of the donor module **44** is 0.1 due to effective PeT, but increases to 0.71 on Zn(II) addition. In the "click" integrated logic molecule **45**, the donor is hardly emissive (Φ_F=0.002, due to effective Förster type energy transfer). The second module (acceptor) derived from compound **42**, even when energy transfer is effective, does not fluoresce brightly because of strong ICT charge donor characteristics of the dialkylamino group. When the final input Hg(II) is added, then strong emission in red is observed (Figure 92).

	λ_{max}		ε_{max}		Φ^a		τ(ns)^b	
Compound	**D**^{c}	**A**^{c}	**D**	**A**	**D**	**A**	τ_1	τ_2
44	562		84000		0.1		3.91	
44+Zn(II)	562		84000		0.71		3.95	
41	611		51000		0.13		3.15	
41+Hg(II)	573		51000		0.56			
42	680		52000		0.036		2.01	
42+Hg(II)	642		58000		0.24			
45	563	682	125300	68000	0.002	0.004	0.32	3.63
45+Zn(II)	567	681	125300	67300	0.024	0.015	0.71	3.58
45+Zn(II)+Hg(II)	567	642	137600	71000	0.036	0.190	0.82	3.70

Table 6. (a) Quantum yields for all compounds were calculated using Sulforhodamine 101 (Φ=0.90 in ethanol) as a reference. (b) Fluorescence lifetimes (τ) corresponds to single-exponential decays if one number is listed (for compounds of **44**, **41** and **42**). (c) D represents the energy for donor unit while A represents the one for acceptor moiety. Compound **44** was excited at 560 nm, **41** at 610 nm, **42** at 680 nm, and **45** at 575 nm. Data under the columns are related to these molecular units

Since the ligands in both of the logic gate modules are highly selective, there is no crosstalk, the metal ions do not interfere or target the "wrong" ligand at the concentrations of the study, at least to an extent to cause problems in signal evaluation. Binding constants of the ligand-metal ion pairs support this argument, and were reported previously.[185] The absorbance spectra obtained for the integrated logic compound **45** under various conditions (Figure 91) shows this unequivocally. Zn(II) ions do not bind to azathiacrown ligand.

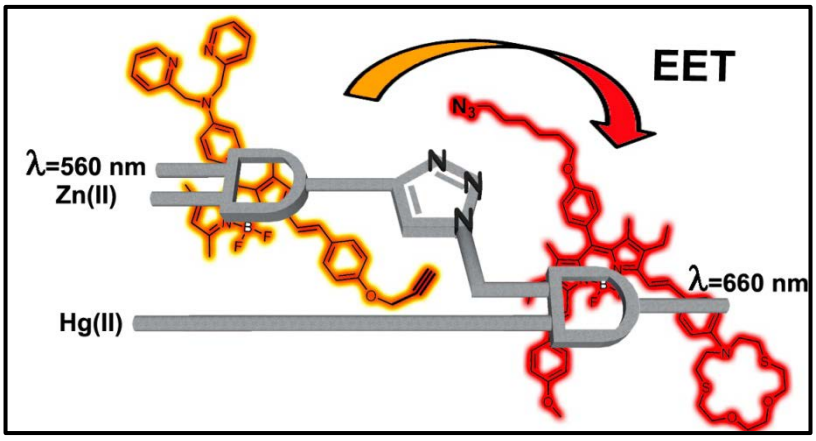

Figure 96. A representation of the two coupled AND logic gates via click chemistry

To the best of our knowledge, our work is the first, which explicitly shows that independent logic gates can be physically brought together by a click reaction to function in an integrated manner. And that idea is an important one, if implemented properly, it could take the molecular logic gate research to a path of solid progress towards advanced information processing.

6.4. Experimental Details

General: ^{1}H NMR and ^{13}C NMR spectra were recorded on Bruker DPX-400 (operating at 400 MHz for ^{1}H NMR and 100 MHz for ^{13}C NMR) in $CDCl_3$ with tetramethylsilane as internal standard. All spectra were recorded at 25 ^{o}C and coupling constants (*J* values) were given in Hz. Chemical shifts were given in parts per million (ppm). Splitting patterns are designated as s (singlet), d (doublet), t (triplet), q (quartet), p (pentet) and m (multiplet). All the ^{13}C spectra were recorded with simultaneous decoupling of proton nuclei. Mass spectra were recorded on Agilent Technologies 6530 Accurate-Mass Q-TOF LC/MS. Absorption spectra were performed by using a Varian Cary-100 spectrophotometer. Fluorescence measurements were conducted on a Varian Eclipse spectrofluometer. Flourescence life time measurements were determined on a HORIBA Jobin Yvon fluorolog, FL-1057. HORIBA Scientific NanoLEDs at 560 nm, 590 nm, 605 nm, 650 nm, and 667 nm (pulse width < 250ps) were used. The instrument response function was

measured with an aqueous Ludox solution. The decays were analyzed with a multi-exponential fitting function by iterative reconvolution and chi-square minimization. The white light used in the reduction of thionine dye was KENGO LIGHTING (F118WH), its voltage and maximum wattage were 230 V – 50 Hz and 500 W respectively. Reactions were monitored by thin layer chromatography using Merck TLC Silica gel 60 F_{254}. Silica gel column chromatography was performed over Merck Silica gel 60 (particle size: 0.040-0.063 mm, 230-400 mesh ASTM). All other reagents and solvents were purchased from Aldrich and used without further purification. 4-(*N*,*N*-di-(pyridine-2-ylmethyl)amino) benzaldehyde,[186] 4-bromohexoxybenzaldehyde[187] and 4-(1,4-dioxa-7,13–dithia–10 azacyclopentadecan–10-yl)benzaldehyde[169] were synthesized according to literature.

Synthesis of target molecule 44

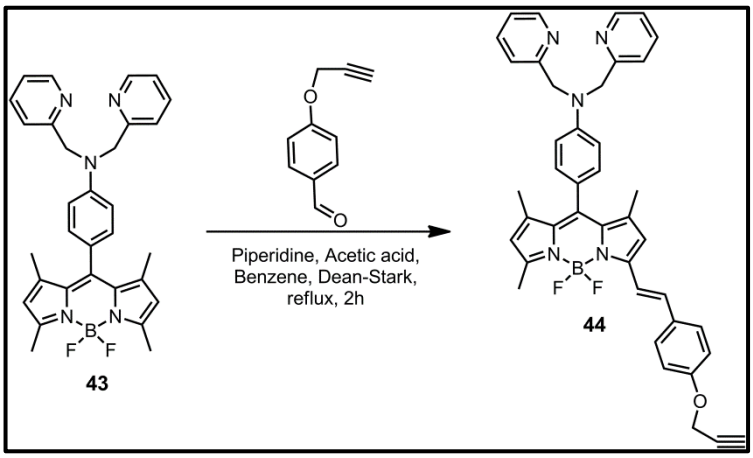

***Synthesis of Compound 43*:** To a 1.0 L round-bottomed flask containing 400 mL argon-degassed CH_2Cl_2 were added 2,4-dimethyl pyrrole (4.4 mmol, 0.4 g), 4-(*N*,*N*-di-(pyridine-2-ylmethyl)amino) benzaldehyde[186] (1.98 mmol, 0.6 g) and one drop of trifluoroacetic acid. The solution was stirred under N_2 at room temperature for 1 day. After addition of a solution of DDQ (1.98 mmol, 0.45 g) in 100 mL of CH_2Cl_2 to the reaction mixture, stirring was continued for 30 min. 5 mL of Et_3N and 5 mL of $BF_3.OEt_2$ were successively added and after 30 min, the reaction mixture was washed with water (3 x 300 mL) and dried over anhydrous Na_2SO_4. The solvent was

evaporated and the residue was purified by silica gel column chromatography using $CHCl_3$: Methanol (97 : 3) as the eluant. Orange solid (0.25 g, 23%).

^{1}H NMR (400 MHz, $CDCl_3$): δ_H 8.60 (2H, d, *J* = 6.48 Hz, ArH), 7.62 (2H, t, *J* = 7.71 Hz, ArH), 7.22 (2H, d, *J* = 7.84 Hz, ArH), 7.18 (2H, t, *J* = 6.58 Hz, ArH), 6.98 (2H, d, *J* = 8.80, ArH), 6.80 (2H, d, *J* = 8.80, ArH), 5.95 (2H, s, ArH), 4.87 (4H, s, C*H*$_2$), 2.52 (6H, s, C*H*$_3$), 1.45 (6H, s, C*H*$_3$) ppm.

^{13}C NMR (100 MHz, $CDCl_3$): δ_C 158.3, 154.8, 149.8, 149.7, 148.8, 143.1, 136.7, 128.9, 123.3, 122.2, 120.9, 113.2, 57.4, 14.5 ppm.

Synthesis of Compound 44: In a 100 mL round-bottomed flask equipped with a Dean-Stark trap and a reflux condenser were added 40 mL of benzene, compound **1** (0.15 mmol, 80 mg), 4-propargyloxy benzaldehyde (0.15 mmol, 24 mg), acetic acid (0.2 mL), and piperidine (0.2 mL). The reaction mixture was stirred at reflux temperature and concentrated nearly to dryness. Progress of the reaction was monitored by TLC (1:1 Hexane : Acetone). When all the starting material had been consumed, water (100 mL) was added and mixture was extracted into $CHCl_3$. The organic layer was dried on Na_2SO_4 and evaporated. Column chromatographic separation (silica gel, 1:1 Hexane : Acetone) of the residue yielded the desired product as a dark purplish-red solid. (21 mg, 20%).

^{1}H NMR (400 MHz, $CDCl_3$): δ_H 8.62 (2H, d, *J* = 4.84 Hz, ArH), 7.65 (2H, t, *J* = 8.54 Hz, ArH), 7.60-7.54 (3H, m: 2H, ArH; 1H, C*H*), 7.26-7.15 (5H, m: 4H, ArH; 1H, C*H*), 7.03 (2H, d, *J* = 8.84 Hz, ArH), 6.98 (2H, d, *J* = 8.85 Hz, ArH), 6.80 (2H, d, *J* = 8.84 Hz, ArH), 6.58 (1H, s, ArH), 5.90 (1H, s, ArH), 4.88 (4H, s, C*H*$_2$), 4.74 (2H, d, *J* = 2.44 Hz, OCH_3), 2.58 (3H, s, C*H*$_3$), 2.55 (1H, t, *J* = 2.46 Hz, CH), 1.48 (3H, s, C*H*$_3$), 1.44 (3H, s, C*H*$_3$) ppm.

^{13}C NMR (100 MHz, $CDCl_3$): δ_C 158.3, 154.5, 153.0, 149.8, 148.8, 142.5, 139.0, 136.7, 135.2, 130.4, 129.2, 128.8, 122.2, 120.9, 117.7, 117.1, 115.1, 113.2, 78.7, 75.8, 57.4, 55.9, 29.7, 14.8, 14.6 ppm.

MS (TOF - ESI): m/z: Calcd: 663.2981 [M^+], Found: 664.30697 [$M+H]^+$, Δ=1.3 ppm.

Synthesis of compound 39:

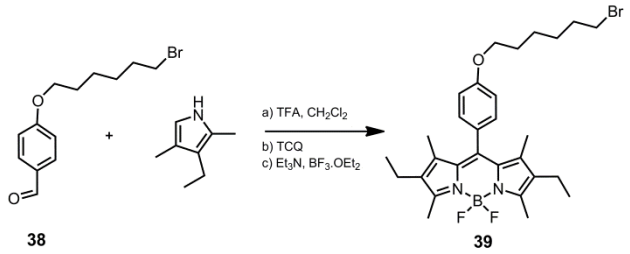

CH_2Cl_2 (300 ml) was purged with Ar gas for 30 min. Compound **38**[187] (1.089 g, 3.82 mmol) and 2,4-dimethyl pyrrole (0.94 g, 7.7 mmol) were added. The color of the solution turned into red after the addition of 3 drops of trifluoroacetic acid. The reaction mixture was stirred at room temperature for 12h. Then, tetrachloro-1,4-benzoquinone (0.93 g, 3.82 mmol) was added and the reaction mixture was stirred at room temperature for 45 min. Then triethyl amine (8 ml) and boron trifluoride diethyl etherate (8 ml) were added sequentially. After stirring at room temperature for 30 min, it was extracted with water. Organic layer was dried with Na_2SO_4 and evaporated under reduced pressure. The product was purified by silica gel column chromatography using $CHCl_3$ as mobile phase. Fraction containing compound **39** was collected then the solvent was removed under reduced pressure (670 mg, 1.2 mmol, 31%).

^{1}H NMR (400 MHz, $CDCl_3$): δ_H 7.15 (d, *J*= 8.56 Hz, 2H), 7.0 (d, *J*= 8.56 Hz, 2H), 4.05 (t, *J*= 6.45 Hz, 2H), 3.59 (t, *J*= 6.64 Hz, 2H), 2.55 (s, 6H), 2.3 (q, J= 7.56, 4H), 1.85 (m, 4H), 1.58 (m, 4H), 1.35 (s, 6H), 1.0 (t, J= 7.52, 6H) ppm.

^{13}C NMR (100 MHz, $CDCl_3$): δ_C 159.47, 153.46, 140.0, 138.43, 132.60, 130.10, 129.44, 127.78, 114.95, 67.87, 44.96, 32.48, 29.11, 26.67, 25.43, 17.06, 14.61, 12.46, 11.84 ppm

Synthesis of compound 40:

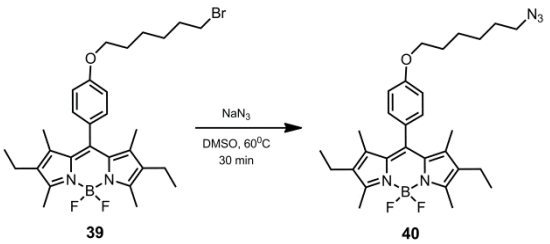

Compound **39** (190 mg, 0.34 mmol) was dissolved in 20 ml DMSO. Excess amount of sodium azide (600 mg, 9.23 mmol) was added. The reaction mixture was stirred for 30 minutes at 60^{o}C. After 30 minutes, sample was extracted with water and $CHCl_3$ a few times to get rid of DMSO and excess NaN_3. Organic layer containing compound **40** was dried with Na_2SO_4 and evaporated under reduced pressure No further purification was required.

^{1}H NMR (400 MHz, $CDCl_3$): δ_H 7.15 (d, *J*= 8.56 Hz, 2H), 7.0 (d, *J*= 8.56 Hz, 2H), 4.05 (t, *J*= 6.45 Hz, 2H), 3.32 (t, *J*= 6.64 Hz, 2H), 2.55 (s, 6H), 2.3 (q, J= 7.56 Hz, 4H), 1.85 (m, 2H), 1.68 (m, 2H), 1.54 (m, 4H), 1.35 (s, 6H), 1.0 (t, J= 7.52 Hz, 6H)

^{13}C NMR (100 MHz, $CDCl_3$): δ_C 159.46, 153.46, 140.33, 138.43, 132.61, 131.19, 127.77, 114.95, 67.86, 51.38, 29.13, 28.80, 26.56, 25.71, 17.07, 14.62, 12.46, 11.84

MS (TOF - ESI): m/z: Calcd: 521.3137 [M^+], Found: 520.3065 [M-H]$^+$, Δ=1.6 ppm

Synthesis of compound 41:

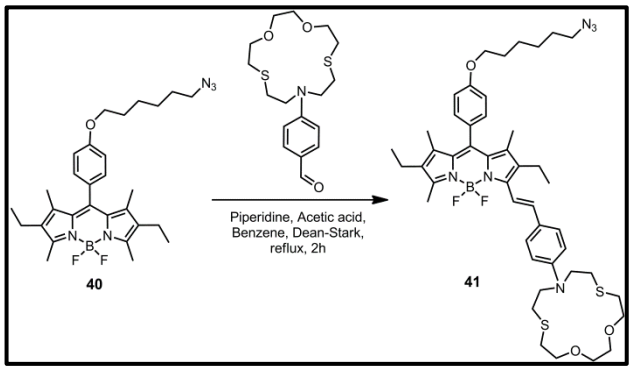

In a 100 mL round-bottomed flask equipped with a Dean-Stark trap and a reflux condenser were added 40 mL of benzene, compound **40** (0.20 mmol, 0.106 g), 4-(1,4- dioxa-7,13-dithia-10-azacyclopentadecan-10-yl) benzaldehyde[169] (0.20 mmol, 0.072 g), acetic acid (0.2 mL), and piperidine (0.2 mL). The reaction mixture was stirred at reflux temperature and concentrated nearly to dryness. Progress of the reaction was monitored by TLC ($CHCl_3$). When all the starting material had been consumed, water (100 mL) was added and mixture was extracted into $CHCl_3$. The organic layer was dried on Na_2SO_4 and evaporated. Column chromatographic separation (silica gel, $CHCl_3$) of the residue yielded desired product as a dark blue solid (44 mg, 25%).

^{1}H NMR (400 MHz, $CDCl_3$): δ_H 7.59 (1H, d, *J* = 16.93 Hz, CH), 7.52 (2H, d, *J* = 8.32 Hz, ArH), 7.19 (3H, m: 2H, ArH; 1H, CH), 7.01 (2H, d, *J* = 8.04 Hz, ArH), 6.67 (2H, d, *J* = 8.24 Hz, ArH), 4.08 (2H, t, *J* = 6.10 Hz, OCH_2), 3.85 (broad 4H, s, OCH_2CH_2), 3.69 (8H, m), 3.34 (2H, t, *J* = 6.59 Hz, N_3CH_2), 2.95 (4H, t, *J* = 7.36 Hz, NCH_2CH_2), 2.80 (broad 4H, SCH_2CH_2), 2.68-2.55 (5H, m: 3H CH_3, 2H CH_2), 2.35 (2H, q, *J* = 7.50 Hz, CH_2CH_3), 1.89 (2H, t, *J* = 7.20 Hz, OCH_2CH_2) 1.70 (2H, t, *J* = 6.15 Hz, $N_3CH_2CH_2$), 1.61-1.48 (4H, m, CH_2CH_2), 1.39 (3H, s, CH_3), 1.38 (3H, s, CH_3), 1.18 (3H, t, *J* = 7.08 Hz, CH_3), 1.01 (3H, t, *J* = 7.22 Hz, CH_3) ppm.

^{13}C NMR (100 MHz, $CDCl_3$): δ_C 159.4, 152.8, 150.5, 147.2, 138.8, 138.5, 137.6, 135.6, 132.9, 132.7, 131.6, 129.7, 129.0, 128.1, 125.8, 115.8, 114.9, 111.8, 74.2, 70.7, 67.8, 51.9, 51.4, 31.3, 29.5, 29.1, 28.8, 26.5, 25.5, 18.4, 17.1, 14.6, 12.6, 11.8, 11.6 ppm.

MS (TOF - ESI): m/z: Calcd: 858.4308 [M^+], Found: 859.4398 [$M+H]^+$, Δ=1.1 ppm.

Synthesis of compound 42:

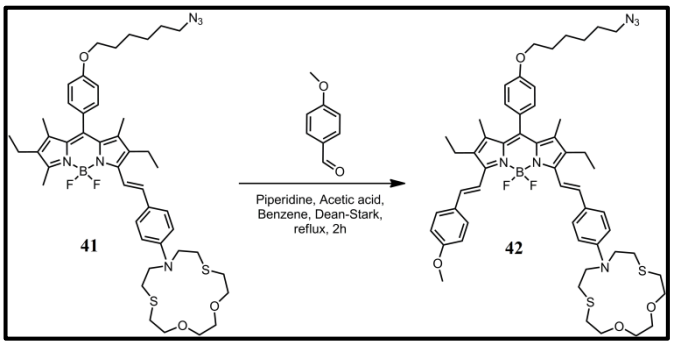

In a 100 mL round-bottomed flask equipped with a Dean-Stark trap and a reflux condenser were added 40 mL of benzene, compound **41** (0.13 mmol, 110 mg), 4-metoxy benzaldehyde (0.26 mmol, 35.4 mg), acetic acid (0.2 mL), and piperidine (0.2 mL). The reaction mixture was stirred at reflux temperature and concentrated nearly to dryness. Progress of the reaction was monitored by TLC (Chloroform : Methanol ; 98 : 2). When all the starting material had been consumed, water (100 mL) was added and mixture was extracted into $CHCl_3$. The organic layer was dried on Na_2SO_4 and evaporated. Column chromatographic separation (silica gel, Chloroform : Methanol ; 98 : 2) of the residue yielded the desired product as a green solid. (65 mg, 44%).

^{1}H NMR (400 MHz, $CDCl_3$): δ_H 7.68 (1H, d, *J* = 16.73 Hz, CH), 7.63 (1H, d, *J* = 16.9 Hz, CH), 7.59 (2H, d, *J* = 8.76 Hz, ArH), 7.54 (2H, d, *J* = 8.80 Hz, ArH), 7.26-7.15 (4H, m: 2H, ArH; 1H, CH; 1H, CH), 7.02 (2H, d, *J* = 8.44 Hz, Ar*H*), 6.97 (2H, d, *J* = 8.68 Hz, ArH), 6.69 (2H, d, *J* = 8.84, ArH), 4.06 (2H, t, *J* = 6.40 Hz, OCH_2), 3.88 (3H, s, OCH_3), 3.84 (4H, t, *J* = 4.98 Hz, OCH_2CH_2), 3.75-3.62 (8H, m, 4H, NCH_2CH_2S, 4H, OCH_2CH_2O), 3.32 (2H, t, *J* = 6.83 Hz, N_3CH_2), 2.92 (4H, t, *J* = 3.88 Hz, OCH_2CH_2S), 2.78 (4H, t, *J* = 4.50 Hz, NCH_2CH_2S), 2.62 (4H, q, *J* = 6.30 Hz, CH_2), 1.89 (2H, m) 1.69 (2H, m), 1.55 (4H, m), 1.39 (6H, s, CH_3), 1.18 (6H, t, *J* = 7.49 Hz) ppm.

^{13}C NMR (100 MHz, $CDCl_3$): δ_C 159.96, 159.45, 159.42, 151.57, 148.98, 147.46, 147.29, 138.98, 137.74, 137.17, 136.41, 135.68, 134.36, 133.70, 133.57, 132.99, 130.62, 130.09, 129.98, 129.75, 129.24, 129.00, 128.64, 128.33, 128.16, 125.87, 118.47, 115.86, 114.92, 114.43, 114.21, 111.87, 74.28, 70.75, 67.89, 55.42, 51.97, 51.41, 31.32, 29.60, 29.17, 28.82, 26.59, 25.74, 18.42, 14.15, 14.00, 11.72, 11.61

MS (TOF - ESI): m/z: Calcd: 976.4726 [M^+], Found: 977.4781 [$M+H]^+$, Δ=2.6 ppm.

Synthesis of compound 42:

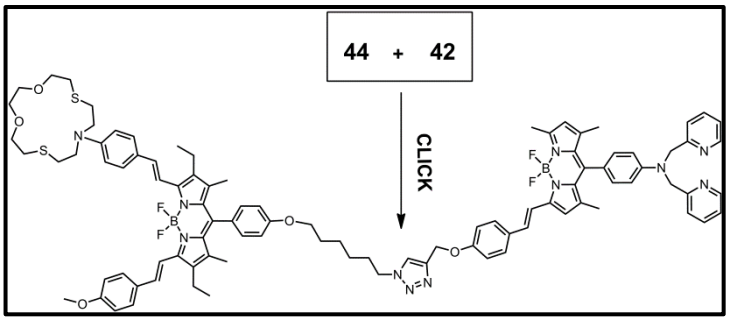

A solution of the compound **44** (0.030 mmol, 20 mg), compound **42** (0.045 mmol, 38 mg). sodium ascorbate (0.022 mmol, 4.3 mg), and $CuSO_4$ (0.011 mmol, 2.73 mg) in a 12:1:1 mixture of $CHCl_3$, EtOH and water (total 14 ml) was stirred at room temperature for 12 h. After evaporation of solvent, the crude product was purified by column chromatography ($CHCl_3$: Methanol, 93:7). Purple solid (32 mg, 55%).

^{1}H NMR (400 MHz, $CDCl_3$): δ_H 8.63 (2H, d, *J* = 4.7 Hz, ArH), 7.72-7.48 (11H, m), 7.26-7.13 (9H, m), 7.06-6.93 (8H, m), 6.85-6.78 (2H, d, *J* = 8.80 Hz, ArH), 6.69 (2H, d, *J* = 8.72 Hz, ArH), 6.58 (1H, s, ArH), 5.98 (1H, s, ArH), 5.28 (2H, s, OCH_2), 4.89

(4H, s, NCH_2), 4.41 (2H, t, *J* = 7.10 Hz), 4.02 (2H, t, *J* = 6.30 Hz), 3.88 (3H, s, OCH_3), 3.83 (4H, t, *J* = 4.98 Hz), 3.75-3.66 (8H, m), 2.95 (4H, t, *J* = 8.80 Hz), 2.80 (4H, t, *J* = 4.98 Hz), 2.63-2.54 (7H, m), 2.00 (2H, m), 1.83 (2H, m), 1.73 (2H, m), 1.58 (2H, m), 1.50 (3H, s), 1.46 (3H, s), 1.38 (6H, s), 1.17 (6H, t, *J* = 7.38 Hz)
^{13}C NMR (100 MHz, $CDCl_3$): δ_C 159.94, 159.41, 158.81, 158.29, 149.79, 148.81, 147.44, 144.01, 136.74, 135.22, 130.07, 129.97, 129.24, 129.13, 128.92, 128.63, 123.40, 122.50, 122.20, 120.95, 117.17, 115.13, 114.90, 114.20, 113.20, 111.86, 74,28, 70.75, 67.78, 62.21, 57.42, 55.41, 51.97, 50.35, 31.32, 30.21, 29.60, 29.08, 26.33, 25.61, 14.81, 14.57, 14.14, 14.00, 11.73 ppm.

6.5. Conclusion

In conclusion, energy transfer (EET) and modulation of inner filter effect (IFE) offer two possible methodologies for concatenating two logic gates. In our IFE-based approach, we concatenated a photochromicity-based AND logic gate to an ion-responsive Bodipy based AND gate, making use of the modulation of IFE. In energy transfer based method, we coupled two ion-responsive Bodipy based AND logic gates, through the increased efficiency of energy transfer. EET approach is particularly appealing because, it involves physical connection of two logic gates through a chemical reaction. There are still issues to be addressed, such as the maximum number of gates that can be integrated based on EET approach, but even the slightest improvements in mimicking silicon circuitry may yield huge leaps of advance due to the molecular nature of these particular designs. While other approaches including self-assembling components are possible, we are confident that clickable molecular logic gates are highly promising. Demonstration of more complex examples of physically integrated logic gates is to be expected. Our work along those lines is in progress.

CHAPTER 7

EPILOGUE

7. EPILOGUE

In this thesis, we have proposed some novel and interesting approaches in the design of fluorescent chemosensors. Targeting of medically important anions, such as cyanide and fluoride, and developing a multianalyte chemosensor for cations were successfully achieved through a rational design. Since Bodipy dyes are very versatile chromophores in many applications, they were exactly the preferred fluorophores used in the design of fluorescent probes provided in this thesis.

In one of those works (chapter 3), we have reported a highly selective and sensitive cyanide sensor operating in the "turn-off-on" mode via decomplexation of Cu(II) ion from a bright fluorescent boradiazaindacene derivative. The system described there can detect cyanide ion concentrations lower than 20.0 μM in water, which is the lowest limit of the blood cyanide concentrations found in fire victims. We can confidently claim that our system is an important member of cyanide sensors emerged in recent years.

In another study (chapter 4), we have presented our work in the expansion of central Bodipy ring via a rational approach. That study has considerable number of features which would make it a valuable and broadly interesting work for readers. Successful use of heteronuclear NMR to elucidate the signaling mechanism in a chemosensor is very rare. In addition, Bodipy dyes are at the focus of considerable attention in recent years, straightforward access into ring expanded derivatives would be of interest just as a result of because of this. Particularly, we were managed to synthesize oxalyl-tethered pyrroles that are doubly bridged with two difluoroboron chelating units to yield bright orange dyes. Addition of fluoride and cyanide anions on to the solutions of that compound resulted in reversible detachment of the otherwise stable difluoroboron bridges, displaying sharp changes in color. In other words, in that approach, the relief of distorted structure of boron bridges by fluoride/cyanide addition played a key role in the recognition process. The structural characterization as well as sensing performance of that novel compound was investigated by ^{11}B NMR, absorption spectroscopic and mass spectrometric techniques.

On the other hand, by using the accumulated knowledge of chemosensor design, we have been investigating their applications to different fields of supramolecular chemistry. We realized that by the help of fluorescent chemosensors we can address some important solutions, at least to a certain point, to the troublesome issues that molecular logic concept faces.

In one of those works (chapter 5), we demonstrated that with a prior knowledge of respective binding affinities of metal ions for various ligands, it should be possible to design molecular logic gates using different metal ions as inputs. Bodipy chemistry is particularly useful in this regard, because it allows straightforward placement of ICT and PET donors on the same molecule. These modulators can then be selectively addressed by exploiting selective metal ion/ligand interactions, resulting in signal changes which can be separately associated with ICT or PET processes. In addition, such designed systems eliminate the need for self-annihilating “inputs”, the use of which in retrospect, look very crafty. In the presented examples, straightforward syntheses of the target molecules, with responses compatible with 3-input AND logic and, a molecular half-adder with non-annihilating inputs, was demonstrated. Outputs compatible with XOR logic has been difficult to attain without the use of self-annihilating (such as acids and bases, either Lewis or Bronsted-Lowry) inputs, but in the half-adder described in this work, this is done by the differential selective interactions between the ligands and the metal ions selected.

Recent research in molecular logic gates produced molecular equivalences of even highly complex digital circuits. However, almost all the integration reported in the literature is “virtual”, meaning that the output of a unimolecular system is adapted to the output of integrated set of logic gates, such that, that unimolecular system represents the equivalence of a certain complex digital design. Although this approach provides some important advantages, it does not truly solve the concatenation issue at the molecular level. For a rational design and implementation towards a sophisticated molecular computing, physical integration/concatenation of molecular (chemical) logic gates should also be provided, like it is in all other digital devices. Since assuring communication between species is a very difficult task at the

molecular level, their physical integration still is one of the foremost problems remaining in the field of molecular logic gates. However, in order to make some further significant advances in this field, there is no doubt that this is the right time for the new methodologies to be developed or put forward as an idea, suggesting alternative solutions to the aforementioned issue.

Realizing this emergency, we have reported a study (chapter 6) where concatenation of two separately functioning molecular logic gates is achieved through energy transfer and modulation of inner filter effect. In other words, energy transfer (EET) and modulation of inner filter effect (IFE) offer two possible methodologies for concatenating two logic gates. We provided Bodipy based molecular systems to illustrate these approaches. In our IFE-based approach, we concatenated a photochromicity-based AND logic gate to an ion-responsive Bodipy based AND gate, making use of the modulation of IFE. In energy transfer based method, we coupled two ion-responsive Bodipy based AND logic gates, through the increased efficiency of energy transfer. EET approach was particularly appealing because, it involves physical connection of two logic gates through a chemical reaction. There are still issues to be addressed, such as the maximum number of gates that can be integrated based on EET approach, but even the slightest improvements in mimicking silicon circuitry may yield huge leaps of advance due to the molecular nature of these particular designs. While other approaches including self-assembling components are possible, we are confident that clickable molecular logic gates are highly promising. Demonstration of more complex examples of physically integrated logic gates is to be expected.

To conclude, we can easily claim that, all the reported approaches (including ours) regarding the molecular logic phenomena are not mature enough to afford a competitive molecular computer or to develop a ready-to-use device, so far. Perhaps, it will happen once the solid state platforms take the place of the solution-based chemistry where most of the molecular logic gates are described today. All in all, the molecular logic phenomenon is a quite recent concept and despite all the improvements that took place, it is still in the 'proof-of-principle' stage.

8. BIBLIOGRAPHY

1. Trend, J. E.; Kipke, C. A.; Rossmann, M.; Yafuso, M.; Patil, S. L. (**1993**) U.S. Patent 5,474,743

2. Lehn, J.M. *Supramolecular Chemistry: Concepts and Perspectives*, VCH, Weinheim, **1995**

3. Vögtle F. *Supramolecular Chemistry An Introduction*, Wiley, Chichester, **1991**

4. Lehn, J.M. *Proc. Natl. Acad. Sci*. USA **2002**, *99,* 4763-4768

5. Lakowicz, J.R. *Principles of Fluorescence Spectroscopy,* Plenum Press, New York, **1999**

6. http://photochemistryportal.net/home/index.php/2009/08/24/light-absorption-and-fate-of-excited-state/

7. Wardle, B. *Principles and Applications of Photochemistry*, John Wiley & Sons, **2009**

8. Kasha, M. *Discussions of the Faraday Society* **1950**, *9,* 14

9. Stokes,G.G. *Org. Lett.* **1852,** *142,* 463-562

10. Lakowicz, J.R. *Principles of Fluorescence Spectroscopy,* Plenum Press, New York, **1999**

11. Weber, G.; Teale, F.W.J. *Transactions of the Faraday Society* **1957**, *53*, 646

12. Berezin, M.Y.; Achilefu, S. *Chem. Rev.* **2010**, *110*, 2641-2684

13. Bates, M.; Huang, B.; Dempsey, G.T.; Zhuang, X. *Science* **2007**, *317*, 1749

14. Marks, K.M.; Nolan, G.P. *Nat. Meth.* **2006**, *3*, 591

15. Demchenko, A.P. *Introduction to Fluorescence Sensing*, Springer, Netherlands, **2009**

16. Haugland, R.P.; Gregory, J.; Spence, M.T.Z.; Johnson, I.D. *Handbook of Fluorescent probes and research products;* Molecular Probes, **2002**

17. Song, L.; Hennink, E.J.; Young, I.T.; Tanke, H.J. *Biophys. J.* **1995**, *68*, 2588

18. Geisow, M.J. *Exp. Cell. Res.* **1984**, *150*, 29

19. Egawa, Y.; Hayashida, R.; Seki, T.; Anzai, J. *Talanta*, **2008**, *76*, 736

20. De Silva, A.P.; Gunaratne, H.Q.N.; Gunnlaugsson, T.; Huxley, A.J.M.; Rademacher, J.T; Rice, T.E. *Chemosensors for Ion and Molecule Recognition*, Ed. Czarnik, A.W. Deseverge, J.P. NATO ASI Series, Series C; Mathematical and Physical Sceinces, Vol.*492*, pp 143-147, Kluwer Academic Publishers, **1997**

21. Gawley, R.E.; Mao, H.; Haque, M.; Thorne, J.B.; Pharr, J.S. *J. Org. Chem.* **2007**, *72*, 2187-2191

22. Xu, Z.; Yoon, J.; Spring, D. R.; *Chem. Soc. Rev.* **2010**, ***39***, 1996

23. Valeur, B. *Molecular Fluorescence*, Wiley-VCH: Weinheim, **2002**

24. Rurack, K.; Resch-Genger, U. *Chem. Soc. Rev*. **2002**, *31*, 116–127

25. Wasielewski. M. et al., *Photosyn. Res*. **1987,** *12*, 181-189

26. Czarnik, A.W. et al., *Fluorescent Chemosensors for Ion and Molecule Recognition* (American Chemical Society: 1993)

27. Akkaya, E.U.; Saki, N. *J. Org. Chem* **2001,** *66*, 1512-1513

28. Fabbrizzi, L.; Poggi, A. *Chem. Soc. Rev*. **1995,** *24*, 197-202

29. De Silva, A.P. et al., *Photoinduced Electron Transfer V* **1993,** 223-264

30. De Silva, A.P.; de Silva, S.A. *J. Chem. Soc. Chem. Commun.* **1986**, 1709

31. De Silva, A.P.; Gunaratne, H.Q.N. and Sandanayake, K.R.A.S. *Tetrahedron Lett.* ***31*****,** **1990**, p. 5193

32. Fabbrizzi, L.; Lichelli, M.; Pallavicini, P.; Perotti, A. and Sacchi, D. *Angew. Chem. Int. Ed. Engl.* ***33*****,** **1994**, p. 1975

33. Wu, Y.; Peng, X.; Guo, B.; Fan, J.; Zhang, Z.; Wang, J.; Cui, A.; Gao, Y. *Org. Biomol. Chem*. **2005**, *3*, 1387

34. Kim, S.K.; Lee, S.H.; Lee, J.Y.; Bartsch, R.A.; Kim, J.S. *J. Am. Chem. Soc.* **2004**, *126*, 16499–16506

35. Turfan, B.; Akkaya, E.U. *Org. Lett.* **2002**, *4*, 2857-2859

36. Nagano, T. et al., *Org. Lett*. **2007,** *9*, 3375-3377

37. Valeur, B.; Badaoui, F.; Bardez, E.; Bourson, J.; Boutin,P.; Chatelain, A.; Devol, I.; Larrey, B.; Lefe`vre, J.P.; Soulet, A.; in: Desvergne, J.-P.; Czarnik, A.W. (Eds.), *Chemosensors of Ion and Molecule Recognition*, NATO ASI Series, Kluwer, Dordrecht, **1997**, p. 195.

38. Valeur, B.; Leray, I. *Coord. Chem. Rev*., **2000**, *205*, 3

39. Löhr,H.G.; Vögtle,F. *Acc. Chem. Res*. **1985,** *18*, 65

40. Mateeva, N.; Enchev, V.; Antonv, L.; Deligeorgiev, T.; Mitewa, M. *J. Incl.Phenom.* **1995**, *93*, 323

41. Martin, M.M.; Be´gin, L.; Bourson, J.; Valeur, B. *J. Fluoresc.* **1994**, *4*, 271

42. Deniz, E.; Isbasar, G. C.; Bozdemir, O. A.; Yildirim, L.T.; Siemiarczuk, A.; Akkaya E. U. *Org. Lett*., **2008**, *10*, 3401

43. Zhou, Y.; Xiao, Y.; Chi, S.; Qian, X. *Org.Lett.* **2008**, *10*, 633

44. Dong,Y.; Bolduc, A.; McGregor, N.; Skene, W.G. *Org.Lett*. **2011**, *13*, 1844

45. Marder, S.R.; Kippelen, B.; Jen, A.K.Y.; Peyghammbarian,N. *Nature (London*) **1997**, *388*, 845

46. Burckstummer, H.; Kronenberg, N.M.; Meerholz, K.; Wurtner, F. *Org.Lett*. **2010**, *12*, 3666

47. Erten-Ela, S.; Yilmaz, M.D.; Icli, B.; Dede, Y.; Icli, S.; Akkaya, E.U. *Org.Lett.* **2008**, *10* (15), 3299-3302

48. Turro, N.J. *Modern Molecular Photochemistry*, University Science Books, Sausalito, **1991**

49. Förster, T. *Ann. Phys*. **1948**, *2*, 55

50. Förster, T. *Disc. Faraday Soc*. **1959**, *27*, 7

51. Sharma, A.; Schulman, S.G. *Introduction to Fluorescence Spectroscopy*, Wiley Science, **1999**

52. Yilmaz, M.D.; Bozdemir, O.A.; Akkaya, E.U. *Org. Lett*. **2006**, *8*, 2871

53. Dexter, D.L. *J. Chem. Phys*., **1953**, *21*, 836

54. Turro, N.J., *Modern Molecular Photochemsitry*, University Science Books, Sausalito, **1991**

55. Wan, C.-W.; Burghart, A.; Chen, J.; Bergström, F.; Johansson, L.B.A.; Wolford, M.F.; Kim, T.G.; Topp, M.R.; Hochtrasser, R.M.; Burgess, K. *Chem Eur J*, **2003**, *9*, 4430–4441

56. Barigelletti, F.; Flamigni, L. *Chem. Soc. Rev*. **2000**, *29*, 1

57. Martinez-Manez, R.; Sancenon, F. *Chem. Rev*., **2003**, *103*, 4419

58. Xu, Z.C.; Yoon, J.; Spring, D.R. *Chem. Soc. Rev*. **2010**, *39*, 1996

59. Kim, J.S.; Quang, D.T. *Chem. Rev*. **2007**, *107*, 3780

60. Wu, J.; Liu, W.; Ge, J.; Zhang, H.; Wang, P. *Chem. Soc. Rev*. **2011**, *40*, 3483

61. Pearson, R.G. *J. Am. Chem. Soc*. **1963**, *85*, 3533

62. Du, J.; Fan, J.; Peng, X.; Li, H.; Wang, J.; Sun, S. *J.Fluoresc*. **2008**, *18*, 919

63. Nolan, E.M.; Lippard, S.J. *J. Am. Chem. Soc*., **2003**, *125*, 14270-14271

64. Coskun, A.; Akkaya, E.U. *J. Am. Chem. Soc*., **2006**, *128*, 14474-14475

65. Yamada, K.; Nomura, Y.; Citterio, D.; Iwasawa, N.; Suzuki, K. *J. Am. Chem. Soc*., **2005**, *127*, 6956-57

66. Rubin, H. *news and reviews in molecular, cellular and developmental biology* **2005,** *27*, 311

67. Eskes, R.; Antonsson, B.; Osen-Sand, A.; Richter, C.; Mazzei,G.; Nichols, A.; Martinou, J.C. *The Journal of cell biology* **1998,** *143*, 217-24

68. Komatsu, H.; Iwasawa, N.; Citterio, D.; Suzuki, Y.; Kubota, T.; Tokuno, K.; Kitamura, Y.; Oka, K.; Suzuki, K. *J. Am. Chem. Soc.* **2004,** *126*, 16353-60

69. Farruggia, G. Lotti, S.; Prodi, L.; Montalti, M.; Zaccheroni, N.; Savage, P.; Trapani, V.; Sale, P.; Wolf, F.I. *J. Am. Chem. Soc.* **2006,** *128*, 344-50

70. Woodroofe, C.C.; Lippard, S.J. *J. Am. Chem. Soc*., **2003**, *125*, 11458-11459

71. Taki, M.; Wolford, J.L.; O`Halloran, T.V. *J. Am. Chem. Soc*., **2004**, *126*, 712-713

72. Xu, Z.; Yoon, J.; Spring, D.R. *Chem. Soc. Rev*. **2010**, *39*, 1996

73. Nolan, E.M.; Lippard, S.J. *Account. Chem. Res*. **2009**, *42*, 193

74. Yubin, D.; Weihong, Z.; Yongshu, X. *Progress in Chemistry* **2011**, *23*, 2478

75. Beer, P.D.; Gale, P.A. *Angew. Chem.Int. Ed.* **2001**, *40*, 486 - 516.

76. Gunnlaugsson, T.; Glynn, M.; Tocci, G.M.; Kruger, P.E.; Pferffer, F.M. *Coord. Chem. Rev*. **2006**, *250*, 3094

77. Christianson, D.W.; Lipscomb, W.N. *Acc. Chem. Res.* **1989**, *22*, 62.

78. Metzger, A.; Lynch, V.M.; Anslyn, E. V. *Angew. Chem. Int. Ed*. **1997**, *36*, 862

79. Simon, M. I.; Strathmann, M. P.; Gautam, N. *Science* **1991**, *252*, 802

80. Lipscomb, W. N.; Strater, N. *Chem. Rev*. **1996**, *96*, 2375

81. Jose, D.; Mishra, S.; Ghosh, A.; Shrivastav, A.; Amitava, *D. Org.Lett*. **2007,** *9 (10)*, 1979

82. Neelakandan, P.; Hariharan, M.; Ramaiah, D. *Org.Lett.* **2005,** *7*, 5765

83. Ward, C. J.; Patel, P.; James, T. D. *Chem. Lett.*, **2001**, 406

84. Black, C. B.; Andrioletti, B.; Try, A. C.; Ruiperez, C.; Sessler, J.L. *J. Am. Chem. Soc.* **1999**, *121*, 10438

85. Hudnall, T.W.; Gabbai, F.P. *Chem. Commun*. **2008**, 4596-4597

86. Treibs, A.; Kreuzer, F.-H. Justus Liebigs Ann. Chem. 1968, *718*, 208

87. López Arbeloa F.; Bañuelos J.; Martínez V.; Arbeloa T.; López Arbeloa I. *Int Rev Phys Chem*, **2005**, *24*, 339–374

88. Shah, M.; Thangaraj, K.; Soong, M.; Wolford, M.; Boyer, J.; Politzer, I.; Pavlopoulos, T. *Heteroat. Chem.*, **1990**, 1, 389

89. Li, Z.; Mintzer, E.; Bittman, R. *J. Org. Chem*., **2006**, 71, 1718

90. Yakubovskyi, V.; Shandura, M.; Mykola, P.; Kovtun, Y. *Eur. J. Org. Chem.*, **2009**, *19*, 3237

91. Wu, L.; Burgess, K. *Chem. Commun*., **2008**, 40, 4933

92. Hattori, S.; Ohkubo, K.; Urano, Y.; Sunahara, H.; Nagano, T.; Wada, Y.; Tkachenko, N.V.; Lemmetyinen, H.; Fukuzumi, S. *J. Phys. Chem. B*. **2005**, *109*, 15368

93. Yogo, T.; Urano, Y.; Ishitsuka, Y.; Maniwa, F.; Nagano, T. *J. Am. Chem. Soc*., **2005**, *127*, 12162

94. Metzker, M.L.; Lu, J.; Gibbs, R.A. *Science*,**1996**, *271*, 1420–1422

95. Harriman, A.; Izzet, G.; Ziessel, R. *J Am Chem Soc*, **2006**, *128*, 10231–10239

96. Loudet, A.; Burgess, K. *Chem. Rev*., **2007**, *107*, 4891–4932

97. Ulrich, G.; Ziessel, R.; Harriman, A. *Angew. Chem. Int. Ed*. **2008**, *47*, 1184–1201

98. Benniston, A.C.; Copley, G. *Phys. Chem. Chem. Phys*. **2009**, *11*, 4124–4131

99. Boens, N.; Leen, V.; Dehaen, W. *Chem. Soc. Rev*. **2012**, *41*, 1130

100. Floyd, T.L. *Digital Fundamentals*, Prentice-Hall International Inc., Upper Saddle River, NJ, **1997**

101. Gibilisco, S. *The Illustrated Dictionary of Electronics*, McGraw-Hill, New York, **2001**

102. Saba, A.; Manna, N. *Digital Principles & Logic Design*, Infinity Science Press, London, **2007**

103. Millman, J.; Grabel, A. *Microelectronics*, McGraw-Hill, London, **1988**

104. Hush, N. *Nat. Mater.* **2003**, *2*, 134

105. Moore, G.E. *Electronics*, **1965**, *38*, 114

106. Moore, G.E. *IEEE Trans. Consum. Electron.*, **1977**, *23*, 10

107. Moore, G.E. *Proc. IEEE*, **1998**, *86*, 53

108. Dubash, M. **2005**, *Moore's Law is dead, says Gordon Moore*, available at: http://news.techworld.com/operating%20systems/3477/moores-law-is-dead-says-gordon-moore/%3E/ [accessed 27 November 2012]

109. Balzani, V.; Credi, A.; Venturi, M. *Proc. Natl.Acad. Sci. U.S.A.* **2002**, *99*, 4814

110. de Silva, A.P.; Gunaratne, H.Q.N.; McCoy, C.P. *Nature*, **1993**, *364*, 42

111. de Silva, A.P; McClenaghan, N.D. *Chem. Eur. J.*, **2002**, *8*, 4935

112. Pischel, U. Angew. Chem. Int. Ed. **2007**, *46*, 4026 –4040.

113. Andreasson, J.; Pischel, U. *Chem. Soc. Rev*., **2010**, *39*, 174

114. de Silva, A.P.; Leydet, Y.; Lincheneau, C.; McClenaghan, N.D. *J. Phys.: Condens. Matter* **2006**, *18*, 1847

115. Andreasson, J.; Pischel, U.; Straight, S.D.; Moore, T.A.; Moore, A.L.; Gust, D *J. Am. Chem. Soc*. **2011**, *133*, 11641

116. Szacilowski, K. *Chem. Rev.*, **2008**, *108*, 3481

117. de Silva, A.P.; McClenaghan, N.D. *J. Am. Chem. Soc.*, **2000**, *122*, 3965

118. Margulies, D.; Melman, G.; Felder, C.E.; Arad-Yellin, R.; Shanzer, A. *J. Am. Chem. Soc*., **2004**, *126*, 15400

119. Wagner, N.; Ashkenasy, G. *Chem. Eur. J*., **2009**, *15*, 1765

120. Zhang, L.; Whitfield, W.A.; Zhu, L. *Chem. Commun*., **2008**, 1880

121. Langford, S.J.; Yann, T. *J. Am. Chem. Soc*., **2003**, *125*, 11198

122. Margulies,D.; Melman, G.; Shanzer, A. *J. Am. Chem. Soc.*, **2006**, *128*, 4865

123. Amelia, M.; Baroncini, M.; Credi, A. *Angew. Chem. Int. Ed.*, **2008**, *47*, 6240

124. Perez-Inestrosa, E.; Montenegro, J.M.; Collado, D.; Suau, R. *Chem. Commun.*, **2008**, 1085

125. Andréasson, J.; Straight, S.D.; Moore, T.A.; Moore, A.L.; Gust, D. *J. Am. Chem. Soc*., **2008**, *130*, 11122

126. Tian, H. *Angew. Chem. Int. Ed*., **2010**, *49*, 4710

127. Ruiter, G.; Van der Boom, M.E.; *J. Mater. Chem*., **2011**, *21*, 17575

128. Pischel, U. *Angew. Chem. Int. Ed.*, **2010**, *49*, 1356

129. Baron, R.; Onopriyenko, A.; Katz, E.; Lioubashevski, O.; Willner, I.; Wang, S.; Tian, H. *Chem. Commun.*, **2006**, *20*, 2147

130. Ruiter, G.; Tartakovsky, E.; Oded, N.; van der Boom, M.E. *Angew. Chem. Int. Ed.*, **2010**, *49*, 169

131. Ruiter, G.; Vvan der Boom, M.E. *Acc. Chem. Res.*, **2011**, *44*, 563

132. Schmidtchen, F. P.; Berger, M. *Chem. Rev*. **1997**, *97*, 1609–1646

133. *Guidelines for Drinking-Water Quality*, World Health Organization, Geneva, 1996

134. Moriva, F.; Hashimoto, Y. J. *Forensic. Sci*. **2001**, ***46***, 1421–1425.

135. Ishii, A.; Seno, H.; Watanabe-Suzuki, K.; Suzuki, O.; Kumazawa, T. *Anal. Chem*. **1998**, *70*, 4873–4876

136. Kim, Y-H.; Hong, J-I. *Chem. Commun*. **2002**, 512-513

137. Chen, C-L.; Chen, Y-H.; Chen, C-Y.; Sun, S-S. *Org. Lett.* **2006**, *8*, 5053-5056

138. Ekmekci, Z.; Yilmaz M. D.; Akkaya, E. U. *Org. Lett.* **2008**, *10*, 461-464

139. Chow, C-F.; Lam, M. H. W. Wong, W-Y. *Inorg. Chem.* **2004**, *43*, 8387-8393

140. Atilgan, S.; Ozdemir, T.; Akkaya, E. U. *Org. Lett*. **2008**, *10*, 4065-4067

141. Ozlem, S.; Akkaya, E. U. *J. Am. Chem. Soc.* **2009**, *131*, 48-49

142. Goze, C.; Ulrich, G.; Ziessel, R. *Org. Lett*., **2006**, *8*, 4445-4448

143. Zeng, L.; Miller, E. W.; Pralle, A.; Isacoff, E. Y.; Chang, C. J. *J. Am. Chem. Soc*. **2006**, *128*, 10-11

144. Matsumoto, T.; Urano, Y.; Shoda, T.; Kojima, H.; Nagano, T. *Org. Lett.* **2007**, *9*, 3375-3377

145. Sunahara, H.; Urano, Y.; Kojima, H.; Nagano, T. *J. Am. Chem. Soc.* **2007**, *129*, 5597-5604

146. Bozdemir, O.A.; Yılmaz, M.D.; Buyukcakir, O.; Siemiarczuk, A.; Tutas, M.; Akkaya, E.U. *New J. Chem.* **2010**, *34*, 151-155

147. Erbas, S,; Gorgulu, A.; Kocakusakogullari, M.; Akkaya E.U. *Chem. Commun*. **2009**, 4956-4958

148. Kolemen, S.; Cakmak, Y.; Erten-Ela, S.; Altay, Y.; Brendel, J.; Thelakkat, M.; Akkaya, E.U. *Org. Lett*. **2010,** *12*, 3812-3815

149. Bouit, P.A.; Kamada, K.; Feneyrou, P.; Berginc, G.; Toupet, L.; Maury, O.; Andraud, C. *Adv. Mater*. **2009**, *21*, 1151-1154

150. Haugland, R. P. *The Handbook-A guide to fluorescent probes and labeling technologies*, 10th ed.; Invitrogen Corp., 2005

151. Jentsch, T. *Curr. Opin. Neurobiol*. **1996**, *6*, 303-308

152. Varner, J.A.: Jensen, K.F.: Horwath, W.: Isaacson, R.L. *Brain Res*. **1998**, *784*, 284-298

153. Bozdemir O.A.; Sozmen, F.; Buyukcakir, O**.**; Guliyev, R.; Cakmak Y.; Akkaya E.U. *Org. Lett.* **2010**, *12*, 1400-1403

154. Hudnall, T.W.; Chiu, C.W.; Gabbai, F.P. *Acc. Chem. Res.* **2009**, *42*, 388-397

155. Xu, Z.; Kim, S. K.; Han, S. J.; Lee, C.; Kociok-Kohn, G.; James, T. D.; Yoon, J. *Eur. J. Org. Chem*. **2009**, 3058–3065

156. Abragam, A. *Principles of Nuclear Magnetism*, Clarendon, Oxford, **1986**.

157. Finze, M.; Bernhardt, E.; Willner, H.; Lehmann, C. *Angew. Chem. Int. Ed.* **2003**, *42*, 1052-1055

158. Bernhardt, E.; Henkel,G.; Willner, H.; Pawelke, G.; Burger, H. *Chem. Eur. J.* **2001**, *7*, 4696-4705

159. Hundnall, T. W.; Gabbai, F. P. *Chem. Commun*. **2008**, 4596–4597

160. Hayes, J. P. *Introduction To Digital Logic Design*; Addison-Wesley Publishing Company: Reading, MA, **1993**

161. Lee, T. H.; Gonzalez, J. I.; Zheng, J.; Dickson, R. M. *Acc. Chem. Res.* **2005**, *38*, 534–541

162. Bissell, R. A.; de Silva, A. P.; Gunaratne, H. Q. N.; Lynch, P. L. M.; Maguire, G. E. M.; Sandanayake, K. R. A. S. *Chem. Soc. Rev.* **1992**, *21*, 187–195

163. Remon, P.; Ferreira, R.; Montenegro, J. M.; Suau, R.; Perez-Inestrosa, E.; Pischel, U. *ChemPhysChem* **2009**, *10*, 2004–2007

164. Baytekin, H. T.; Akkaya, E. U. *Org. Lett.* **2000**, *2*, 1725–1727

165. Coskun, A.; Deniz, E.; Akkaya, E. U. *Org. Lett.* **2005**, *7*, 5187–5189

166. de Silva, A. P.; Gunarante, H. Q. N.; Gunnlaugsson, T.; Huxley, A. J. M.; McCoy, C. P.; Rademacher, J. T.; Rice, T. E. *Chem. Rev.* **1997**, *97*, 1515–1566

167. Wong, B. A.; Friedle, S.; Lippard, S. J. *J. Am. Chem. Soc.* **2009**, *131*, 7142–7152

168. Peng, X.; Du, J.; Fan, J.; Wang, J.; Wu, Y.; Zhao, J.; Sun, S.; Xu, T. *J. Am. Chem. Soc.* **2007**, *129*, 1500–1501

169. Ishikawa, J. *Bull. Chem. Soc. Jpn.* **1995**, *68*, 3071–3076

170. Das, S.; Thomas, K. G.; Thomas, K. J.; Kamat, P. V.; George, M. V. *J. Phys. Chem.* **1994**, *98*, 9291–9296

171. Guliyev, R.; Coskun, A.; Akkaya, E. U. *J. Am. Chem. Soc.* **2009**, *131*, 9007–9013

172. Connors, K. A. *Binding Constants: The Measurement of Molecular Complex Stability*; John Wiley & Sons: New York, **1987**

173. Peng, X.; Du, J.; Fan, J.; Wang, J.; Wu,Y.; Zhao, J.; Sun, S.; Xu, T. *J. Am. Chem. Soc.* **2007,** *129*, 1500-1501

174. Vladimirova, M. P.; Simova, S. D.; Stanoeva, E. R.; Mitewa, M. I. *Dyes and Pigm.* **2001**, *50*, 157-162

175. Zhirnov, V.V.; Cavin, R.K; Hutchby, J.A.; Bourianoff, G.I. *Proc. IEEE*, **2003**, *91*, 1934-1939

176. Baron, R.; Lioubashevski, O;. Katz, E.; Niazov, T.; Willner, I. *Angew. Chem. Int. Ed*. **2006**, *45*, 1572

177. Niazov, T.; Baron, R.; Katz, E.; Lioubashevski, O.; Willner, I. *Proc. Nat. Acad. Sci. USA* **2006**, *103*, 17160

178. Strack, G.; Ornatska, M.; Pita, M.; Katz, E. *J. Am. Chem. Soc.* **2008**, *130*, 4234-4235

179. Gupta, T.; Van der Boom, M.E. *Angew. Chem. Int. Ed.* **2008**, *47*, 2260–2262

180. Gupta, T.; Van der Boom, M.E. *Angew. Chem. Int. Ed.* **2008**, *47*, 5322

181. Silvi, S.; Constable, E.C.; Housecroft, C.E.; Beves, J.E.; Dunphy, E.L.; Tomasulo, M.; Raymo, F.M.; Credi, A. *Chem. Eur. J.* **2009**, *15*, 178–185

182. Raymo, F.M.; Giordani, S. *Proc. Natl. Acad. Sci. U. S. A.*, **2002**, *99*, 4941–4944

183. Remacle, F.; Speiser, S.; Levine, R.D. *J. Phys. Chem. B*, **2001**, *105*, 5589–5591

184. Salman, H.; Eichen, Y.; Speiser, S. *Mat. Sci. Eng.C* **2006**, *26*, 881-885

185. Bozdemir, O.A.; Guliyev, R; Buyukcakir, O.; Selcuk, S.; Kolemen, S.; Gulseren, G.; Nalbantoglu, T.; Boyaci, H.; Akkaya, E.U. *J. Am. Chem. Soc.* **2010**, *132*, 8029–8036

186. Peng, X.; Du, J.; Fan, J.; Wang, J.; Wu, Y.; Zhao, J.; Sun, J.; Xu, T. *J. Am. Chem. Soc*. **2007**, *129*, 1500-1501.

187. Kim, O.; Je, J.; Melinger, J.S. *J. Am. Chem. Soc.*, **2006**, 128, 4532–4533